

For Reference

NOT TO BE TAKEN FROM THIS ROOM

For Reference

NOT TO BE TAKEN FROM THIS ROOM

Ex LIBRIS
UNIVERSITATIS
ALBERTAEÆSIS



THE UNIVERSITY OF ALBERTA

THE THREE DIMENSIONAL ISING MODEL ON A
TRIPLE OF RELATED LATTICES

by



JOSEPH ALLEN LEU

A THESIS

SUBMITTED TO THE FACULTY OF GRADUATE STUDIES
IN PARTIAL FULFILLMENT OF THE REQUIREMENTS FOR THE DEGREE
OF DOCTOR OF PHILOSOPHY

DEPARTMENT OF PHYSICS

EDMONTON, ALBERTA

SPRING, 1970

ABSTRACT

The Ising model of a ferromagnet has been investigated in detail on a triple of related lattices which heretofore have not been studied. These lattices, which we call the hydrogen peroxide, hyperkagomé, and hypertriangular have coordination numbers of three, four, and six respectively, and may be looked upon as three dimensional analogues of the more familiar two dimensional lattices, honeycomb, kagomé, and triangular.

High and low temperature exact series expansions have been derived for the partition function, energy, specific heat, and initial susceptibility of the hydrogen peroxide and hypertriangular lattices. The exact series expansion of the spontaneous magnetization has also been derived for the hydrogen peroxide lattice.

The star - triangle and decoration transformations, which relate the Ising partition functions of the hydrogen peroxide, hyperkagomé, and hypertriangular lattices to each other, have been utilized to obtain the properties of the hyperkagomé lattice from those of the hydrogen peroxide lattice. For a given pair of the triple of related lattices we have utilized these transformations to obtain expressions relating the specific heat amplitudes and the

Digitized by the Internet Archive
in 2023 with funding from
University of Alberta Library

<https://archive.org/details/Leu1970>

susceptibility amplitudes.

A problem which is very similar to the calculation of the initial susceptibility of an Ising ferromagnet, namely the self-avoiding walk problem, has also been studied for the hydrogen peroxide and hypertriangular lattices. Exact series expansions of the self-avoiding walk generating function have been derived for both lattices.

A numerical analysis utilizing the ratio and Padé approximant methods has been performed on the series expansions to obtain estimates of the critical constants and critical indices of the Ising model. Estimates for the critical index and the attrition parameter of the self-avoiding walk problem have been obtained in a similar manner.

An empirical formula giving the critical point of an Ising ferromagnet as a function of coordination number has also been found.

ACKNOWLEDGEMENTS

I am greatly indebted to my supervisor Dr. D. D. Betts for suggesting this problem and for his constant encouragement and advice during the course of this work. I would also like to thank Dr. C. J. Elliott who assisted with the computer programing.

I would like to thank the Department of Physics, University of Alberta, and the National Research Council of Canada for their financial support. Part of this research was supported by the U. S. Air Force and that support is gratefully acknowledged.

My gratitude is also extended to Marge Lybacki and Mary Lou Senf who showed great patience in typing the manuscript.

Finally I would like to thank my wife Mary whose patience and forbearing made a difficult task less so.

CONTENTS

	Page
Chapter I INTRODUCTION	
A. Critical Point Phenomena	1
B. The Ising Model	24
C. Scope of this Thesis	33
Chapter II THE HYDROGEN PEROXIDE, HYPERTRI- ANGULAR AND HYPERKAGOMÉ LATTICES	34
Chapter III HIGH TEMPERATURE SERIES EXPANSIONS	
A. The Zero Field Partition Function	49
B. The Initial Susceptibility	60
Chapter IV LOW TEMPERATURE SERIES EXPANSIONS OF FERROMAGNETS AND ANTIFERROMAGNETS	
A. The Direct Method	64
B. The Shadow Lattice Method	75
Chapter V ISING MODEL TRANSFORMATIONS	
A. The Star-Triangle Transformation	89
B. The Decoration Transformation	96
C. Exact Relationships between the Thermodynamic Variables	104

	Page
Chapter VI SELF-AVOIDING WALKS	
A. Relationship to Ising Model	113
B. Enumeration of Self-Avoiding Walks	115
Chapter VII ANALYSIS OF SERIES EXPANSIONS	
A. Methods of Analysis	122
B. The Ising Model	128
C. The Self-Avoiding Walk Problem	136
Chapter VIII REVIEW AND DISCUSSION	
A. The Ising Model	140
B. The Self-Avoiding Walk Problem	152
Appendix A Partition function coefficients for the hypertriangular lattice	154
Appendix B Lattice constants of non-magnetic and magnetic graphs for the hypertriangular lattice	156
Appendix C Symbolic equations for calculating on the hypertriangular lattice the lattice constants of separated non-magnetic and magnetic graphs	162
Appendix D Star lattice constants for the hydrogen peroxide and hypertriangular lattices	169

	Page
Appendix E Susceptibility coefficients for the hypertriangular lattice calculated by the direct method	178
Appendix F Low temperature ferromagnetic polynom- ials and series expansions for the hypertriangular lattice	192
Appendix G Partial generating functions for the hydrogen peroxide lattice	195
Appendix H Shadow configurations for the hydrogen peroxide lattice	197
Appendix I Low temperature ferromagnetic polynom- ials for the hydrogen peroxide lattice	232
Appendix J Configurational data for calculating self-avoiding walks on the hydrogen peroxide and hypertriangular lattices	235
Appendix K Tables of Padé approximant estimates of critical parameters for the hypertri- angular and hydrogen peroxide lattices	243
References	267

TABLES

	Page
1.1 Experimental values for critical indices	19
1.2 Critical indices for the mean field theory and the Ising model	22
3.1 The first six series coefficients for the zero field partition function of the hypertriangular lattice	53
3.2 The first four series coefficients for the initial susceptibility of the hypertriangular lattice	53
7.1 Ratio estimates of critical parameters of the Ising model on the hydrogen peroxide and hypertriangular lattices	132
7.2 Ratio estimates of critical parameters of the self-avoiding walk problem on the hydrogen peroxide and hypertriangular lattices	138
8.1 High temperature critical properties of the two dimensional Ising model	142
8.2 High temperature critical properties of the three dimensional Ising model	143

	Page
4.1 Topological breakdown of the perturbations on the hydrogen peroxide lattice contributing to [7,6]	69
4.2 Shadow configurations for the hydrogen peroxide lattice	78
5.1 The star-triangle transformation	90
5.2 The decoration transformation	97
6.1 The result of adding a step to a self-avoiding walk of $(n-1)$ steps	116
6.2 The three topologically distinct linear graphs that result from the addition of a step to the tail of a tadpole	117
7.1 Plot of successive ratios b_n/b_{n-1} against $1/n$ for the initial susceptibility of the hypertriangular lattice	131
7.2 Plot of successive ratios c_n/c_{n-1} against $1/n$ for the self-avoiding walk generating function of the hypertriangular lattice	137
8.1 Plot of $v_C = \tanh(J/kT_C)$ against $1/q$ for two and three dimensional Ising models	144
8.2 Plot of $\tanh(-U_C/kT_C)$ against $1/q$ for two and three dimensional Ising models	147

Page

8.3	Plot of S_c/k against $1/q$ for two and three dimensional Ising models	148
8.4	Plot of the critical ratios $P_c/\rho_c kT_c$ against $1/q$ for two and three dimensional Ising models	149

CHAPTER I

INTRODUCTION

A. Critical Point Phenomena

The study of critical phenomena was initiated a century ago with the measurements by Andrews (1869) near the critical point of carbon dioxide. Subsequent experiments have shown that a number of physical systems of a diverse nature, fluids, ferromagnets, antiferromagnets, binary liquids, and binary alloys, all have well defined critical points and all show very similar behaviour in the vicinity of the critical point. One could also mention critical point phenomena associated with superfluids, superconductors, ferroelectrics and antiferroelectrics. The origin of critical phenomena in these systems is however of a different nature from those systems we have mentioned above so we will say no more about them.

The major part of this thesis is concerned with the theory of critical phenomena described in terms of an Ising model of a ferromagnet. Hence it is necessary that we first give a brief review of the experimental facts as we know them. An excellent review of the methods and results of experimental investigations of critical point

phenomena has been given by Heller (1967). We will limit most of our discussion of experimental results to critical phenomena associated with gas-liquid and magnetic systems as they have been subject to more extensive investigations than other systems.

Our discussion of the experimental and theoretical aspects of critical phenomena will concentrate on the manner in which various thermodynamic functions behave as the temperature approaches its critical value.

Experience has shown that in the neighbourhood of the critical point certain thermodynamic functions behave as

$$W \approx A_+(x-x_c)^p, \quad x \rightarrow x_{c+}, \quad (1-1)$$

where W is the thermodynamic function of interest and x is the independent thermodynamic variable. The exponent p is called the critical exponent or critical index of W and A_+ is called the amplitude. In case W diverges at the critical point we will write

$$W \approx A_+(x-x_c)^{-p}, \quad x \rightarrow x_{c+}. \quad (1-2)$$

The form

$$W \approx A_+(x-x_c)^{1/p}, \quad x \rightarrow x_{c+} \quad (1-3)$$

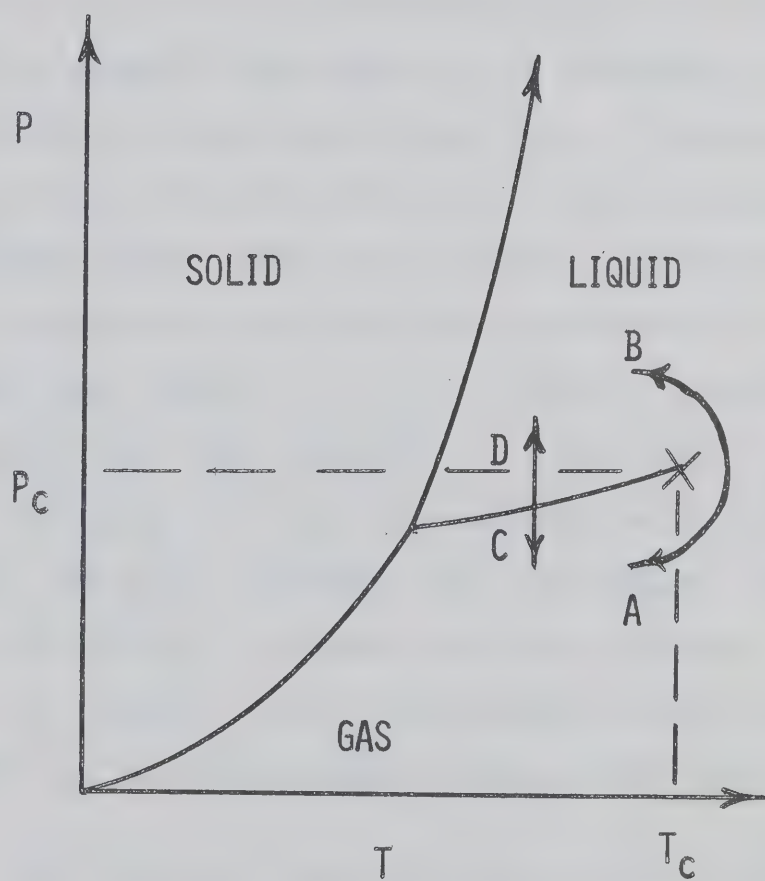
will also occur. In each case p is called the critical index of the thermodynamic function W . It has become established notation to specify by Greek letters the critical indices of certain thermodynamic functions, e.g. α for specific heat, β for magnetization, γ for susceptibility etc. There is one other form of critical point behaviour which often occurs in the critical region,

$$W \approx A \ln(x-x_c) + B, \quad x \rightarrow x_{c+}. \quad (1-4)$$

A logarithmic divergence such as (1-4) can be described by a critical index $p = 0$.

The phase diagram for a typical single component system is depicted in Fig. 1.1. The point labelled X at the end of the vapour pressure curve, beyond which it is impossible to make any distinction between the liquid and gas phases is called the critical point ($P=P_c$, $T=T_c$). A transition from the gas to the liquid phase along curve AB (Fig. 1.1) is continuous and does not give rise to any

Fig. 1.1. The phase diagram for a simple substance exhibiting gas, liquid, and solid phases. The point labelled X is the critical point ($T = T_c$, $P = P_c$) .



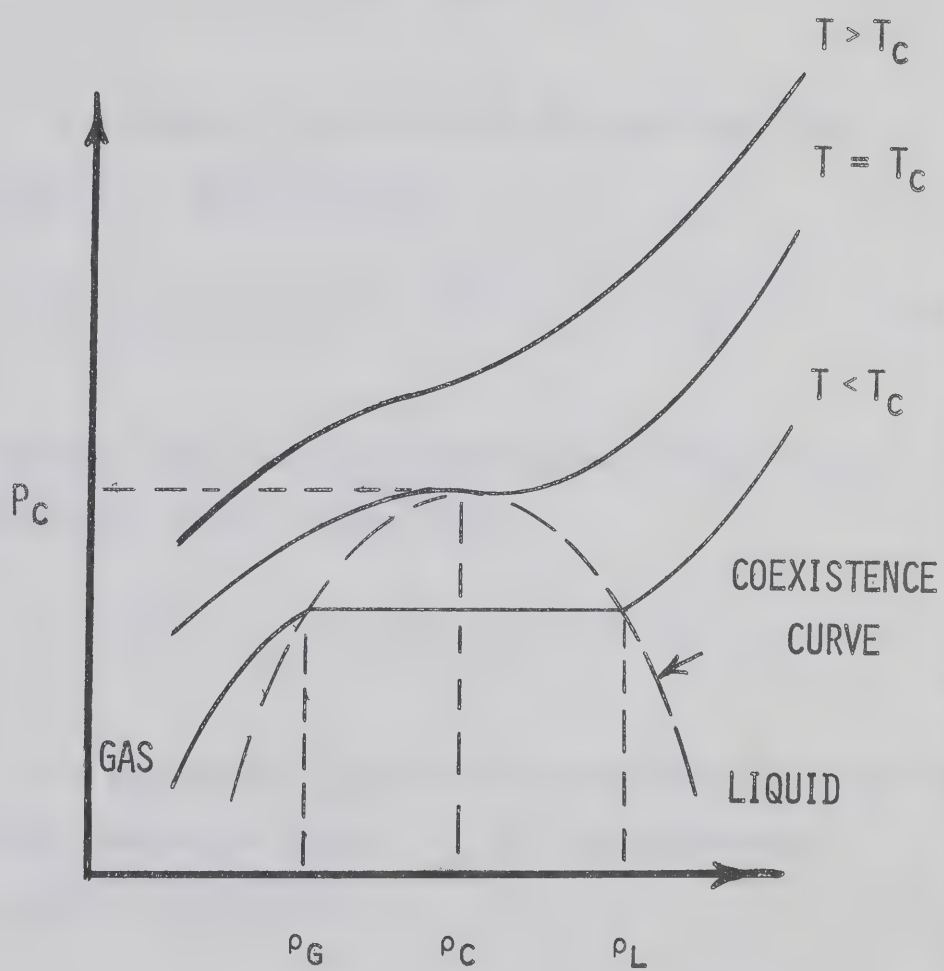
anomalous behaviour in the derivatives of the free energy, while the transition from the gas to the liquid phase along curve CD (Fig. 1.1) is discontinuous.

A more convenient description of the critical region of a fluid and the phenomena associated with it can be given in terms of the shape of the isotherms in the region of the critical point (Fig. 1.2). The pressure is a monotonically increasing function of the density for temperatures greater than the critical temperature T_C , and its derivatives are finite and continuous. As T_C is approached from above ($T \rightarrow T_{C+}$), $(\partial P / \partial \rho)_T$ decreases and has a minimum for some value of ρ until at $T = T_C$ and $\rho = \rho_C$, $(\partial P / \partial \rho)_T = 0$. As the temperature is lowered below T_C the fluid separates into two phases, gas and liquid, and $(\partial P / \partial \rho)_T$ vanishes over the interval $\rho_G < \rho < \rho_L$, where ρ_G is the maximum density of the gas phase and ρ_L is the minimum density of the liquid phase.

The shape of the isotherms in the critical region can be characterized as follows. For simple gases (Ar, Xe, CO₂, ect.) the top of the coexistence curve can be described by the form

$$\rho_L - \rho_G \sim (T_C - T)^\beta, \quad T \rightarrow T_{C-}. \quad (1-5)$$

Fig. 1.2. The isotherms of a simple fluid. The coexistence curve is indicated by the dashed line and the critical point is at (P_c, ρ_c) .



An analysis of the data from the classic experiment on Xe (Weinberger and Schneider 1952, Fisher 1964(a)) yields

$$\beta = 0.345 \pm 0.015 .$$

The shape of the critical isotherm near the critical point is described by

$$P - P_C \sim |\rho - \rho_C|^\delta, \quad T = T_C, \quad \rho \rightarrow \rho_C . \quad (1-6)$$

Widom and Rice (1955) analyzed experimental data for a number of simple gases. They found

$$\delta = 4.2 \pm 0.2 .$$

The appropriate quantity to describe the shape of the critical isotherms above T_C is the isothermal compressibility, defined by

$$K_T = - \frac{1}{V} \left(\frac{\partial V}{\partial P} \right)_T = \frac{1}{\rho} \left(\frac{\partial \rho}{\partial P} \right)_T , \quad (1-7)$$

which according to our above statements approaches infinity as $T \rightarrow T_{C+}$. The behaviour of the isothermal compressibility in the critical region can be described by

$$K_T \sim (T - T_c)^{-\gamma}, \quad \rho = \rho_c, \quad T \rightarrow T_{c+}. \quad (1-8)$$

The experimental evidence for CO_2 (Heller 1967) suggests

$$\gamma = 1.35 \pm 0.15.$$

The behaviour of the compressibility along the coexistence curve as the critical point is approached from below can be similarly described,

$$K_T(\rho_G) \sim K_T(\rho_L) \sim (T_c - T)^{-\gamma'}, \quad T \rightarrow T_{c-}. \quad (1-9)$$

An analysis of the data for CO_2 (Heller 1967) indicates

$$\gamma' = 1.1 \pm 0.4.$$

Recent experiments (Voronel' et al. 1965, Moldover 1966) have revealed a very striking anomaly associated with the specific heat at constant volume as one approaches the critical point from above and below along the critical isochor ($\rho = \rho_c$). The experimental evidence (Kadanoff et al. 1967) suggests

$$\begin{aligned}
C_V &\sim (T-T_C)^{-\alpha}, & T \rightarrow T_{C+} \\
C_V &\sim (T_C-T)^{-\alpha'}, & T \rightarrow T_{C-}
\end{aligned}
\quad \rho = \rho_C \quad (1-10)$$

where

$$0 \leq \alpha \leq 0.4 ,$$

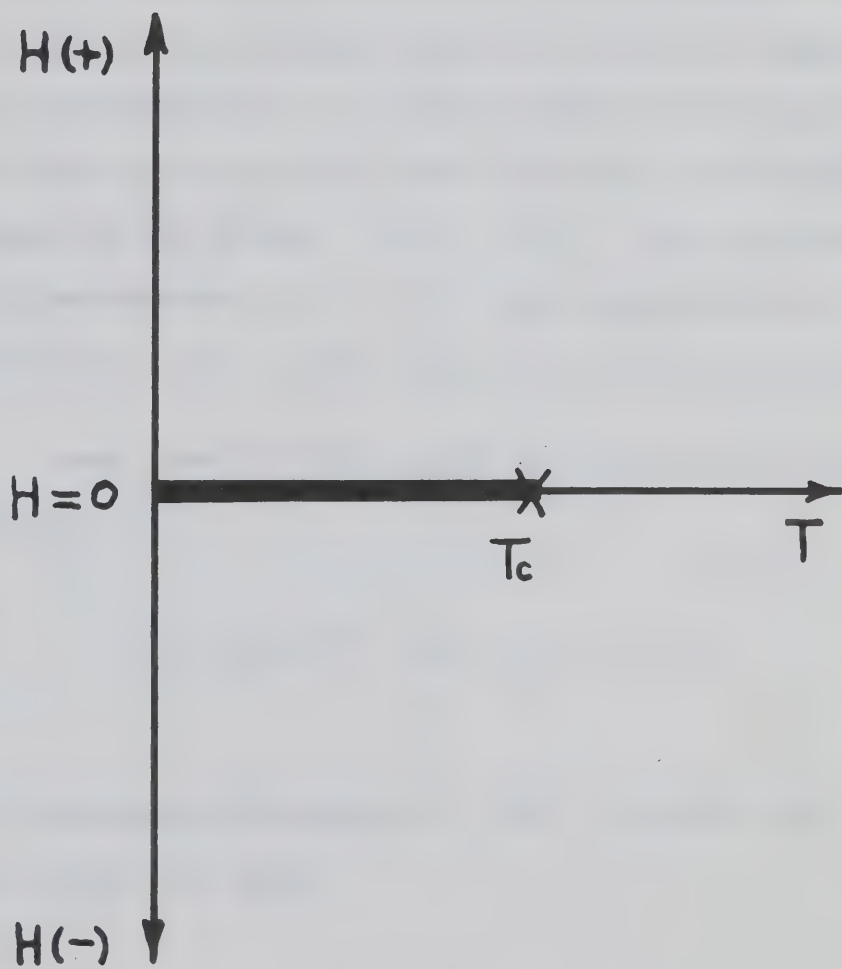
$$0 \leq \alpha' \leq 0.25 .$$

A value of α (or α') equal to zero would indicate a logarithmic divergence.

Guggenheim (1945) has shown that most simple gases obey a law of corresponding states. This suggests that the values of the critical indices listed above should be valid for all such gases.

The phase diagram of an idealized ferromagnet is illustrated in Fig. 1.3. There are two phases, an ordered phase represented by the heavy line on the T axis, and a disordered phase represented by the remainder of the diagram. The ordered phase, for which there exists a spontaneous magnetization, occurs only for $H = 0$ and $T < T_C$. The point labelled $X(T=T_C)$ is the ferromagnetic

Fig. 1.3. The phase diagram of a ferromagnet. The point $X(T=T_C, H=0)$ is the ferromagnetic Curie point.



Curie point or critical point.

The critical point phenomena of a ferromagnet can also be explained in terms of the shape of the isotherms (Fig. 1.4). For a given direction of the magnetic field H and temperatures greater than the critical temperature T_C the magnetization is a monotonically increasing function of the field and has finite and continuous derivatives for all values of the field. For $T < T_C$ the isotherms show a discontinuity at $H = 0$, the magnetization tending to the limits $I_+(0)$ and $I_-(0)$ as H tends to zero.

Near the critical point the spontaneous magnetization behaves as

$$I \sim (T_C - T)^\beta, \quad T \rightarrow T_{C-}, \quad H = 0. \quad (1-11)$$

For the insulating ferromagnet EuS (Heller and Benedeck 1965) one finds

$$\beta \approx 0.33 \pm 0.02.$$

The shape of the critical isotherm can be described by

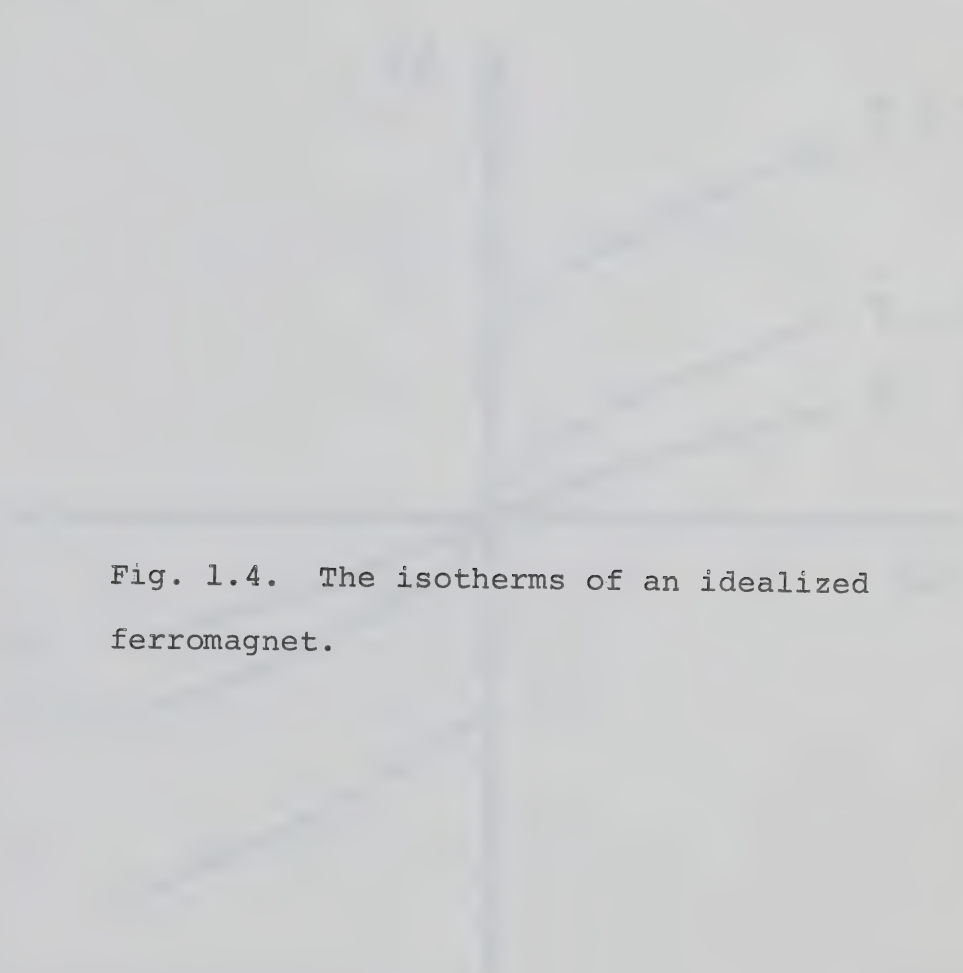
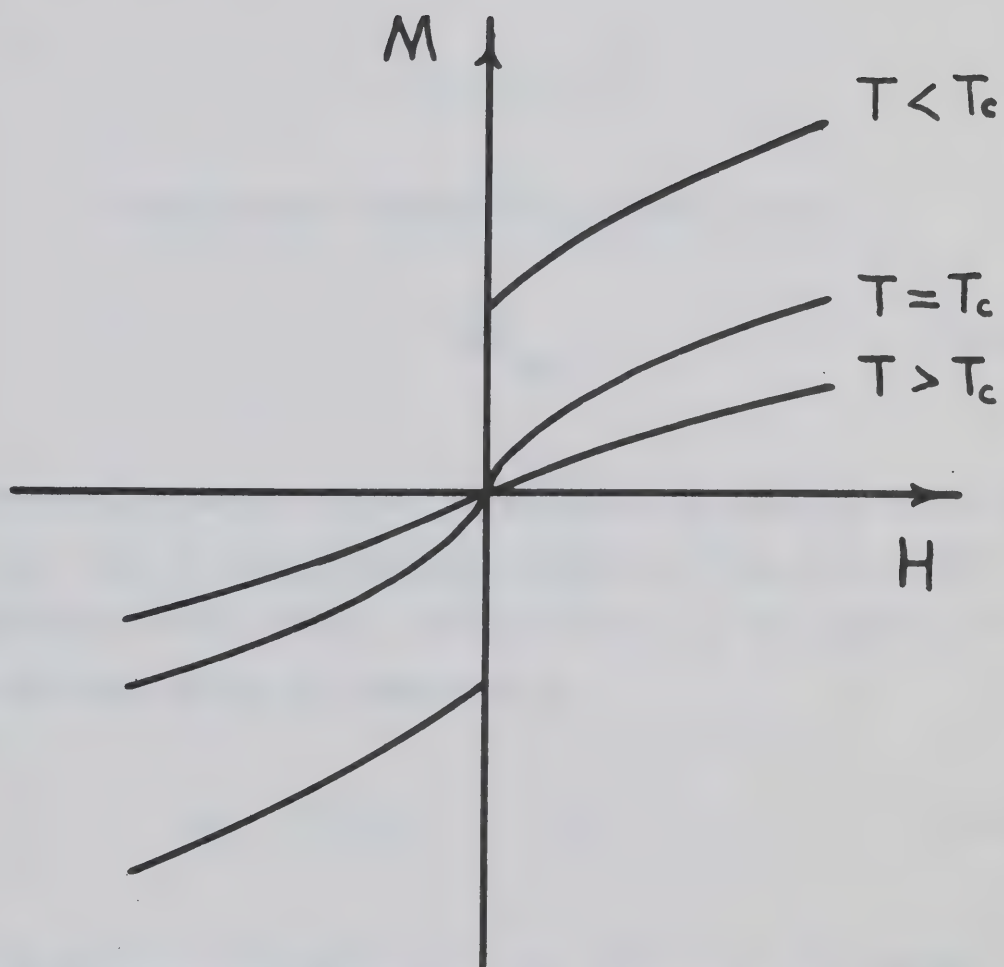


Fig. 1.4. The isotherms of an idealized ferromagnet.



$$|I| \sim |H|^{1/\delta}, \quad T = T_c, \quad H \rightarrow 0. \quad (1-12)$$

Kouvel and Fisher (1964) analyzed some experimental data for nickel and found

$$\delta = 4.2 \pm 0.1.$$

The initial susceptibility defined by

$$\chi_0 = \left(\frac{\partial I}{\partial H} \right)_{H=0} \quad (1-13)$$

increases gradually as the temperature is lowered until at $T = T_c$ and $H = 0$ it becomes infinite (Fig. 1.5). The behaviour of the initial susceptibility in the region of the critical point is described by

$$\chi_0 \sim (T - T_c)^{-\gamma}, \quad T \rightarrow T_{c+}, \quad H = 0. \quad (1-14)$$

A very accurate experiment on Fe (Noakes et al. 1966) indicates

$$\gamma = 1.333 \pm 0.015.$$


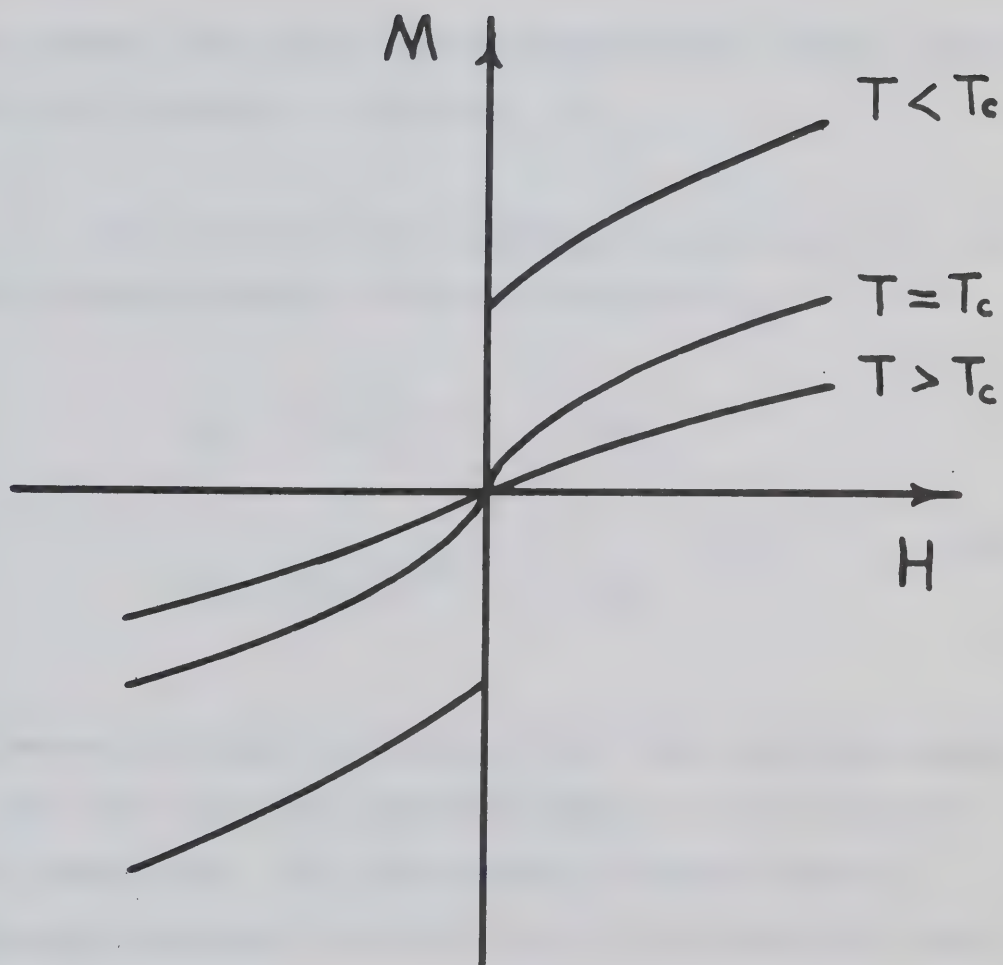


Fig. 1.5. The spontaneous magnetization and initial susceptibility of a ferromagnet.



One would expect similar behaviour for the initial susceptibility below T_c

$$\chi \sim (T_c - T)^{-\gamma'}, \quad T \rightarrow T_{c-}, \quad H = 0. \quad (1-15)$$

At the present time there are no experimental results which enable one to predict a value for γ' .

The critical point behaviour of the specific heat C_H at constant magnetic field is described by

$$\begin{aligned} C_H &\sim (T - T_c)^{-\alpha}, \quad T \rightarrow T_{c+}, \\ &H = 0, \quad (1-16) \\ C_H &\sim (T_c - T)^{-\alpha'}, \quad T \rightarrow T_{c-}, \end{aligned}$$

Experiments performed by Teaney (1966) show the ferromagnets EuS and EuO both have magnetic specific heat anomalies of the lambda type. The experimental results are not sufficiently accurate to allow one to fix a definite value for α and α' . All that can be said is that the results are consistent with a logarithmic behaviour or a small non zero value for the critical index.

In simple antiferromagnets the quantity analogous to the spontaneous magnetization of a ferromagnet is the

sublattice magnetization. Experiments performed on the antiferromagnet MnF_2 by Heller and Benedeck (1962) give

$$\beta = 0.335 \pm 0.005.$$

Teaney (1965) has made accurate measurements of the specific heat of the antiferromagnetic MnF_2 . The behaviour of the specific heat in the critical region (Kadanoff et al. 1967) is consistent with

$$C_H \sim (T - T_C)^{-\alpha}, \quad T \rightarrow T_{C+},$$

$$H = 0, \quad (1-17)$$

$$C_H \sim (T_C - T)^{-\alpha'}, \quad T \rightarrow T_{C-},$$

where

$$0 \leq \alpha \leq 0.16,$$

$$0 \leq \alpha' \leq 0.18.$$

In order to have a critical isotherm and susceptibility of an antiferromagnet analogous to those of a ferromagnet it is necessary to place the antiferro-

magnet in a staggered field, a field which points in opposite directions for neighbouring spins. There is no known way of realizing such a field experimentally, hence there is no direct experimental analogue between the critical isotherm and susceptibility of a ferromagnet and antiferromagnet.

Many binary fluid mixtures exhibit a critical temperature below which the fluid separates into two phases. One can define a coexistence curve analogous to that of a gas-liquid system. Some recent accurate measurements on mixtures of C Cl_4 and $n - \text{C}_7\text{F}_{16}$ (Thompson and Rice 1964) indicate that the index β describing the shape of the coexistence curve in the critical region is given by

$$\beta \approx 0.34 \pm 0.02 .$$

One other type of transition which we shall mention here is the order-disorder transition in a binary alloy. A binary alloy in which like atoms attract unlike atoms is analogous to an antiferromagnet. The quantity analogous to the sublattice magnetization is the order parameter. A very accurate experiment has been performed on very pure beta brass (Als-Neilsen and Deitrich 1967).

An analysis of the experimental data suggest

$$\beta = 0.305 \pm 0.005 .$$

The behaviour of the diffuse scattering at the superlattice peak was also investigated. This provides information on the analogue of the staggered susceptibility. The results showed

$$\gamma = 1.25 \pm 0.02 .$$

In light of the results for β and γ found from our work on the Ising model the above results for beta brass are perhaps the most significant of all the experimental results we have quoted.

The experimental evidence we have cited is summarized in Table 1.1. The values of the critical indices suggest that phenomena associated with critical points are very general and display only a very weak dependence on a particular type of system, i.e. magnetic, gas-liquid, etc. Thus it should seem quite reasonable to seek expressions relating the critical indices to one another. Using rigorous thermodynamic arguments, the relation between the specific heat at constant field C_H

TABLE 1.1

Experimental values for critical indices

Index	Gas-Liquid	Ferromagnet	Anti-ferromagnet	Binary Liquid	Binary Alloy
α	$0 \leq \alpha \leq 0.4$	$\alpha \geq 0$	$0 \leq \alpha \leq 0.16$		
γ	1.35	1.333			1.25
δ	4.2	4.2			
α'	$0 \leq \alpha' \leq 0.25$	$\alpha' \geq 0$	$0 \leq \alpha' \leq 0.18$		
β	0.345	0.33	0.335	0.34	0.305
γ'	1.1				

and the specific heat at constant magnetization C_M and the fact that C_M is non-negative, Rushbrooke (1963) derived the inequality

$$\alpha' + 2\beta + \gamma' \geq 2 . \quad (1-18)$$

Griffiths (1965) gave a rigorous derivation, based on the convexity properties of the free energy, of the inequality

$$\alpha' + \beta(1+\delta) \geq 0 . \quad (1-19)$$

A non-rigorous theory has recently been developed (Widom 1965, Kadanoff 1966, Kadanoff et al. 1967), which enables all of the critical indices to be expressed in terms of two fundamental indices. The theory (scaling law theory) predicts that the inequalities in (1-18) and (1-19) are replaced by equalities and that corresponding indices above and below the critical point are equal, i.e.

$$\left. \begin{aligned} \alpha' + 2\beta + \gamma' &= 2 \\ \alpha' + \beta(\delta+1) &= 2 \\ \alpha &= \alpha' \\ \gamma &= \gamma' \end{aligned} \right\} . \quad (1-20)$$

The experimental values for the set of critical indices describing the critical point behaviour of real systems are not known to sufficient accuracy to enable one to draw a definite conclusion on the validity of the scaling law hypothesis which leads to (1-20). The critical indices of the mean field theory and also those of the two dimensional Ising model satisfy (1-20). However, numerical investigations indicate (1-20) does not hold for the three dimensional Ising model (see Table 1.2). We shall have more to say about equations (1-18), (1-19), and (1-20) in Chapter VIII.

Several attempts have been made towards a theoretical description of the experimental facts as outlined above. The first of these were of a phenomenological nature, the **Van** der Waals theory of the gas-liquid critical point and the Weiss theory of ferromagnetism, which are now commonly known as mean field theories. The predictions of the mean field theories disagree both qualitatively and quantitatively with the results of experiment.

An explanation based on a statistical mechanical approach did not come until much later with the advent of the Ising (1925) and Heisenberg (1928) models of ferromagnetism.

TABLE 1.2

Critical indices for mean field theories (M.F.T.) and Ising models
previous to present investigation.

Index	M. F. T.	Ising model, 2-dimensions	Ising model, 3-dimensions
α	(0) discontinuity	(0) log	0.125 (b)
γ	1	$7/4$	1.250 (c)
δ	3	15.00 (a)	5.20 (a)
α'	(0) discontinuity	(0) log	0.066 (d)
β	$1/2$	$1/8$	0.312 (d)
γ'	1	$7/4$	1.310 (d)
<hr/>			
(a)	Gaunt et al. 1964)	(c) (Domb and Sykes 1961)	
(b)	(Sykes, Martin, Hunter 1967)	(d) (Baker and Gaunt 1967)	

Theoretical investigations of the Ising and Heisenberg models have shown these two models, or modifications thereof, are capable of explaining much of the observed critical point behaviour in real systems. Our work concentrates on the Ising model of a ferromagnet, so we will review in the next section the development of the Ising model from 1925 to the present.

B. The Ising Model

What has now come to be known as the Ising model was first proposed as a model of ferromagnetism in 1920 to Ernst Ising by his supervisor W. Lenz (Brush 1967). The Ising model represented the first attempt to give a statistical mechanical interpretation to the phenomena of ferromagnetism.

The classical Ising model of a ferromagnet associates with each site of a crystal lattice a spin (magnetic moment m) which can point in two directions, "up" and "down", relative to an external magnetic field H . The two states of the i th spin are usually described by the variable $\sigma_i = +1$ for "spin up" and $\sigma_i = -1$ for "spin down". In addition to the energy of interaction ($-mH\sigma_i$) of the magnetic moment with the magnetic field, there is also assumed to exist an interaction between neighbouring spins, $-J$ if the two spins point in the same direction and J if they point in opposite directions, where J is a positive constant. The energy of the system is given by

$$E = -J \sum_{\langle i,j \rangle} \sigma_i \sigma_j - mH \sum_i \sigma_i \quad (1-21)$$

where $\langle i,j \rangle$ indicates the first sum is over nearest neighbours only. Equation (1-21) can be taken as the

definition of the classical Ising model. Having defined the energy the next step is to calculate (in principal at least) the partition function from which the thermodynamic quantities of interest can be obtained in a straight forward manner. The greater part of this thesis is concerned with just such a calculation for a triple of related three dimensional lattices on which the Ising model (1.21) has not previously been studied.

Interest in the Ising model is primarily of a pedagogical nature as it is one of the few many body problems that has proven exactly soluble, others being a class of two dimensional problems (the ice problem, KDP model of a ferroelectric, and F model of an antiferroelectric), which have been solved by Lieb (1967(a), (b), (c)), and the one dimensional Van der Waals gas, which has been solved exactly (Kac et al. 1963). Despite the fact the expression for the energy (1-21) is extremely simple, studies of the Ising model have shown that the simple nearest neighbour interaction between spins is the essential ingredient in explaining the existence and behaviour of ferromagnetic systems near their critical points.

Use of the Ising model is not restricted to a study of ferromagnets only. The model can serve as an equally valid description of an antiferromagnet upon

replacing J by $-J$, as a model for liquid-gas condensation; the lattice gas (Yang and Lee 1952); and as a model for binary alloys and liquids as well.

Though as we have pointed out in the previous paragraph the great pedagogical interest in the Ising model stems from the fact it serves as a prototype for many different types of cooperative phenomena, there is experimental justification for studying such a model as well. For those insulating ferromagnets and antiferromagnets exhibiting a large anisotropy in the g factor ($g_{\parallel} > g_{\perp}$) the Ising model provides a more valid description than the Heisenberg model which applies only to isotropic systems. Recent experimental evidence (Als-Neilsen and Deitrich 1967) suggests the Ising model can provide a valid description of a binary alloy.

Ising (1925) was able to solve the model exactly in one dimension for all temperatures and all values of the magnetic field by a straight forward combinatorial approach. The one dimensional model did not exhibit a phase transition for $T > 0$. However, at $T = 0$, the susceptibility becomes exponentially infinite, indicating the onset of a spontaneous magnetization. In this sense the one dimensional model can be said to have a critical point at $T = 0$. As a result of his studies, Ising erroneously concluded that the two

dimensional model would also fail to exhibit ferromagnetic properties. Ising had failed to appreciate the importance of correlations between spins in two or more directions.

The first convincing argument that the two dimensional model would exhibit ferromagnetic properties was given by Peierls (1936). The first exact results for the two dimensional Ising model were obtained by Krammers and Wannier (1941) who discovered a certain symmetry property between the high and low temperature partition functions for the square lattice which enabled them to locate the position of the critical point exactly if it existed. An exact closed form expression for the zero field partition function for the rectangular lattice was first given in the classic paper of Onsager (1944), where he showed that the specific heat was logarithmically infinite on both sides of the critical point.

Onsager (see Wannier, 1945) was also able to shed light on the reason for the symmetry property first observed by Krammers and Wannier. Onsager pointed out that the observed symmetry was unique to two dimensional lattices and could be given a topological explanation based on the fact that two dimensional lattices are planar and therefore dual lattices (Ore 1963) can be constructed from them. The square lattice is self dual, the reason that Krammers and

Wannier were able to locate the critical point exactly.

In 1948 Onsager (see Onsager 1949) enunciated his famous result for the spontaneous magnetization of the rectangular lattice

$$I = [1 - (\sinh 2K_x \sinh 2K_y)^{-2}]^{1/8}, \quad (1-22)$$

where

$$K_x = J_x/kT, \quad (1-23)$$

$$K_y = J_y/kT.$$

The derivation of this result has never been published by Onsager, only quoted in the above reference. The first published derivation of (1-22) was given by Yang (1952). Following the work of Onsager and Yang exact expressions for the zero field partition function and spontaneous magnetization for several other two dimensional lattices were obtained. The results, however, were of the same general form as those for the square lattice, the critical indices in fact were found to be the same for all two dimensional lattices.

To this date no exact expression has been obtained for the partition function of the two dimensional Ising model in a non zero field, and hence no exact expression has been obtained for the initial susceptibility. By examining the relationship between the correlations for pairs of spins and the initial susceptibility Fisher (1959(a)) was able to show in a semirigorous manner that near the critical point the initial susceptibility behaved as

$$\chi_0 \approx C(1 - T_c/T)^{-1/4}, \quad T \rightarrow T_{c+}, H=0. \quad (1-24)$$

The three dimensional Ising model has so far resisted all efforts to obtain an exact solution, in fact an exact result of any kind has yet to be found. The only rigorous results obtained so far for the three dimensional Ising model are those of Griffiths (1964-67) which show that the three dimensional Ising model does indeed undergo a transition.

In the absence of any exact analytical results for the three dimensional Ising model, most efforts at elucidating the behaviour of the thermodynamic functions in the critical region have been limited to two alternative methods, improved closed form approximations and exact series expansions.

In order to construct a closed form approximation it is necessary to neglect some of the statistical mechanical details of the problem so that the partition function can be summed. The disadvantage of this approach is that the details which one is forced to neglect are usually all important. Hence one simply reproduces the already well known mean field results which predict the wrong type of behaviour, both qualitatively and quantitatively, in the critical region.

Our approach to the Ising model in this thesis is that of exact series expansions, the coefficients of the series being known exactly as far as they go. The method involves an exact calculation of the leading terms (usually the first ten to twenty terms) of the power series expansion of the thermodynamic quantity of interest. One then attempts to estimate the critical parameters by employing suitable numerical techniques. The method has been tested on the two dimensional model and it has proven capable of giving excellent estimates of the critical parameters, many of which are known exactly. The impetus for this method was provided by Domb, Sykes, Fisher and their colleagues at Kings College, London. As a result of their efforts and those of others who have utilized this method a considerable amount of numerical information has been compiled on the

behaviour of the three dimensional Ising model in the region of the critical point (see Table 1.2).

For example, in the region just above the critical point it is now fairly well established that the initial ferromagnetic susceptibility behaves as

$$\chi_0 \approx C_+(1-T_c/T)^{-5/4}, \quad T \rightarrow T_{c+}, \quad H=0. \quad (1-25)$$

There is also strong evidence to suggest that the specific heat singularity above T_c is not logarithmic. The work of Sykes, Martin, and Hunter (1967) suggest that near T_c the specific heat behaves as

$$C_H \approx A_+(1-T_c/T)^{-1/8}, \quad T \rightarrow T_{c+}, \quad H=0. \quad (1-26)$$

On the low temperature side of T_c the values of the critical indices are much less certain. Probably the best previous estimates of the low temperature critical indices have been given by Baker and Gaunt (1967). They find

$$\left. \begin{aligned} \beta &\approx 0.312^{+0.003}_{-0.006} \\ \gamma' &\approx 1.310^{+0.030}_{-0.050} \\ \alpha' &\approx 0.066^{+0.160}_{-0.040} \end{aligned} \right\} . \quad (1-27)$$

The primary purpose of this research has been to obtain improved estimates of the low temperature critical indices. Such information is not only desirable from the standpoint of making a comparison with experiment but it can also serve as a guide to the validity of the scaling law hypothesis (Widom 1965, Kadanoff 1966, Kadanoff et al. 1967).

C. Scope of this Thesis.

The structure of the three dimensional lattices on which we have applied the Ising model is discussed in Chapter II. The derivation of high temperature series expansions for the zero field partition function and initial susceptibility is outlined in Chapter III. The derivation of the low temperature series expansion for the partition function is discussed in Chapter IV. In Chapter V we review some well known Ising model transformations which are applicable to the lattices we have worked with. The self-avoiding walk problem, its relationship to the Ising model and the derivation of the corresponding series expansions, is discussed in Chapter VI. Numerical methods utilized to obtain estimates of critical parameters are outlined in Chapter VII. A review and discussion of the results of this research project appear in Chapter VIII.

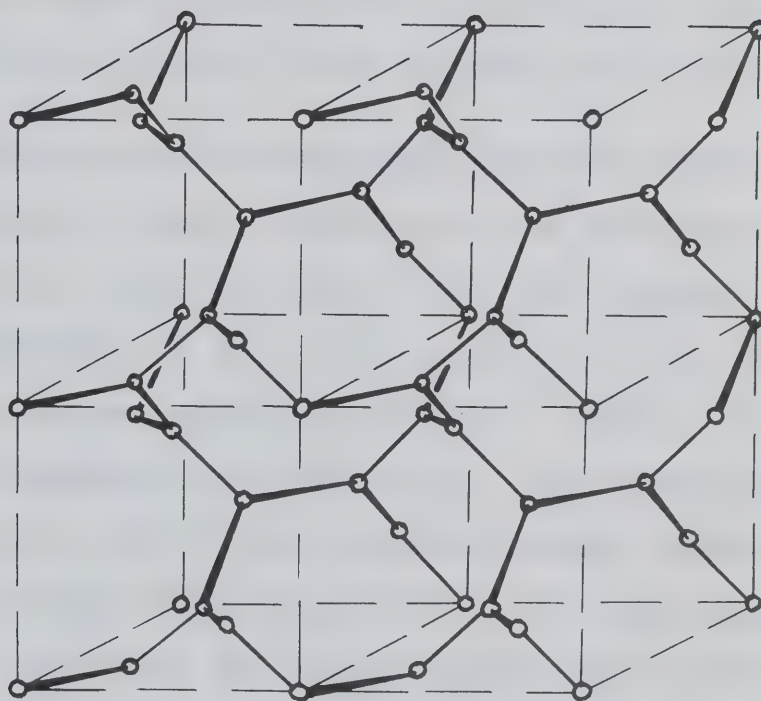
CHAPTER II

THE HYDROGEN PEROXIDE, HYPERTRIANGULAR, AND
HYPERKAGOMÉ LATTICES

Prior to the work reported on in this thesis, most investigations of the three dimensional Ising model have been confined to five regular lattices, the face centered cubic, body centered cubic, simple cubic, cristobalite, and diamond, having coordination numbers 12, 8, 6, 6, and 4 respectively. By a regular lattice we mean one which can be superimposed on itself by a combination of translation and improper rotation in such a way that any point can be superimposed on any other point and any bond can be superimposed on any other bond. In other words, in a regular lattice all points and all bonds are equivalent.

The lattice of primary importance in this investigation is an idealized hydrogen peroxide lattice (Fig. 2.1). This lattice was first reported on in the literature by Heesch and Laves (1933) and a detailed description of this and other similar lattices appears in Wells (1954). This lattice belongs to the cubic system and has the space group $O^8(I4_32)$ (Henry and Lonsdale 1952). The lattice is not centrosymmetric and so can occur in "left-handed" and "right-handed" forms. The lattice consists of four interpenetrating

Fig. 2.1. The hydrogen peroxide lattice.



body centered cubic lattices (Fig. 2.2) and so has four atoms per unit cell. A coordinate system can be chosen such that the atoms in a cubic unit cell have coordinates $(0,0,0)$; $(1/4,1/4,0)$; $(1/2,1/4,1/4)$; $(3/4,0,1/4)$; $(0,3/4,3/4)$; $(1/4,1/2,3/4)$; $(1/2,1/2,1/2)$; $(3/4,3/4,1/2)$ (Fig. 2.3). Idealized crystalline hydrogen peroxide is the only known substance to have such a structure (Wells, private communication), hence the name of the lattice. The hydrogen peroxide lattice may be constructed by picking out one quarter of the lattice points of a face centered cubic lattice.

Real crystalline hydrogen peroxide differs from our ideal model in that it belongs to the tetragonal system (Abrahams et al. 1951) instead of the cubic system. The lattice parameters are $a = 4.06$ Å and $b = 8.00$ Å. The corresponding space group is $D_4^h(P4_12_12)$ (Henry and Lonsdale 1952), enantiomorphous with $D_4^8(P_432_12)$. The oxygen-oxygen bond distance is 1.49 Å, the distance between oxygen atoms across the hydrogen bond being 2.78 Å. The angle made by the hydrogen bond with the oxygen-oxygen bond is 97° and the azimuthal angle between planes containing the hydrogen bonds and the oxygen-oxygen bond is 94° (Fig. 2.4). The hydrogen bonds form a four fold infinite helix in a plane perpendicular to the c-axis (Fig. 2.5). On the basis of

Fig. 2.2. . The four interpenetrating body centered cubic lattices which make up the hydrogen peroxide lattice.

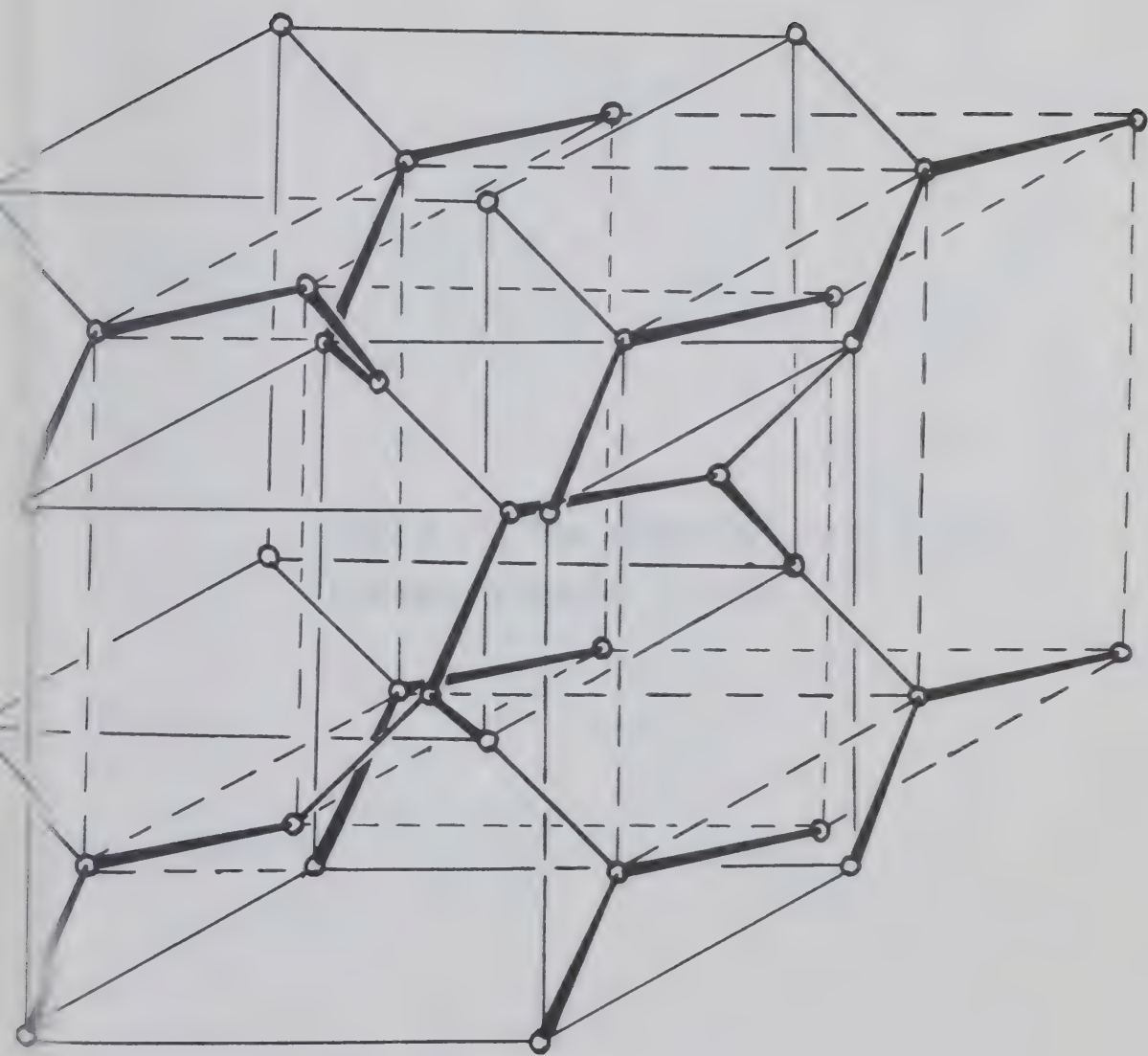
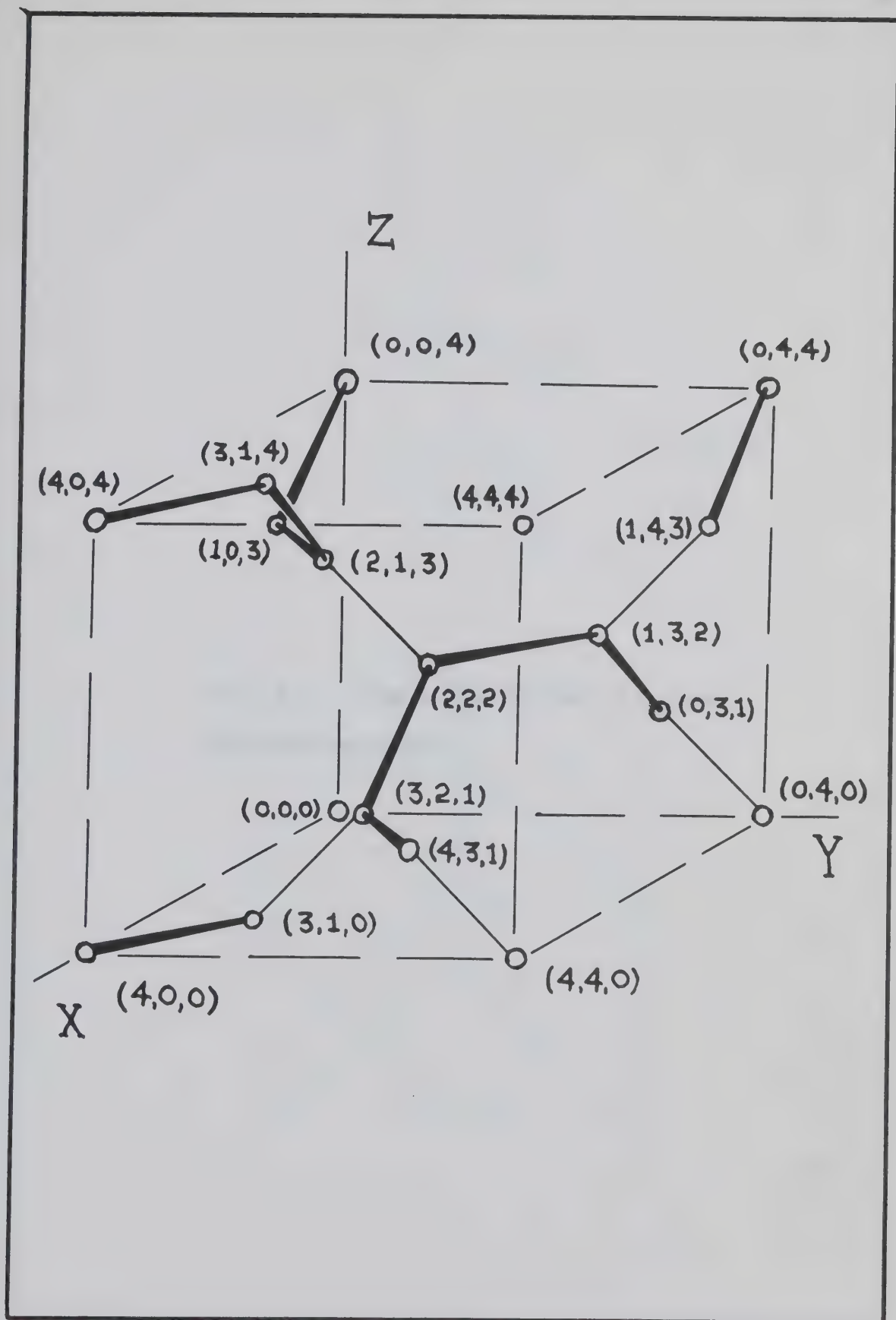


Fig. 2.3. The cubic unit cell of the hydrogen peroxide lattice.





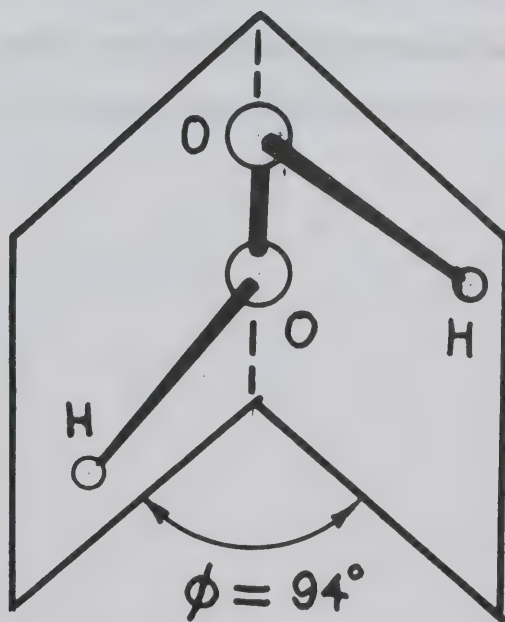
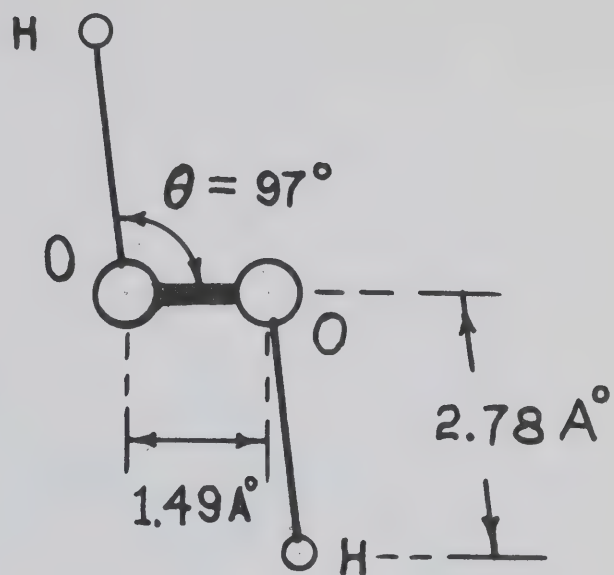


Fig. 2.4. The shape of the hydrogen peroxide molecule.





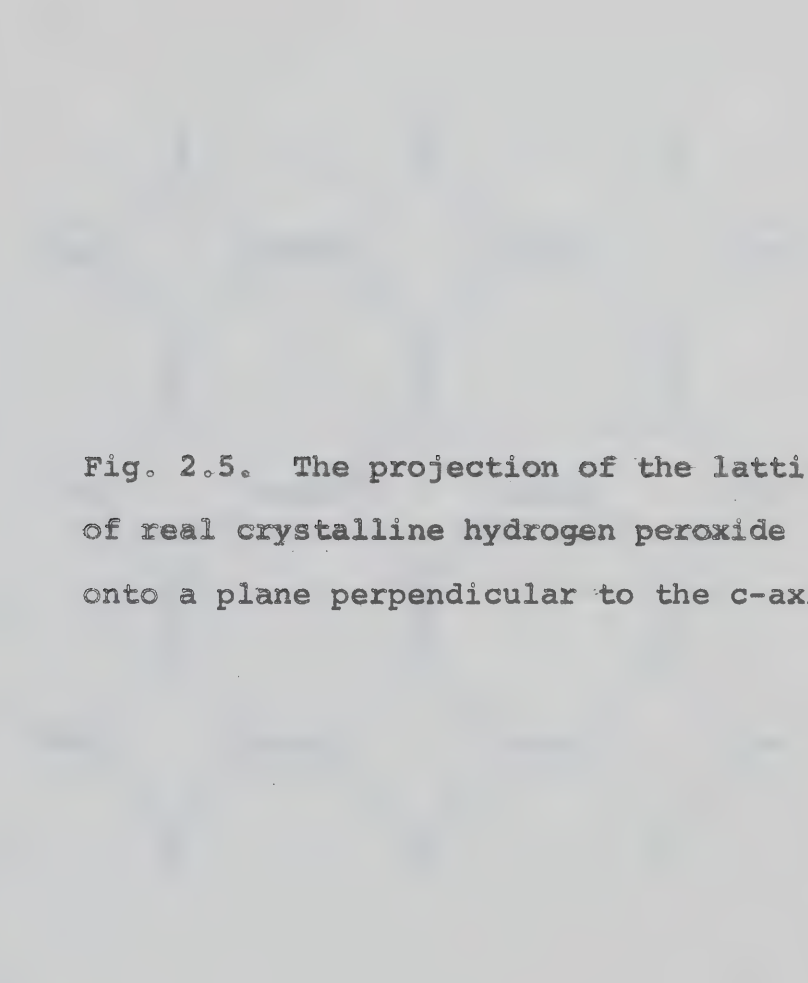
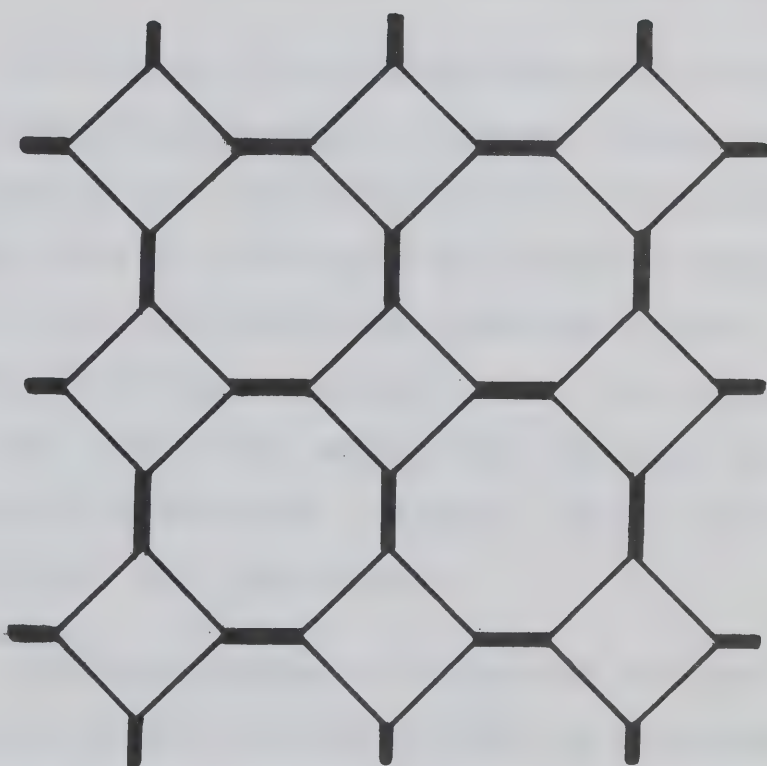


Fig. 2.5. The projection of the lattice
of real crystalline hydrogen peroxide
onto a plane perpendicular to the c-axis.



the structure outlined above, it was concluded (Abrahams et al. 1951) that crystalline hydrogen peroxide has no measurable entropy at absolute zero. For those interested in a more detailed description of hydrogen peroxide, from its discovery to the present, one may refer to the lengthy treatise by Schumb, Satterfield, and Wentworth (1955).

In studies of the three dimensional Ising model, the hydrogen peroxide lattice occupies a unique position. It is a lattice with the lowest possible coordination number ($q=3$) and it can be looked upon as the three dimensional analogue of the two dimensional honeycomb lattice. Furthermore, from the hydrogen peroxide lattice it is possible to construct two other three dimensional lattices, the hypertriangular and hyperkagomé lattices, having coordination numbers six and four respectively.

The hypertriangular lattice can be formed from the hydrogen peroxide lattice by first bi-colouring the sites of the hydrogen peroxide lattice (Fig. 2.6) followed by a removal of all sites belonging to one of the two given colours. The remaining sites form what we call the hypertriangular lattice (Fig. 2.7). The hypertriangular lattice serves as a three dimensional analogue of the two dimensional triangular lattice.

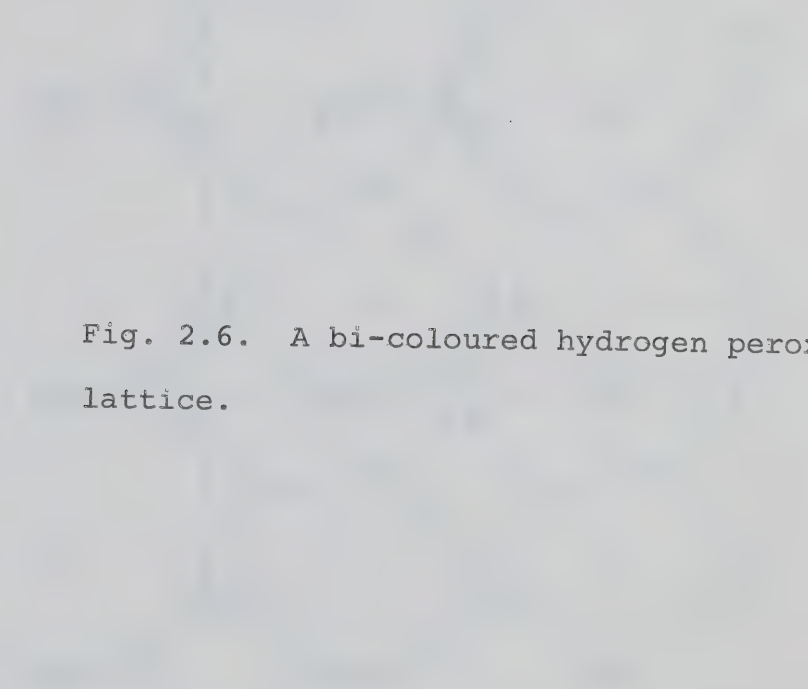


Fig. 2.6. A bi-coloured hydrogen peroxide lattice.

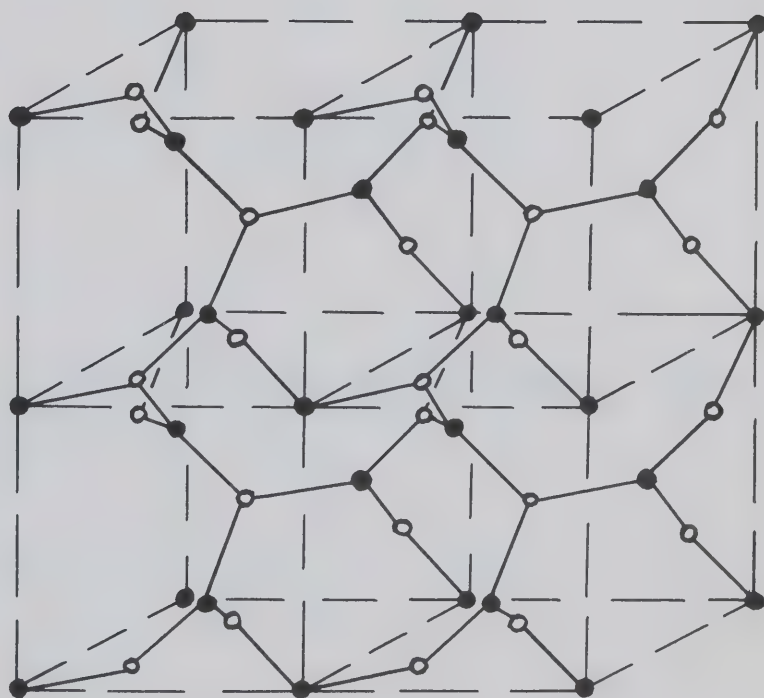
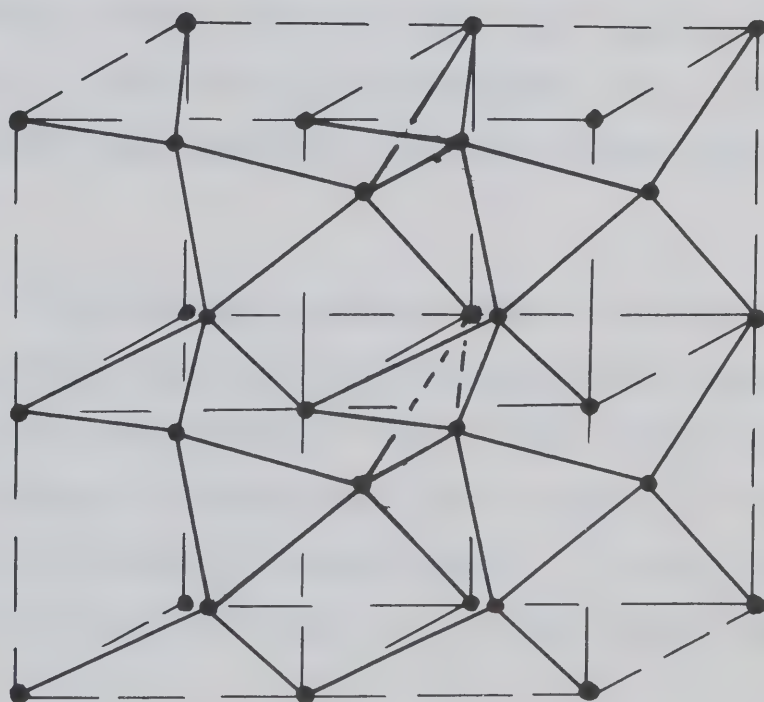


Fig. 2.7. The hypertriangular lattice.



The hyperkagomé lattice can be constructed from the hydrogen peroxide lattice in the following manner. At the mid point of each bond of the hydrogen peroxide lattice we place a new lattice site, thus forming a decorated hydrogen peroxide lattice (Fig. 2.8). These new lattice sites are then connected together and the original hydrogen peroxide sites are removed. The remaining lattice of coordination number four is called the hyperkagomé lattice (Fig. 2.9). This lattice can be looked upon as being a three dimensional analogue of the two dimensional kagomé lattice.

The hydrogen peroxide lattice is a loose packed lattice whereas both the hypertriangular and hyperkagomé lattices are close packed. By a loose packed lattice we mean a lattice in which there are no circuits (loops) made up of an odd number of bonds (edges). A close packed lattice has loops with both an even and an odd number of edges.

One may be inclined to ask the following question, namely, why study the hydrogen peroxide lattice since it would seem to be of little direct experimental interest? The hydrogen peroxide lattice, as we have already pointed out, occupies a unique position in studies of the three dimensional Ising model. Because of its low coordination

Fig. 2.8. The decorated hydrogen peroxide lattice.

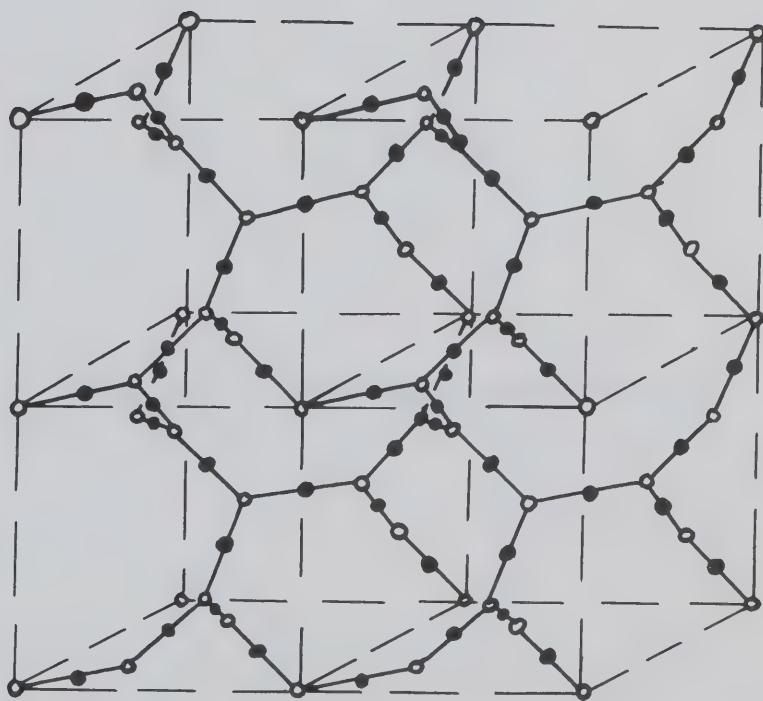
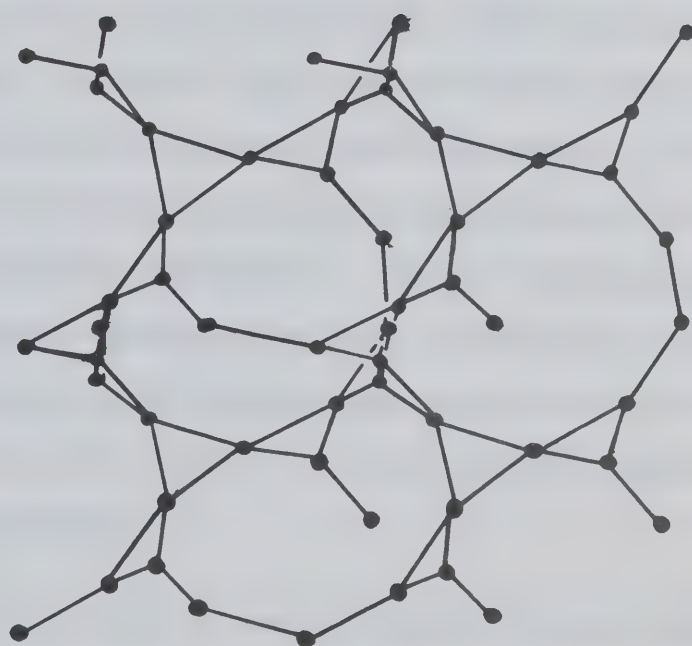


Fig. 2.9. The hyperkagomé lattice.



number, the coefficient of the low temperature series expansions for the Ising model on the hydrogen-peroxide lattice are all of the same sign, a fact which tends to make the lattice more suitable for study than lattices of higher coordination number. A notable exception of course being the diamond lattice with a coordination number of four (Essam and Sykes 1963). The low coordination number of the hydrogen peroxide lattice also gives rise to a considerable simplification in the configurational counting problem which arises in the derivation of high temperature series expansions for the Ising model. Another reason for studying such a lattice is that the hydrogen peroxide, hypertriangular, and hyperkagomé lattices are all related by certain well known transformations, which are described in Chapter V. These transformations serve as a valuable check as to the correctness of the underlying counting problem and they also provide an independent means of checking the results of the numerical analysis of the series expansions.

The behaviour of the spontaneous magnetization, initial susceptibility, and zero field specific heat can all be interpreted in terms of their corresponding correlation functions (see Kadanoff et al. 1967). For example, the initial susceptibility can be formulated in terms of a sum over spin-spin correlation functions. As the critical point is approached,

the range of correlation grows, becoming infinite at the critical point, with the result that the susceptibility becomes infinite at the critical point. This divergence in the range of correlation is the precise cause of this and all other singularities in the thermodynamic derivatives. Since one expects the long range correlations to be independent of all but the grossest features of the interaction, a change in the behaviour of the long range correlations from one lattice to another of the same dimensionality is not expected. In fact the solutions for the two dimensional Ising model bear this out, the correlations for the square and triangular lattices being basically the same. In three dimensions as far as one can tell, the critical indices are also lattice independent. Hence, our numerical estimates of the critical indices for the Ising model on the hydrogen peroxide lattice are also expected to be valid for other three dimensional lattices.

CHAPTER III

HIGH TEMPERATURE SERIES EXPANSIONSA. The Zero Field Partition Function

In this chapter we briefly review some of the standard techniques used to derive high temperature series expansions. A thorough review of the various methods of deriving high temperature series expansions for the Ising model has been given by Domb (1960). It is not the intention of the author to give a lengthy review of the concepts of graph theory, which are widely used in deriving the expansions we are seeking. The reader unfamiliar with such concepts should refer to Domb (1960) or Sykes, Essam, Heap, and Hiley (1966).

The energy of the spin one-half Ising model with nearest neighbour interactions only can be written in the form (c.f. Chap. I, eq'n. (1-21)),

$$E = -J \sum_{\langle i,j \rangle} \sigma_i \sigma_j - m H \sum_i \sigma_i, \quad (3-1)$$

where J is the interaction energy between neighbouring sites, m is the magnetic moment, and H is the external magnetic field. The σ variables take the values ± 1 according to

whether the magnetic moment is parallel or antiparallel to the magnetic field.

The thermodynamics of the Ising model are computed from the partition function, which for a regular lattice of N sites takes the form

$$Z_N(\beta, H) = \sum_{\sigma_1=\pm 1, \dots, \sigma_N=\pm 1} \exp \beta [J \sum_i \sigma_i \sigma_j + mH \sum_i \sigma_i], \quad (3-2)$$

where $\beta = 1/kT$ and the outermost sum is over the 2^N possible values of the σ_i for the N lattice sites. Since the σ variables commute (3-2) can be written as a product

$$Z_N(\beta, H) = \sum_{\sigma_1=\pm 1, \dots, \sigma_N=\pm 1} \prod_{\langle i, j \rangle} \exp(K \sigma_i \sigma_j) \prod_i \exp(\beta m H \sigma_i), \quad (3-3)$$

where $K = \beta J/kT$. The $\sigma_i \sigma_j$ satisfy the following relations,

$$\left. \begin{aligned} (\sigma_i \sigma_j)^2 &= (\sigma_i \sigma_j)^4 = (\sigma_i \sigma_j)^6 = \dots = 1 \\ (\sigma_i \sigma_j) &= (\sigma_i \sigma_j)^3 = (\sigma_i \sigma_j)^5 = \dots \end{aligned} \right\} \quad (3-4)$$

Hence we can write

$$\exp(K \sigma_i \sigma_j) = \cosh K + \sigma_i \sigma_j \sinh K. \quad (3-5)$$

Equation (3-5) is the well known Van der Waerden identity (Van der Waerden 1941). The first product in (3-3) can now be written as

$$\begin{aligned}
\prod_{\langle i,j \rangle} (\cosh K + \sigma_i \sigma_j \sinh K) &= \prod_{\langle i,j \rangle} \cosh K (1 + \sigma_i \sigma_j \tanh K) \\
&= (\cosh K)^{qN/2} \sum_{i,j,\dots} [1 + (\sigma_i \sigma_j) \tanh K \\
&\quad + (\sigma_i \sigma_j) (\sigma_k \sigma_l) \tanh^2 K + \dots],
\end{aligned}
\tag{3-6}$$

where $qN/2$ is the number of nearest neighbour bonds in the lattice. Setting $H=0$, the second factor in (3-3) becomes equal to unity and the zero field partition function is given by

$$\begin{aligned}
Z_N(\beta, 0) &= (\cosh K)^{qN/2} \sum_{\sigma_1=1, \dots, \sigma_N=\pm 1} \sum_{i,j,\dots} [1 + (\sigma_i \sigma_j) \tanh K \\
&\quad + (\sigma_i \sigma_j) (\sigma_k \sigma_l) \tanh^2 K + \dots].
\end{aligned}
\tag{3-7}$$

We can now give a graph theoretical interpretation to (3-7). The only terms in (3-7) that will give a non-zero contribution are those which contain the σ_i 's to an even power as the sum over states will cancel all terms which contain a σ_i to an odd power. With each $(\sigma_i \sigma_j)$ we associate a nearest neighbour bond (an edge of a graph) of the lattice, and since only even powers of the σ_i can occur in a given term, an even number of edges must meet at the i th vertex, or in the terminology of graph theory each vertex is of even degree. Thus with each term of (3-7) we can associate one

or more graphs, whose vertices are all of even degree. Such graphs, connected and separated, are referred to as non-magnetic graphs.

The partition function can now be written as

$$Z_N(\beta, 0) = 2^N (\cosh K)^{qN/2} \left\{ 1 + \sum_{\ell=1}^{qN/2} p(\ell, N) \tanh^\ell K \right\}, \quad (3-8)$$

where $p(\ell, N)$ denotes the total number of ways of constructing (embedding) in a given lattice all graphs of ℓ lines whose vertices are all of even degree. The $p(\ell, N)$ are in general polynomials of degree ℓ in N , hence the notation. 2^N in (3-8) arises when we perform the sum over states.

The procedure outlined in the preceding paragraphs is perhaps best illustrated by means of an example. The first six $p(\ell, N)$ for the hypertriangular lattice are shown in Table 3.1

In Table 3.1 we have enclosed in parenthesis those graphs contributing to a given $p(\ell, N)$. This notation denotes the number of such graphs per lattice site and is commonly referred to as the lattice constant for a given graph.

Instead of (3-8) what we are really interested in is the dimensionless Helmholtz free energy per site defined

TABLE 3.1

The first six coefficients in the power series expansion for the zero field partition function of the hypertriangular lattice.

$p(1,N)$	$= 0$	$p(4,N)$	$= 0$
$p(2,N)$	$= 0$	$p(5,N)$	$= N \left(\text{pentagon} \right)$
$p(3,N)$	$= N \left(\triangle \right)$		$= 3N$
	$= N$	$p(6,N)$	$= N \left(\text{hexagon} \right) + N \left(\text{bowtie} \right)$
			$+ N \left(\triangle \triangle \right)$
			$= 1/2 N^2 + 14 1/2 N$

TABLE 3.2

The first four coefficients, calculated by the direct method, in the susceptibility series for the hypertriangular lattice.

$b_1 = \left(\diagup \right) = 3$	$b_3 = \left(\diagup \diagdown \right) = 72$
$b_2 = \left(\wedge \right) = 15$	$b_4 = \left(\wedge \wedge \right) + \left(\text{trident} \right)$
	$+ \left(\triangle \diagup \right)$
	$= 345$

by

$$-f/kT = \lim_{N \rightarrow \infty} \{\ln Z_N(\beta, 0)\}/N. \quad (3-9)$$

Hence

$$\begin{aligned} -f/kT = \ln 2 + (q/2) \ln (\cosh K) \\ + \lim_{N \rightarrow \infty} \{\ln [1 + \sum_{\ell=1}^{qN/2} p(\ell, N) v^\ell]\}/N, \end{aligned} \quad (3-10)$$

where $v = \tanh K$. It is customary to denote the logarithm of the configurational partition function per site by $\ln \Lambda$, i. e.

$$\ln \Lambda = \{\ln [1 + \sum_{\ell=1}^{qN/2} p(\ell, N) v^\ell]\}/N, \quad (3-11)$$

hence

$$-f/kT = \ln 2 + (q/2) \ln (\cosh K) + \lim_{N \rightarrow \infty} \ln \Lambda. \quad (3-12)$$

Upon formally working out the logarithm in (3-11) one finds

$$\ln \Lambda = \sum_{\ell=1}^{qN/2} p_{\ell}^{(1)} v^\ell, \quad (3-13)$$

where $p_{\ell}^{(1)}$ is just the coefficient of N in $p(\ell, N)$.

For example, for the hypertriangular lattice we have (c. f. Table 3.1)

$$\ln \Lambda = \frac{1}{N} \ln [1 + p(3, N)v^3 + p(5, N)v^5 + p(6, N)v^6 + \dots]. \quad (3-14)$$

Expressing $(\Delta \Delta)$ in terms of connected lattice constants (see Appendix C, page 162) and expanding the logarithm on the right-hand side of (3-19) we have

$$\begin{aligned} \ln \Lambda &= \frac{1}{N} \{ N(\Delta)v^3 + N(\text{pentagon})v^5 + [\frac{1}{2}N^2(\Delta)^2 + N(\text{hexagon}) - \frac{1}{2}N(\Delta)]v^6 \\ &\quad - [N^2(\Delta)^2v^6 + \dots]/2 + \dots \} \\ &= (\Delta)v^3 + (\text{pentagon})v^5 + [(\text{hexagon}) - \frac{1}{2}(\Delta)]v^6 + \dots \\ &= p_3^{(1)}v^3 + p_5^{(1)}v^5 + p_6^{(1)}v^6 + \dots \end{aligned} \quad (3-15)$$

The coefficients in (3-15) are all linear in configurational lattice constants and no configurations with cutting points enter, a result which exactly parallels the Mayer theory of cluster integral expansions in the theory of imperfect gases. A rigorous derivation of the cluster expansion method as applied to lattice statistical problems has been given by Sykes et al. (1966).

The reason we must stipulate $N \rightarrow \infty$ is that if we do not, the partition function will just be a finite polynomial, which is everywhere analytic and hence would show no singular behaviour. Hence the free energy per site for a regular lattice of coordination number q and N sites in the limit $N \rightarrow \infty$ can be written as

$$(-f/kT) = \ln 2 + (q/2) \ln (\cosh K) + \sum_{\ell=1}^{\infty} p_{\ell}^{(1)} v^{\ell}, \quad (3-16)$$

where we now have

$$\ln \Lambda = \sum_{\ell=1}^{\infty} p_{\ell}^{(1)} v^{\ell}. \quad (3-17)$$

Using the techniques outlined above we have derived the series expansion for the free energy of the hydrogen peroxide lattice up to order twenty-eight and for the hypertriangular lattice up to order fourteen.

The dimensionless free energy per site for the hydrogen peroxide lattice is given by

$$\begin{aligned} (-f/kT) = & \ln 2 + (3/2) \ln (\cosh K) + 1 \frac{1}{2} v^{10} \\ & + 1 \frac{1}{2} v^{14} + 10 \frac{1}{2} v^{16} + 23 \frac{1}{2} v^{18} \\ & + 6 \frac{3}{4} v^{20} + 178 \frac{1}{2} v^{22} + 484 v^{24} \\ & + 774 v^{26} + 3023 \frac{1}{4} v^{28} + \dots, \end{aligned} \quad (3-18)$$

and for the hypertriangular lattice by

$$\begin{aligned} (-f/kT) = & \ln 2 + 3 \ln (\cosh K) + v^3 + 3v^5 + 14 \frac{1}{2} v^6 \\ & + 33v^7 + 57v^8 + 218 \frac{1}{3} v^9 + 961 \frac{1}{2} v^{10} \\ & + 3045v^{11} + 8925 \frac{1}{4} v^{12} + 32676v^{13} \\ & + 129352 \frac{1}{2} v^{14} + \dots. \end{aligned} \quad (3-19)$$

The coefficients of v in (3-19) up to and including v^{12} were calculated by graphical enumeration on the hypertriangular lattice. The last two terms of (3-19) were obtained from (3-18) via the star-triangle transformation as outlined in Chapter V.

The configurational data required to derive the first twelve terms of the zero field partition function and dimensionless free energy for the hypertriangular lattice are given in Appendix A. The only connected graphs which contribute to the first twenty-eight terms of the zero field partition function and dimensionless free energy for the hydrogen peroxide lattice are the p-graphs (polygons) listed in Appendix D, where we have tabulated separately for both lattices the "star" graphs (see Sykes, Essam, Heap, and Hiley 1966), which are required in the calculation of the lattice constants of the separated configurations listed in Appendix C.

The remainder of the thermodynamic functions of interest, with the exception of the initial susceptibility, can be obtained from (3-16) by differentiation. The internal energy per site is given by

$$U = kT^2 \frac{\partial}{\partial T} (-f/kT) \quad (3-20)$$

and the zero field specific heat per site by

$$C = \partial U / \partial T \quad (3-21)$$

For the hydrogen peroxide lattice we have

$$\begin{aligned} U/J = & -1 \frac{1}{2} v - 15v^9 + 15v^{11} - 21v^{13} - 147v^{15} \\ & - 254v^{17} + 288v^{19} - 3792v^{21} - 7689v^{23} \\ & - 8508v^{25} + 64527v^{27} + \dots, \end{aligned} \quad (3-22)$$

$$\begin{aligned} C/k = K^2 [& 1 \frac{1}{2} - 1 \frac{1}{2} v^2 + 135v^8 - 300v^{10} + 438v^{12} \\ & + 1932v^{14} + 2130v^{16} - 9807v^{18} + 85104v^{20} \\ & + 97215v^{22} + 35853v^{24} + 1529529v^{26} + \dots, \end{aligned} \quad (3-23)$$

whereas for the hypertriangular lattice we have

$$\begin{aligned} U/J = & -3v - 3v^2 - 12v^4 - 87v^5 - 216v^6 - 369v^7 \\ & - 1734v^8 - 9159v^9 - 31530v^{10} - 97488v^{11} \\ & - 391293v^{12} - 1703832v^{13} - \dots, \end{aligned} \quad (3-24)$$

$$\begin{aligned} C/k = K^2 [& 3 + 6v - 3v^2 + 42v^3 + 1248v^5 + 2148v^6 \\ & + 12576v^7 + 79848v^8 + 301428v^9 + 989937v^{10} \\ & + 4380216v^{11} + 21077448v^{12} + \dots. \end{aligned} \quad (3-25)$$

In terms of the variable K alone we have for the hydrogen peroxide lattice

$$\begin{aligned}
C/k = & 1.5K^2 - 1.5K^4 + K^6 - 0.566666K^8 + 135.2952381K^{10} \\
& - 660.1462434K^{12} + 2002.070046K^{14} - 2394.318471K^{16} \\
& + 401.5388552K^{18} - 8224.447893K^{20} + 145141.528K^{22} \\
& - 677416.1035K^{24} + 1829923.386K^{26} - 1989842.638K^{28} \\
& + \dots,
\end{aligned} \tag{3-26}$$

and for the hypertrinagular lattice we have

$$\begin{aligned}
C/k = & 3K^2 + 6K^3 - 3K^4 + 40K^5 + 437K^6 + 1206.8K^7 \\
& + 1566.866667K^8 + 10526.47619K^9 + 76074.59048K^{10} \\
& + 274283.2423K^{11} + 781916.7583K^{12} \\
& + 3515116.625K^{13} + 18106355.75K^{14} + \dots.
\end{aligned} \tag{3-27}$$

The entropy per site is obtained from the relation

$$S/k = (U/kT) - (f/kT). \tag{3-28}$$

B. The Initial Susceptibility

In the previous section we have concerned ourselves with the calculation of the zero field partition function and the thermodynamic variables derivable from it. In order to derive the initial susceptibility per site defined by

$$\chi_0 = (\partial^2 / \partial H^2) (f/kT) \big|_{H=0}, \quad (3-29)$$

we must also consider the effect of the factor containing the magnetic field H in (3-3). The end result is given by

$$\bar{\chi} = \chi_0 / (Nm^2/kT) = 1 + 2 \sum_{\ell=1}^{\infty} b_{\ell} v^{\ell}, \quad (3-30)$$

where $\bar{\chi}$ is the reduced initial susceptibility per site.

b_{ℓ} is the coefficient of N in the total number of ways of embedding in the lattice all graphs of ℓ lines and exactly two vertices of odd degree. Such graphs are referred to as magnetic graphs. This method of calculating the initial susceptibility we shall refer to as the direct method.

The calculation of the first nine terms in the susceptibility series for the hypertriangular lattice using the direct method is given in Appendix E. For example, those graphs contributing to the first four terms of $\bar{\chi}$ for the hypertriangular lattice are shown in Table 3.2.

The calculation of the initial susceptibility by the method of (3-30) requires the enumeration of graphs having vertices of degree one. As these graphs are exceedingly numerous, this method is very susceptible to error and excessively labourious.

Sykes (1961) discovered a theorem which greatly reduces the labour involved in calculating the series for the initial susceptibility. Sykes' theorem, as later derived from graph-combinatorial arguments by Nagle and Temperley (1968) can be written in the form

$$\begin{aligned} \bar{\chi} = 1 + (1-\sigma v)^{-2} [q v (1-\sigma v) - 2(1-v^2) \sum_{\vec{p}} g(\vec{p}) \ell v^{\ell} \\ + (1+v)^2 \sum_{\vec{p}} g(\vec{p}) v^{\ell} \sum_{s=0}^q s(s-2) p_s \\ + 2(1+v)^2 \sum_{\vec{p}} g(\vec{p}) v^{\ell} (s_1-1)(s_j-1)], \end{aligned} \quad (3-31)$$

where $\sigma = (q-1)$, q being the coordination number of the lattice. $\vec{p} = (p_0, p_1, p_2, \dots, p_q)$ is a $(q+1)$ tuple or vector partially describing a graph by the number p_s of its vertices of degree s . $g(\vec{p})$ is the number of graphs with description \vec{p} , which may be embedded in the lattice and for which $p_0 = 0$.

In (3-31) the singly primed summation is over all graphs (nonmagnetic) whose vertices are all of even degree, while the doubly primed summation is over all graphs (magnetic) with exactly two odd vertices, i and j , of odd degree s_i and s_j . Note that if either s_i or s_j or both equal one, the graph does not contribute to (3-31).

Using Sykes' theorem we have derived the first twenty-seven terms in the expansion of the reduced initial susceptibility per site for the hydrogen peroxide lattice

$$\begin{aligned}
 \bar{\chi} = & 1 + 3v + 6v^2 + 12v^3 + 24v^4 + 48v^5 + 96v^6 \\
 & + 192v^7 + 384v^8 + 768v^9 + 1506v^{10} + 2952v^{11} \\
 & + 5814v^{12} + 11448v^{13} + 22494v^{14} + 44192v^{15} \\
 & + 86514v^{16} + 169320v^{17} + 330858v^{18} + 646524v^{19} \\
 & + 1263696v^{20} + 2469456v^{21} + 4817616v^{22} \\
 & + 9397740v^{23} + 18315734v^{24} + 35694200v^{25} \\
 & + 69538944v^{26} + 135463148v^{27} + \dots
 \end{aligned} \tag{3-32}$$

For the hypertriangular lattice we have obtained the first twelve terms in the series for the susceptibility by way of Sykes' theorem. We have also added one more term by star-triangle transformation from (3-32) (c.f. eq'n (5-37)). The initial susceptibility for the hypertriangular lattice is given by

$$\begin{aligned}
\bar{\chi} = & 1 + 6v + 30v^2 + 144v^3 + 690v^4 + 3276v^5 \\
& + 15360v^6 + 71532v^7 + 332166v^8 + 1537836v^9 \\
& + 7097244v^{10} + 32677584v^{11} + 150203012v^{12} \\
& + 689366094v^{13} + \dots
\end{aligned}
\tag{3-33}$$

The graphs required to derive the susceptibility series for the hypertriangular lattice via Sykes' theorem are given in Appendix B. For the hydrogen peroxide lattice the only connected graphs required in calculating the first twenty-seven terms of the susceptibility in this way are the p-graphs and theta graphs of Appendix D, and the dumbbell graphs of Appendix J.

CHAPTER IV

LOW TEMPERATURE SERIES EXPANSIONS OF
FERROMAGNETS AND ANTIFERROMAGNETS

A. The Direct Method.

Consider an Ising model of a ferromagnet at $T = 0$. All the spins are aligned and give rise to a spontaneous magnetization. As the temperature is raised above $T = 0$ thermal fluctuations will perturb the ground state. The probability of any given perturbation will be given by the appropriate Boltzmann factor. As overturning almost any spin causes an increase in energy, the most important perturbations will correspond to a relatively few overturned spins. Thus we can group the perturbations according to the number of overturned spins, the energy of any particular perturbation depending on the relative positions of these spins.

Denote by $-J$ the interaction energy of a pair of aligned first neighbour spins and by $-mH$ the interaction energy of a spin aligned with the magnetic field H . Then if we overturn s spins of magnetic moment m with r first neighbour bonds between them there will be a gain in energy of

$$2(qs-2r)J + 2msH \quad , \quad (4-1)$$

where q is the coordination number of the lattice, i.e. the number of first nearest neighbours. Thus the Boltzmann factor for a perturbation having its energy given by (4-1) will be

$$\exp\{-2(qs-2r)J-2msH\}/kT \quad . \quad (4-2)$$

Letting $\exp(-4J/kT) = u = z^2$ and $\exp(-2mH/kT) = \mu$,
(4-2) can be written as

$$\exp\{-2(qs-2r)J-2msH\}/kT = u^{\frac{1}{2}qs-r} \mu^s \quad . \quad (4-3)$$

The energy of the ground state is given by

$$\epsilon_0 = -N\left(\frac{1}{2}qJ+mH\right) \quad . \quad (4-4)$$

Thus we can write the partition function as follows

$$Q_N(u, \mu) = \exp(-\epsilon_0/kT) \Lambda_N(u, \mu) \quad , \quad (4-5)$$

where

$$\Lambda_N(u, \mu) = \sum_{s,r} G_N(s, r) u^{\frac{1}{2}qs-r} \mu^s \quad . \quad (4-6)$$

For a given lattice the $G_N(s,r)$ in (4-6) denote the total number of strong embeddings (c.f. Domb 1960, Sykes et al. 1966) of s spins with r nearest neighbour bonds between them. In general $G_N(s,r)$ will be a polynomial in N . For the hydrogen peroxide lattice the first few $G_N(s,r)$ are given by

$$\begin{array}{rcl}
 G_N(1,0) & = & N \\
 G_N(2,1) & = & 1\frac{1}{2}N \\
 G_N(2,0) & = & \frac{1}{2}N^2 - 2N \\
 G_N(3,2) & = & 3N \\
 G_N(3,1) & = & 1\frac{1}{2}N^2 - 9N \\
 G_N(3,0) & = & \frac{1}{6}N^3 - 2N^2 + 6\frac{1}{3}N \\
 \vdots & = & \vdots
 \end{array} \quad (4-7)$$

The free energy per spin is given by

$$f = -kT \lim_{N \rightarrow \infty} \frac{\ln Q_N(u, \mu)}{N} \quad (4-8)$$

$$= -\frac{1}{2}qJ - mH - kT \lim_{N \rightarrow \infty} \frac{\ln \Lambda_N(u, \mu)}{N} \quad (4-9)$$

Exactly the same arguments are valid here as were applied in Sect. A of Chapter III in dealing with the taking of the limit, i.e. upon taking $\lim_{N \rightarrow \infty} [\ln \Lambda_N(u, \mu)]/N$ we find that only the coefficient of N in $G_N(s, r)$ fails to vanish and hence

$$\lim_{N \rightarrow \infty} [\ln \Lambda_N(u, \mu)]/N = \ln \Lambda(u, \mu) = \sum_{s, r} [s, r] u^{\frac{1}{2}qs - r} \mu^s \quad (4-10)$$

where by $[s, r]$ we mean coefficient of N in $G_N(s, r)$.

It is customary to group the expansion (4-10) as a series in powers of μ , the successive coefficients then being finite polynomials in u , $L_s(u)$, defined by

$$\ln \Lambda(u, \mu) = \sum_s L_s(u) \mu^s. \quad (4-11)$$

The polynomials $L_s(u)$ are called low temperature ferromagnetic polynomials. A given polynomial $L_s(u)$ is completely specified by a knowledge of all perturbations with s overturned spins,

$$L_s(u) = \sum_{r=0}^{s(s-1)} [s, r] u^{\frac{1}{2}qs - r}. \quad (4-12)$$

When using the method outlined above, which we call the direct method, one usually groups the perturbations according to the topology of their nearest neighbour linkages. As an example, we have listed in Fig. 4.1 those perturbations on the hydrogen peroxide lattice contributing to [7,6].

The low temperature ferromagnetic polynomials of the hypertriangular lattice which have been derived via the direct method are listed in Appendix F.

We will now describe the low temperature anti-ferromagnetic counting problem. We consider a lattice which can be decomposed into two equivalent sublattices. By this we mean that each site of the lattice can be coloured in one of two ways such that a given site is surrounded by nearest neighbours all of the opposite colour. In the terminology of graph theory the lattice is bi-colourable (c.f. Fig. 2.6). Let one of the sublattices be denoted by A and the other by B , and to avoid the use of fractions we consider a lattice of $2N$ sites, N of which are A -sites and N B -sites. Furthermore, as we are now discussing an antiferromagnet for which $J < 0$, we shall take $J' = -J$.

For small fields the lowest energy state is now one of antiparallel ordering in which each A -spin is in

Fig. 4.1. Topological breakdown of the perturbations on the hydrogen peroxide lattice contributing to [7,6]. The coefficient of z^9 in $L_7(z) = 143$.



(48N)



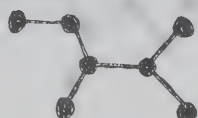
(24N)



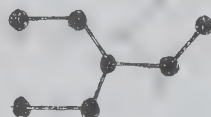
(48N)



(3N)



(12N)



(8N)

$$G_N(7,6) = 143N$$

Total Contribution to $[7,6] = 143$

a state which is the opposite of its first nearest neighbours each of which is a B-spin. If we perturb such a state by overturning s A-spins and t B-spins with r nearest neighbour bonds between them the resultant gain in energy will be

$$2[q(s+t)-2r]J' + 2msH - 2mtH, \quad (4-13)$$

where we have chosen the direction of the field as that of the unperturbed A-sites. It should be pointed out that equation (4-13) for the case of zero field reduces to (4-1), which simply expresses the well known result that in zero field the configurational problem for a loose packed Ising antiferromagnet is isomorphic with the ferromagnetic one.

We now introduce the variables $y = \exp(-2J'/kT)$ and $\omega = y^2$. The energy of the ground state is given by $\epsilon_0^a = -NqJ'/2$. Hence the partition function is given by

$$Q_N^a(\omega, \mu) = \exp(-\epsilon_0^a/kT) \Lambda_N^a(\omega, \mu), \quad (4-14)$$

where
$$\Lambda_N^a(\omega, \mu) = \sum_{s,t,r} G_N(s+t, r) \omega^{\frac{1}{2}q(s+t)} \mu^{s-t}. \quad (4-15)$$

The free energy per spin is given by

$$f = -\frac{1}{2}qJ' - kT \ln \Lambda^a(\omega, \mu) \quad , \quad (4-16)$$

$$\text{where } \ln \Lambda^a(\omega, \mu) = \sum_{s,t,r} [s+t, r] \omega^{\frac{1}{2}q(s+t)-r} s_{\mu}^{-t} \quad . \quad (4-17)$$

For zero field the low temperature expansion of the partition function will be given by

$$\ln \Lambda^a(\omega, 1) = \sum_{s,t,r} [s+t, r] \omega^{\frac{1}{2}q(s+t)-r} \quad , \quad (4-18)$$

where as in the discussion of the ferromagnetic problem we denote by $[s+t, r]$ the coefficient of N in $G_N(s+t; r)$.

Now consider the case of a ferromagnetic loose packed lattice. Again we denote one sublattice by A and the other by B . To the A -sites we assign a magnetic moment m_A and to the B -sites we assign a magnetic moment m_B . In our previous description of the ferromagnetic problem we were concerned with perturbations of s spins with r first neighbour bonds between them. We are now concerned with enumerating perturbations consisting of s A -spins, t B -spins , with r first neighbour bonds

between them. The coefficient of N in the total number of ways of embedding s A-spins, t B-spins, with r first neighbour bonds between them will be denoted by $[s,t;r]$.

The expression for the free energy per site will be given by

$$f = -\frac{1}{2}qJ - m_A H - m_B H - kT \ln \Lambda(u, \mu, \nu), \quad (4-19)$$

where

$$\ln \Lambda(u, \mu, \nu) = \sum [s,t;r] u^{\frac{1}{2}q(s+t)-r} \mu^s \nu^t. \quad (4-20)$$

The variables μ and ν are defined by

$$\exp(-2m_A H/kT) = \mu$$

$$\exp(-2m_B H/kT) = \nu.$$

If we set $\nu = 1/\mu$ and $u = \omega$ we have

$$\ln \Lambda(\omega, \mu) = \sum_{s,t,r} [s,t;r] \omega^{\frac{1}{2}q(s+t)-r} \mu^s \mu^{-t}, \quad (4-21)$$

which can be looked upon as a formal isomorphism with (4-17). We have retained the $[s,t;r]$ of the ferromagnetic problem

even in the presence of a field. The isomorphism between $\ln \Lambda^a(\omega, \mu)$ (4-17) and $\ln \Lambda(\omega, \mu)$ (4-21) is only formal since the two series have different regions of physical validity.

The low temperature polynomials for the sublattice ferromagnetic problem are defined by

$$L_{s,t} = \sum_r [s,t;r] u^{\frac{1}{2}q(s+t)-r} \quad (4-22)$$

Again the method of topological breakdown can be used to enumerate the various $[s,t;r]$.

While the above method (the direct method) is simple and quite straight forward it is difficult to derive more than a few terms as the number of perturbations contributing to a given $[s,r]$ or $[s,t;r]$ increases rapidly. A further disadvantage is that there is no systematic way of checking whether one in fact has listed all the perturbations correctly or if one has calculated the contribution of a given perturbation correctly. However, there is another method, being both more sophisticated and more powerful and essentially self-checking, by which we can attack the problem of enumerating the required perturbations. We shall proceed to describe this method in the following section.

B. The Shadow Lattice Method.

We shall now describe a method, which was introduced by Sykes, Essam, and Gaunt (1965), of enumerating low temperature perturbations on a loose packed lattice. This method eliminates the need for any topological description of the perturbations contributing to a given $[s,t;r]$ and instead simply provides us with the numerical values of the required $[s,t;r]$.

We define a generating function F by

$$F(X,Y,b) = \sum_{s,t,r} [s,t;r] X^s Y^t b^r . \quad (4-23)$$

If we could find a closed form expansion for F we would in fact have the equivalent of an exact solution to the low temperature enumeration problem. Instead of using the generating function F , we shall find it more convenient to work with a partial generating function $F_\lambda(X,b)$ defined by

$$F(X,Y,b) = \sum_{\lambda} Y^\lambda F_\lambda(X,b) , \quad (4-24)$$

where

$$F_{\lambda}(X,b) = \sum_{s,r} [s,\lambda;r] X^s b^r . \quad (4-25)$$

The partial generating function $F_{\lambda}(X,b)$ is equivalent to an exact solution of the problem when the number of overturned spins, λ , on one sublattice is held constant. In fact since the sublattices are symmetric, a knowledge of the first n partial generating functions makes it possible to determine all the $[s,t;r]$ for $s + t \leq 2n + 1$.

We shall now show how one can derive the first three partial generating functions for the hydrogen peroxide lattice. The derivation of partial generating functions of higher order will be quite straight forward.

The zeroth order generating function F_0 corresponds to configurations for which all the sites are on one sublattice, say the A-sublattice. As the sites of a given sublattice are not nearest neighbours of each other, $r = 0$ always. Since we have an infinite lattice of $2N$ sites, the first site on the A sublattice may be chosen in N ways, the second in $(N-1)$ ways and so on.

If we want to choose s A-sites and no B-sites the number of ways we can do this is simply

$$N(N-1)(N-2) \cdots (N-s+1)/s! . \quad (4-26)$$

We want $[s,0;0]$, which is simply the coefficient of N in (4-26), hence

$$[s,0;0] = \frac{(-1)^{s+1}}{s} . \quad (4-27)$$

Therefore for F_0 we have

$$F_0(X,b) = \ln(1+X) . \quad (4-28)$$

To derive F_1 we must choose one site on the B sublattice, and there are N ways of doing this. Upon choosing the B-site we observe that it casts a "shadow" on its three nearest neighbours, all of which are A-sites (see Fig. 2.6 and Fig. 4.2(a)) in the sense that if an A-site is chosen from the sites of the shadow a nearest neighbour bond is formed.

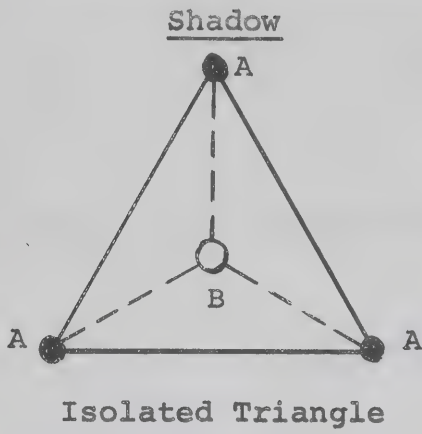
If we choose α A-sites from the three sites in the shadow and β A-sites from the remaining $(N-3)$ sites we shall obtain α nearest neighbour bonds in

$$N \binom{3}{\alpha} (N-3) (N-4) \cdots (N-\beta+1) / \beta! \quad (4-29)$$

ways. The coefficient of N in (4-29) is given by

Fig. 4.2 (a) A B-site (o) and its corresponding "shadow" composed of three A-sites (●). The dashed lines indicate nearest neighbour bonds while the solid lines connecting the A-sites form the "shadow."

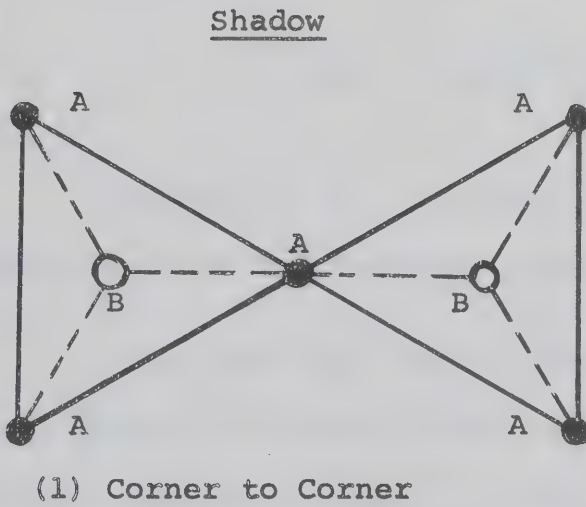
(b) The possible overlappings of the shadow cast by two B-sites. The figures refer to the hydrogen peroxide lattice. The A-sites (and also the B-sites) each form the sites of a hypertriangular lattice. The occurrence factors are just the number of strong embeddings of the given configuration on the hypertriangular lattice.



Occurrence Factor

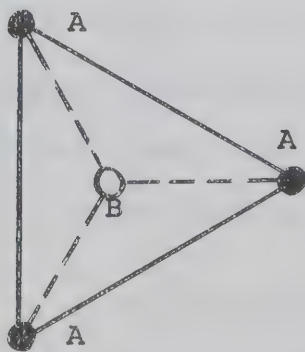
(N)

(a)

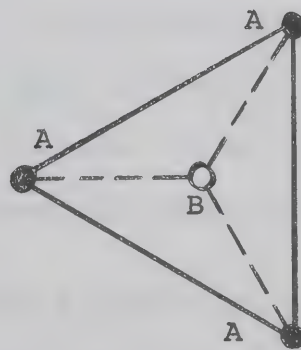


Occurrence Factor

(3N)



(2) Separated



(b)

$(\frac{1}{2} N^2 - 3 \frac{1}{2} N)$

$$\binom{\beta}{\alpha} \binom{-3}{\beta} . \quad (4-30)$$

The term in F_1 corresponding to (4-30) is thus

$$(xb)^\alpha x^\beta \binom{\beta}{\alpha} \binom{-3}{\beta} , \quad (4-31)$$

and therefore by the binomial theorem we have

$$F_1(X,b) = (1+bX)^3 (1+X)^{-3} . \quad (4-32)$$

To derive F_2 we turn over two B-sites and observe that the shadows may overlap as shown in Fig. 4.2(b).

Consider the configuration of two triangles placed corner to corner in Fig. 4.2(b). Since the two triangles have one corner in common, only five A-sites are shaded by the two B-sites. Of these five sites the one on the common corner will create two first neighbour bonds if chosen since it is adjacent to both B-sites. If one of the remaining four A-sites is chosen one first neighbour bond will be formed. If an A-site other than one of these five is chosen no bonds will be formed.

Let us now choose from this configuration α A-sites, which each form two first neighbour bonds, and

β A-sites , which each form one first neighbour bond, and
 γ A-sites which form no first neighbour bonds. The
 α A-sites can be chosen in

$$\left(\begin{matrix} 1 \\ \alpha \end{matrix} \right)$$

ways; the β A-sites can be chosen in

$$\left(\begin{matrix} 4 \\ \beta \end{matrix} \right)$$

ways, and the remaining γ A-sites can be chosen in

$$(N-5)(N-6) \cdots (N-5-\gamma+1)/\gamma! \quad (4-33)$$

ways.

The corner to corner configuration of two triangles can be placed on the hypertriangular lattice in $3N$ ways, therefore on the hydrogen peroxide lattice the number of ways of choosing two B-sites casting a shadow of the corner to corner type plus $\alpha+\beta+\gamma$ A-sites with $2\alpha + \beta$ bonds between them is

$$3N \left(\begin{matrix} 1 \\ \alpha \end{matrix} \right) \left(\begin{matrix} 4 \\ \beta \end{matrix} \right) (N-5)(N-6) \cdots (N-5-\gamma+1)/\gamma! \quad (4-34)$$

and the term linear in N in this is simply

$$3 \binom{1}{\alpha} \binom{4}{\beta} \binom{-5}{\gamma} . \quad (4-35)$$

Hence the contribution of configuration (1) of Fig. 4.2(b) to F_2 is given by

$$3 \sum_{\alpha, \beta, \gamma} \binom{1}{\alpha} (b^2 x)^\alpha \binom{4}{\beta} (bx)^\beta \binom{-5}{\gamma} x^\gamma = 3(1+b^2 x)(1+bx)^4 \times (1+x)^{-5} . \quad (4-36)$$

For the two separated triangles there are six A-sites that can form a first neighbour bond with a B-site and hence $(N-6)$ A-sites that will form no first neighbour bonds. Choosing α A-sites from the six A-sites of the shadow and β A-sites from the remaining $(N-6)$ A-sites, we can form on the hydrogen peroxide lattice configurations of $\alpha + \beta$ A-sites and two B-sites with α first neighbour bonds in

$$\left(\frac{1}{2}N^2 - 3\frac{1}{2}N\right) \binom{6}{\alpha} (N-6)(N-7) \cdots (N-6-\beta+1) / \beta! \quad (4-37)$$

ways. The coefficient of N in (4-37) is given by

$$- 3\frac{1}{2} \binom{6}{\alpha} \binom{-6}{\beta} .$$

Hence the separated configuration gives the following contribution to F_2

$$- 3\frac{1}{2} \sum_{\alpha, \beta} \binom{6}{\alpha} (bX)^\alpha \binom{-6}{\beta} X^\beta = - 3\frac{1}{2} (1+bX)^6 (1+X)^{-6} . \quad (4-38)$$

Therefore the second partial generating function for the hydrogen peroxide lattice is simply

$$\begin{aligned} F_2(X, b) &= 3(1+bX)^4 (1+b^2X) (1+X)^{-5} \\ &= 3\frac{1}{2} (1+bX)^6 (1+X)^{-6} . \end{aligned} \quad (4-39)$$

The general term in $F_n(X, b)$ will be of the form

$$(1+bX)^\alpha (1+b^2X)^\beta (1+b^3X)^\gamma \cdots / (1+X)^{\alpha+\beta+\gamma+\cdots} , \quad (4-40)$$

which we shall denote by the following code

$$(\lambda, \alpha, \beta, \gamma, \cdots), \quad \lambda = \alpha + \beta + \gamma + \cdots, \quad (4-41)$$

which forms a convenient description for supplying such data to a computer. The brackets are closed when the factors to the right terminate. However, any intermediate zeros must be included in the code.

Very simply the code tells us the following. For a given "shadow" composed of λ A-sites, α of these each form one first neighbour bond with the B-sites, β A-sites each form two first neighbour bonds with the B-sites, and so on. The coded form of F_1 and F_2 are shown below.

$$\left. \begin{aligned} F_1(X,b) &= (3,3) \\ F_2(X,b) &= 3(5,4,1) - 3\frac{1}{2}(6,6) \end{aligned} \right\} \cdot \quad (4-42)$$

In this manner we have calculated completely the first seven partial generating functions for the hydrogen peroxide lattice and we have also calculated the leading terms of F_8 , F_9 , F_{10} , and F_{11} , which are listed in coded form in Appendix G. The shadow configurations required to calculate the partial generating functions of the hydrogen peroxide lattice are listed in Appendix H.

In order to obtain the various $[s, \lambda; r]$ from the partial generating functions it is necessary to expand them in the form of a power series. This can only conveniently be done on a computer and for this purpose the coded partial generating functions form the input data. We have written a program to perform such a task. However, as the output is very extensive we shall not list it here. We have pointed out previously that this method is essentially self-checking since the two sublattices are symmetric, i.e. $[s, \lambda; r] = [\lambda, s; r]$. This is a great advantage of the shadow lattice method over others.

As an example of how we use the partial generating functions consider the topological description of the perturbation of Fig. (4.1). We need the coefficient of b^6 for all $s+t = 7$. Expanding the first three partial generating functions we find the coefficient of b^6 is given by

$$3X^5Y^2 + 140X^4Y^3 + 140X^3Y^4 + 3X^2Y^5. \quad (4-43)$$

Adding the coefficients together we obtain

$$\begin{aligned} [7,6] &= 286 \quad \text{for } 2N \text{ sites} \\ &= 143 \quad \text{for } N \text{ sites,} \end{aligned}$$

which is the same as [7,6] quoted in Fig. 4.1.

The first seven partial generating functions are sufficient to determine completely the first fifteen low temperature ferromagnetic polynomials for the hydrogen peroxide lattice. We have also calculated the leading terms of higher order polynomials up to and including $L_{22}(z)$. The low temperature ferromagnetic polynomials for the hydrogen peroxide lattice are listed in Appendix I.

In addition to the energy, specific heat, and initial susceptibility, which have been previously defined, we are also interested in the spontaneous magnetization defined by

$$I = - \frac{\partial f}{\partial H} \Big|_{H=0} . \quad (4-44)$$

From the polynomials listed in Appendix I, we have calculated ferromagnetic low temperature series expansions for the Ising model on the hydrogen peroxide lattice. The series are as follows:

free energy

$$\begin{aligned}
 (-f/kT) &= (q/2) \cdot K + z^3 + 1 \frac{1}{2} z^4 + 3 z^5 + 5 z^6 \\
 &+ 9 z^7 + 15 \frac{3}{4} z^8 + 28 \frac{1}{3} z^9 + 52 \frac{1}{2} z^{10} \\
 &+ 108 z^{11} + 254 z^{12} + 657 z^{13} \\
 &+ 1738 \frac{1}{2} z^{14} + 4511 \frac{1}{5} z^{15} \\
 &+ 11463 \frac{3}{8} z^{16} + \dots,
 \end{aligned} \tag{4-45}$$

configurational energy

$$\begin{aligned}
 U/J &= (-q/2) + 6 z^3 + 12 z^4 + 30 z^5 + 60 z^6 \\
 &+ 126 z^7 + 252 z^8 + 510 z^9 + 1050 z^{10} \\
 &+ 2376 z^{11} + 6096 z^{12} + 17082 z^{13} \\
 &+ 48678 z^{14} + 135336 z^{15} + 366828 z^{16} \\
 &+ \dots,
 \end{aligned} \tag{4-46}$$

specific heat

$$\begin{aligned}
 C/k(\ln z)^2 &= 9 z^3 + 24 z^4 + 75 z^5 + 180 z^6 + 430 \frac{1}{2} z^7 \\
 &+ 1008 z^8 + 2295 z^9 + 5250 z^{10} + 13068 z^{11} \\
 &+ 36576 z^{12} + 111033 z^{13} + 347462 z^{14} \\
 &+ 1015020 z^{15} + 2934624 z^{16} + \dots,
 \end{aligned} \tag{4-47}$$

spontaneous magnetization

$$\begin{aligned}\bar{I} = & 1 - 2 z^3 - 6 z^4 - 18 z^5 - 48 z^6 - 126 z^7 - 234 z^8 \\ & - 830 z^9 - 2154 z^{10} - 5784 z^{11} - 16146 z^{12} \\ & - 46302 z^{13} - 134082 z^{14} - 387724 z^{15} - 1119024 z^{16} \\ & - \dots, \end{aligned} \quad (4-48)$$

and initial susceptibility

$$\begin{aligned}\bar{\chi} = & 4 z^3 + 24 z^4 + 108 z^5 + 416 z^6 + 1476 z^7 + 4968 z^8 \\ & + 17156 z^9 + 51912 z^{10} + 167568 z^{11} + 545456 z^{12} \\ & + 1787364 z^{13} + 5838360 z^{14} + 18949712 z^{15} \\ & + 61171104 z^{16} + \dots \end{aligned} \quad (4-49)$$

The ferromagnetic low temperature series expansions for the hypertriangular lattice are listed in Appendix F.

CHAPTER V

ISING MODEL TRANSFORMATIONSA. The Star-Triangle Transformation

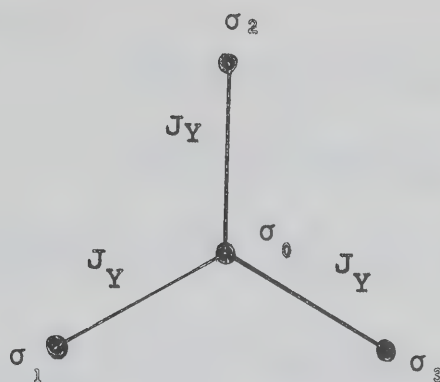
The star-triangle transformation was originally developed by Onsager (see Wannier 1945). By utilizing both the star-triangle and dual transformation Onsager was able to calculate exactly the critical points of the triangular and honeycomb lattices. In this work the dual transformation is of no direct interest as it is applicable to two dimensional lattices only.

The star-triangle transformation replaces a star consisting of three spins interacting with a central spin by a triangle of spins interacting with one another (Fig. 5.1). The partition function for the star (Fig. 5.1(a)) is given by

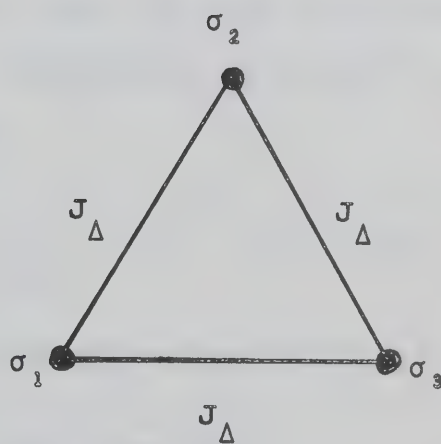
$$Z_Y = \sum_{\substack{\sigma_0 = \pm 1 \\ \sigma_1, \sigma_2, \sigma_3 = \pm 1}} \exp K_Y (\sigma_0 \sigma_1 + \sigma_0 \sigma_2 + \sigma_0 \sigma_3), \quad (5-1)$$

where $K_Y = J_Y/kT$. Since the σ variables commute and obey the Van der Waerden identity (3-5), we can write (5-1) as

Fig. 5.1. The star-triangle transformation.



(a)



(b)

$$\begin{aligned}
 Z_Y = \cosh^3 K_Y \sum_{\sigma_0=\pm 1} [1 + (\sigma_0\sigma_1 + \sigma_0\sigma_2 + \sigma_0\sigma_3) \tanh K_Y \\
 + (\sigma_1\sigma_2 + \sigma_1\sigma_3 + \sigma_2\sigma_3) \tanh^2 K_Y \\
 + \sigma_0\sigma_1\sigma_2\sigma_3 \tanh^3 K_Y]. \quad (5-2)
 \end{aligned}$$

Upon performing the sum over σ_0 in (5-2) we obtain

$$Z_Y = 2 \cosh^3 K_Y \sum_{\sigma_1, \sigma_2, \sigma_3=\pm 1} [1 + (\sigma_1\sigma_2 + \sigma_1\sigma_3 + \sigma_2\sigma_3) \tanh^2 K_Y] \quad (5-3)$$

for the "star" partition function.

The partition function for the triangle of spins (Fig. 5.1(b)) is given by

$$Z_\Delta = \sum_{\sigma_1, \sigma_2, \sigma_3=\pm 1} \exp K_\Delta (\sigma_1\sigma_2 + \sigma_1\sigma_3 + \sigma_2\sigma_3), \quad (5-4)$$

where $K_\Delta = J_\Delta/kT$. Again we make use of the properties of the σ variables, commutativity plus the Van der Waerden identity to obtain

$$\begin{aligned}
 Z_\Delta = \cosh^3 K_\Delta \sum_{\sigma_1, \sigma_2, \sigma_3=\pm 1} [1 + (\sigma_1\sigma_2 + \sigma_1\sigma_3 + \sigma_2\sigma_3) \\
 \times (\tanh K_\Delta + \tanh^2 K_\Delta) + \tanh^3 K_\Delta], \quad (5-5)
 \end{aligned}$$

which can be cast into the form

$$Z_{\Delta} = (\cosh^3 K_{\Delta} + \sinh^3 K_{\Delta}) \sum_{\sigma_1, \sigma_2, \sigma_3 = \pm 1} [1 + (\sigma_1 \sigma_2 + \sigma_1 \sigma_3 + \sigma_2 \sigma_3)] \\ \times \left(\frac{\cosh^2 K_{\Delta} \sinh K_{\Delta} + \cosh K_{\Delta} \sinh^2 K_{\Delta}}{\cosh^3 K_{\Delta} + \sinh^3 K_{\Delta}} \right)]. \quad (5-6)$$

Comparing (5-3) and (5-6) we see that if we choose K_{Δ} to satisfy

$$\frac{\cosh K_{\Delta} \sinh K_{\Delta} (\cosh K_{\Delta} + \sinh K_{\Delta})}{\cosh^3 K_{\Delta} + \sinh^3 K_{\Delta}} = \tanh^2 K_Y, \quad (5-7)$$

the partition functions of the star and triangle will be related to each other by the simple factor

$$\zeta = 2 \cosh^3 K_Y / (\cosh^3 K_{\Delta} + \sinh^3 K_{\Delta}), \quad (5-8)$$

that is

$$Z_Y = \zeta Z_{\Delta}. \quad (5-9)$$

Equations (5-7) and (5-9) constitute the star-triangle transformation.

The temperature variables ($K_Y = J_Y/kT$, $K_{\Delta} = J_{\Delta}/kT$) of star-triangle lattices are related through (5-7), which can be greatly simplified by the use of certain well known hyperbolic identities to yield

$$\exp (4 K_{\Delta}) = 2 \cosh (2 K_Y) - 1. \quad (5-10)$$

In terms of the variables $z = \exp (-2J/kT)$, we have

$$z_{\Delta}^2 = z_Y / (1 - z_Y + z_Y^2), \quad (5-11)$$

and in terms of $v = \tanh (J/kT) = \tanh K$, we have

$$v_Y^2 = (v_{\Delta} + v_{\Delta}^2) / (1 + v_{\Delta}^3). \quad (5-12)$$

If we apply the star-triangle transformation to a lattice of connected stars we can write

$$Z_{2N} (K_Y) = \zeta^N Z_N (K_{\Delta}), \quad (5-13)$$

where Y and Δ denote "star" and "triangle" lattices respectively. The subscripts $2N$ and N refer to the number of sites on the respective lattices. In three dimensions we have

$$\left. \begin{aligned} Y &= \text{HP (hydrogen peroxide)} \\ \Delta &= \text{HT (hypertriangular)} \end{aligned} \right\}$$

and in two dimensions we have

$$\left. \begin{aligned} Y &= \text{HC (honeycomb)} \\ \Delta &= \text{T (triangular)} \end{aligned} \right\}.$$

The significance of the star-triangle transformation for this work is that it provides us with an exact

relationship between the critical points of the hydrogen peroxide and hypertriangular lattices, and hence provides us with a valuable check of our numerical analysis of the series of Chapter III. The star-triangle transformation also enables us to derive from the hydrogen peroxide lattice the partition function and initial susceptibility of the hypertriangular lattice. We shall have more to say about this in Section C of this Chapter.

B. The Decoration Transformation

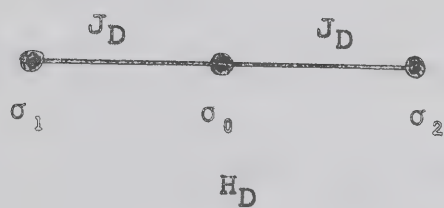
The decoration transformation was first suggested by Syozi (1951) and later developed by Naya (1954). The decoration transformation combined with the star-triangle transformation enables one to calculate exactly the solution of the Ising model on the kagomé lattice from the solution of the Ising model on the honeycomb lattice. In this work we shall combine the decoration transformation with the star-triangle transformation to calculate the properties of the Ising model on the hyperkagomé lattice (Fig. 2.9) from the properties of the Ising model on the hydrogen peroxide lattice (Fig. 2.1).

The decoration transformation replaces a central spin interacting with two neighbouring spins plus the interaction with the magnetic field by a single bond connecting the two outer spins plus a new interaction with the magnetic field. The partition function for the system shown in Fig. 5.2(a) is given by

$$Z_D = \sum_{\substack{\sigma_0=\pm 1 \\ \sigma_1, \sigma_2=\pm 1}} \exp (K_D \sigma_0 \sigma_1 + K_D \sigma_0 \sigma_2 + L_D \sigma_0), \quad (5-14)$$

where $K_D = J_D/kT$, $L_D = mH_D/kT$. The subscript D denotes a decorated system. Again using the commutivity of the σ

Fig. 5.2. The decoration transformation.



(a)



(b)

variables plus the Van der Waerden identity, (5-14) can be written as

$$\begin{aligned}
 Z_D = \cosh^2 K_D \cosh L_D \sum_{\substack{\sigma_0 = \pm 1 \\ \sigma_1, \sigma_2 = \pm 1}} \{ & 1 + (\sigma_1 + \sigma_2) \tanh K_D \tanh L_D \\
 & + \sigma_1 \sigma_2 \tanh^2 K_D + \sigma_0 [(\sigma_1 + \sigma_2) \tanh K_D + \tanh L_D \\
 & + \sigma_1 \sigma_2 \tanh^2 K_D \tanh L_D] \}. \quad (5-15)
 \end{aligned}$$

Performing the sum over σ_0 we are left with

$$\begin{aligned}
 Z_D = 2 \cosh^2 K_D \cosh L_D \sum_{\sigma_1, \sigma_2 = \pm 1} [& 1 + (\sigma_1 + \sigma_2) \tanh K_D \tanh L_D \\
 & + \sigma_1 \sigma_2 \tanh^2 K_D] \}. \quad (5-16)
 \end{aligned}$$

The partition function for the system shown in Fig. 5.2(b) is given by

$$Z = \sum_{\sigma_1, \sigma_2 = \pm 1} \exp (K \sigma_1 \sigma_2 + L \sigma_1 + L \sigma_2), \quad (5-17)$$

where $K = J/kT$ and $L = mH/kT$. Using arguments previously given (5-17) can be written in the form

$$\begin{aligned}
 Z = & \left(\frac{\cosh K \cosh^2 L}{1 + \tanh K \tanh^2 L} \right) \sum_{\sigma_1, \sigma_2 = \pm 1} [1 + (\sigma_1 + \sigma_2) \\
 & \times \left(\frac{\tanh L + \tanh K \tanh L}{1 + \tanh K \tanh^2 L} \right) + \sigma_1 \sigma_2 \left(\frac{\tanh K + \tanh^2 L}{1 + \tanh K \tanh^2 L} \right)] \}. \quad (5-18)
 \end{aligned}$$

Comparing (5-16) with (5-18) we see that if we require

$$\left. \begin{aligned} \tanh K_D \tanh L_D &= \frac{\tanh L + \tanh K \tanh L}{1 + \tanh K \tanh^2 L} \\ \tanh^2 K_D &= \frac{\tanh K + \tanh^2 L}{1 + \tanh K \tanh^2 L} \end{aligned} \right\} \quad (5-19)$$

the partition functions for the decorated system (Fig. 5.2(a)) and the undecorated system (Fig. 5.2(b)) will be related in the following way:

$$Z_D = \xi Z, \quad (5-20)$$

where

$$\xi = 2 \left(\frac{\cosh^2 K_D \cosh L_D}{\cosh K \cosh^2 L} \right) (1 + \tanh K \tanh^2 L). \quad (5-21)$$

From (5-19) we see that for zero field the relationship between the temperature variables ($K_D = J_D/kT$, $K = J/kT$) of decorated and undecorated Ising lattices is given by

$$\tanh^2 K_D = \tanh K \quad (5-22)$$

or

$$v_D^2 = v. \quad (5-23)$$

In terms of the variable z we have

$$z = 2 z_D / (1 + z_D^2). \quad (5-24)$$

If we apply the decoration transformation (5-20, -21) to a lattice of N sites and coordination number q we will get a decorated lattice of $N + (qN/2)$ sites. The corresponding partition functions will be related by

$$\frac{Z(K_D)}{N + (qN/2)} = \xi^{qN/2} \frac{Z(K)}{N}. \quad (5-25)$$

Applying the decoration transformation to the hydrogen peroxide lattice (Fig. 2.1) we get the decorated hydrogen peroxide lattice (Fig. 2.8). The partition functions of hydrogen peroxide and decorated hydrogen peroxide lattices are related by

$$\frac{Z(K_{DHP})}{5N} = \xi^{3N} \frac{Z(K_{HP})}{2N}, \quad (5-26)$$

where DHP and HP denote the decorated hydrogen peroxide and hydrogen peroxide lattices respectively. We have taken the number of sites on the hydrogen peroxide lattice as $2N$, and since the hydrogen peroxide lattice has a coordination number of three, we obtain $5N$ sites for the decorated hydrogen peroxide lattice.

If we now apply the star-triangle transformation to the open circles (o) of the decorated hydrogen peroxide lattice (Fig. 2.8) we get the hyperkagomé lattice of Fig. 2.9.

The partition functions for these two lattices are related by

$$Z_{5N}(K_{DHP}) = \zeta^{2N} Z_{3N}(K_{HK}), \quad (5-27)$$

where HK denotes the hyperkagomé lattice. The hyperkagomé lattice has only $3N$ sites as $2N$ sites of the decorated hydrogen peroxide lattice are removed in the process of carrying out the star-triangle transformation.

The relationship between the partition functions of the hyperkagomé and hydrogen peroxide lattices is obtained by combining (5-26) and (5-27). For zero magnetic field we have

$$Z_{3N}(K_{HK}) = \left[2 \frac{(\cosh^3 K_{HK} + \sinh^3 K_{HK})^2}{\cosh^3 K_{HP}} \right]^N Z_{2N}(K_{HP}). \quad (5-28)$$

Equation (5-28) enables us to calculate from the hydrogen peroxide lattice the zero field partition function, energy, and specific heat of the hyperkagomé lattice.

The relationship between the temperature variables ($K_{HK} = J_{HK}/kT$, $K_{HP} = J_{HP}/kT$) of hyperkagomé and hydrogen peroxide lattices is obtained from (5-7) and (5-22). The result is

$$\exp(4K_{HK}) = (1 + 3 \tanh K_{HP}) / (1 + \tanh K_{HP}). \quad (5-29)$$

In terms of the variable v we have

$$v_{HP} = (v_{HK} + v_{HK}^2)/(1 + v_{HK}^3), \quad (5-30)$$

and in terms of z we have

$$z_{HK}^2 = z_{HP}/(2 - z_{HP}). \quad (5-31)$$

The development we have outlined above has been concerned only with the transformation from the hydrogen peroxide lattice to the hyperkagomé lattice, which are three dimensional lattices. Exactly the same procedure holds for the transformation from the honeycomb lattice to the kagomé lattice, which are two dimensional lattices. The only change that is required is one of notation, $HP \rightarrow HC$, and $HK \rightarrow K$, where HC and K stand for the honeycomb and kagomé lattices respectively. A very thorough review of the star-triangle and decoration transformations with arbitrary interactions has been given by Fisher (1959(b)).

C. Exact Relationships Between the Thermodynamic Variables

The star-triangle and decoration transformations discussed in the previous section make it possible to determine from the hydrogen peroxide lattice the thermodynamic variables (partition function, energy, specific heat, etc.) of the hypertriangular and hyperkagomé lattices.

The partition functions of star-triangle lattices are related by (5-13), and hence the relationship between the dimensionless Helmholtz free energy per site for star-triangle lattices is given by

$$\frac{L}{2N} \ln Z_{2N}^Y(K^Y) = \frac{1}{2} [\ln z + \frac{1}{N} \ln Z_N^\Delta(K^\Delta)] \quad (5-32)$$

where (c.f. eq'ns 3-9, -10)

$$\frac{1}{2N} \ln Z_{2N}^Y(K^Y) = \ln 2 + \frac{3}{2} \ln \cosh K^Y + \sum_{\ell=1}^{\infty} p_{\ell}^{(1)} v_Y^{\ell} \quad (5-33)$$

and

$$\frac{1}{N} \ln Z_N^\Delta(K^\Delta) = \ln 2 + 3 \ln \cosh K^\Delta + \sum_{\ell=1}^{\infty} p_{\ell}^{(1)} v_{\Delta}^{\ell} \quad (5-34)$$

The meaning of the coefficient $p_{\ell}^{(1)}$ was explained in

(3-13). From (5-8) we have

$$\ln \zeta = \ln 2 + 3 \ln (\cosh K_Y) - 3 \ln (\cosh K_\Delta) - \ln (1 + v_\Delta^3). \quad (5-35)$$

Hence

$$\sum_{\ell=1}^{\infty} p_\ell^{(1)} v_\Delta^\ell = \ln (1 + v_\Delta^3) + 2 \sum_{\ell=1}^{\infty} p_\ell^{(1)} v_Y^\ell, \quad (5-36)$$

where the relationship between v_Y and v_Δ is given by (5-12).

From (5-36) we see that if we know the first $2N$ terms of the free energy for the star lattice (denoted by Y), we can calculate the first N terms of the free energy for the triangle lattice (denoted by Δ). The same holds true for the internal energy and specific heat as they are found from the free energy by differentiation.

In this way we obtained from the series for the free energy of the hydrogen peroxide lattice, for which we have calculated the first twenty-eight terms, the first fourteen terms in the series for the free energy of the hypertriangular lattice. The first twelve terms in the series for the free energy of the hypertriangular lattice were also calculated directly from the hypertriangular lattice (see Appendix A) and as far as they go the two

series agree exactly.

Fisher (1959(b)) has shown how one can relate the initial susceptibilities of star-triangle lattices. The result is simply

$$\bar{\chi}(v_{\Delta}) = 1/2 [\bar{\chi}(+v_Y) + \bar{\chi}(-v_Y)]. \quad (5-37)$$

As was the case with the free energy, the first $2N$ terms in the series for the initial susceptibility for the star lattice give rise to the first N terms in the series for the initial susceptibility of the triangle lattice. Thus from the first twenty-six terms in the susceptibility series for the hydrogen peroxide lattice we obtained the first thirteen terms in the susceptibility series for the hypertriangular lattice. The first twelve terms in the series for the initial susceptibility of the hypertriangular lattice were also calculated independently of the hydrogen peroxide lattice (see Appendix B). The results of the two methods agree exactly, indicating that for both lattices the graphical enumeration is correct.

As was pointed out in Chapter I, in the critical region the specific heat and initial susceptibility can be represented by the asymptotic forms

$$C = A_+ (1 - K/K_c)^{-\alpha} \quad (5-38)$$

$$\bar{\chi} = C_+ (1 - K/K_c)^{-\gamma} \quad (5-39)$$

where A_+ and C_+ denote the amplitude of the specific heat and initial susceptibility respectively. By the use of equation (5-13) and (5-28) we can derive exact expressions, valid in the critical region, which relate the amplitude on one lattice to that of the other lattice.

For example, for star-triangle lattices the partition functions are related by (5-13). Since we are interested only in the singular part of the partition function the factor ϵ in (5-13) can be neglected. Thus for the singular part of the dimensionless Helmholtz free energy per site we have

$$(-f/kT)^\Delta \equiv \frac{1}{N} \ln Z_N^\Delta(K^\Delta) = 2 \left[\frac{1}{2N} \ln Z_{2N}^Y(K^Y) \right] \equiv 2(-f/kT)^Y. \quad (5-40)$$

The specific heat is defined by

$$C = kK^2 \partial^2 (-f/kT) / \partial K^2 \quad (5-41)$$

From (5-10) we have

$$\exp(-4K_c^\Delta) \frac{\partial}{\partial K^\Delta} = (\sinh 2K_c^Y)^{-1} \frac{\partial}{\partial K^Y} \quad (5-42)$$

Hence in the critical region we have

$$(K_Y^C)^2 \exp(-8K_C^\Delta) C^\Delta(K_C^\Delta) = 2(K_C^\Delta)^2 (\sinh 2K_C^Y)^{-2} C^Y(K_C^Y) \quad (5-43)$$

Upon substituting in (5-43) the asymptotic form (5-38)

we get

$$\begin{aligned} (K_C^Y)^2 \exp(-8K_C^\Delta) A_+^\Delta (1 - K^\Delta/K_C^\Delta)^{-\alpha} \\ = 2(K_C^\Delta)^2 (\sinh 2K_C^Y)^{-2} A_+^Y (1 - K_C^Y/K_C^Y)^{-\alpha} \end{aligned} \quad (5-44)$$

Taking the logarithm of (5-44) and applying (5-42) we find

$$K_C^Y \exp(-4K_C^\Delta) (1 - K^\Delta/K_C^\Delta)^{-1} = K_C^\Delta (\sinh 2K_C^Y)^{-1} (1 - K_C^Y/K_C^Y)^{-1} \quad (5-45)$$

From (5-44) and (5-45) we find for the final result

$$A_+^Y/A_+^\Delta = \frac{1}{2} [(K_C^Y/K_C^\Delta) \exp(-4K_C^\Delta) \sinh 2K_C^Y]^{2-\alpha} \quad (5-46)$$

which is valid for star-triangle lattices of arbitrary dimension.

An expression similar to (5-46) can be derived for the amplitude of the susceptibility of star-triangle lattices. For example, on a star-lattice, which has a coordination number of three and $2N$ sites consisting of primed and unprimed sublattices, the reduced initial

susceptibility per site is given by

$$\bar{\chi}^Y = \chi_0^Y / (2Nm^2/kT) = \frac{1}{2} \sum_{i=1}^N (\langle \sigma_i \sigma_i \rangle + 2 \langle \sigma_i \sigma'_i \rangle \langle \sigma'_i \sigma'_i \rangle). \quad (5-47)$$

These three sums are in general distinct, but in the critical region where the spin correlations become long range, the sums become equal, hence

$$\bar{\chi}^Y = 2 \sum_{i=1}^N \langle \sigma_i \sigma_i \rangle = W_{2N}^Y(K^Y) / Z_{2N}^Y(K^Y) \quad (5-48)$$

where

$$W_{2N}^Y(K^Y) = 2 \sum_{i=1}^N \sum_{\sigma_i=\pm 1} \cdots \sum_{\sigma_N=\pm 1} \sigma_i \sigma_i \left(\sum_{\sigma'_1=\pm 1} \cdots \sum_{\sigma'_N=\pm 1} \right) \times \exp K^Y \sum_{i=1}^N \sum_{\delta=1}^3 \sigma'_i \sigma_\delta. \quad (5-49)$$

The subscript δ indicates the three nearest neighbours of the i th spin. The star-triangle relation can be applied to (5-49) and we end up with

$$\bar{\chi}^Y(K^Y) = 2 \bar{\chi}^\Delta(K^\Delta). \quad (5-50)$$

Now proceeding exactly as in the case for the specific heat we find

$$C_+^Y/C_+^\Delta = 2[(K_c^Y/K_c^\Delta) \exp(-4K_c^\Delta) \sinh 2K_c^Y]^{-\gamma}. \quad (5-51)$$

Results similar to (5-46) and (5-51) can be obtained for the hydrogen peroxide and hyperkagomé lattices (honeycomb and kagomé lattices in two dimensions). The procedure is exactly as outlined for the star-triangle lattices except now one has the intermediate decoration process. Instead of (5-13) one now uses (5-28) and in place of (5-42) one has

$$\begin{aligned} \exp(-4K_c^{HK}) \frac{\partial}{\partial K^{HK}} \\ = [(1 - \tanh K_c^{HP})/(1 + \tanh K_c^{HP})] \frac{\partial}{\partial K^{HP}}. \end{aligned} \quad (5-52)$$

The specific heat amplitude relation is given

by

$$\frac{A_+^{HK}}{A_+^{HP}} = \frac{2}{3} \left[\left(\frac{K_c^{HK}}{K_c^{HP}} \right) \exp(4K_c^{HK}) \frac{1 - \tanh K_c^{HP}}{1 + \tanh K_c^{HP}} \right]^{2-\alpha} \quad (5-53)$$

while the amplitudes of the initial susceptibilities are related by

$$\frac{C_+^{HK}}{C_+^{HP}} = \frac{3}{2} \left[\left(\frac{K_c^{HK}}{K_c^{HP}} \right) \exp(4K_c^{HK}) \frac{1 - \tanh K_c^{HP}}{1 + \tanh K_c^{HP}} \right]^{-\gamma} \quad (5-54)$$

For the two dimensional honeycomb and kagomé lattices one has only to make the following change in notation in (5-53) and (5-54): $HP \rightarrow HC$, $HK \rightarrow K$.

The symmetry between (5-46), (5-51) and (5-53), (5-54) is quite obvious. In fact, having derived the amplitude relationships for the star-triangle lattices one could write down by inspection the expressions (5-53) and (5-54). However, (5-53) and (5-54) were derived independently of the results for the star-triangle lattices.

The validity of the expressions (5-46, -51, -53, -54) can be tested for two dimensions. In two dimensions, where the star lattice is the honeycomb lattice and the triangle lattice is the triangular lattice, $\alpha = 0$, $\gamma = 7/4$, $\exp(4K_C^T) = 3$, and $\sinh 2K_C^{HC} = \sqrt{3}$ yield

$$A_+^{HC}/A_+^T = 0.957994\dots$$

and

$$C_+^{HC}/C_+^T = 1.132234\dots$$

in precise agreement with the ratios as quoted, for example, by Fisher (1967). For the kagomé lattice

$\exp(4K_C^K) = 3 + 2\sqrt{3}$ and we find

$$A_+^K/A_+^{HC} = 1.004091\dots$$

and

$$C_+^K/C_+^{HC} = 1.048238\dots$$

The first ratio agrees exactly with the ratio as computed from the individual specific heat amplitude estimates as quoted by Fisher (1967). However, using the estimates of the amplitudes of the susceptibility from Fisher's table we find

$$C_+^K/C_+^{HC} = 0.9723\dots.$$

This 8% discrepancy indicates either that our relation (5-54) is incorrect or that the estimate of the amplitude of the susceptibility of the kagomé lattice is in error. The other three expressions for the amplitude ratios are clearly correct and the fourth, as already pointed out, could be written down by symmetry, and thus we believe (5-54) is correct. Sykes (private communication) has recently reexamined the susceptibility series for the kagomé lattice and could find no error. It is the view of the author that this controversy is still unresolved.

CHAPTER VI

SELF-AVOIDING WALKSA. Relationship To Ising Model

Self-avoiding walks are random walks with the restrictions that there can be no immediate reversals and no self intersections. Hence self-avoiding walks define a non-Markovian process and the statistical properties of such walks are not well known. The generating function for self-avoiding walks is define by

$$C(x) = 1 + \sum_{\ell=1} c_{\ell} x^{\ell} , \quad (6-1)$$

where c_{ℓ} is the number of self-avoiding walks of length ℓ on a lattice. The problem is to determine the asymptotic behaviour of the c_{ℓ} .

The relationship between the self-avoiding walk problem and the Ising model has been studied by Temperley (1956) and by Fisher and Sykes (1959). A more recent review has been given by Domb (1969). It is now generally recognized that the relationship between the two problems is very subtle and not entirely clear. Nonetheless the self-avoiding walk problem provides a very good

approximation to the high temperature ferromagnetic susceptibility of the Ising model. For example, the asymptotic behaviour of self-avoiding walks can be represented by the form

$$C(x) \sim (1-\mu x)^{-\gamma}, \quad (6-2)$$

where μ (the "critical point") is called the attrition parameter and for a very long walk represents the number of ways the walk can be continued for one more step. A rigorous proof of the existence of the attrition parameter was given by Hammersley (1957). The numerical values found for the attrition parameter μ and the index γ in (6-2) differ only by a few per cent from the values of the corresponding quantities for the high temperature ferromagnetic susceptibility of the Ising model.

B. Enumeration of Self-Avoiding Walks

The enumeration of self-avoiding walks is usually carried out in one of two ways, a sampling of walks of very long length via Monte-Carlo techniques (Gans 1965) or an exact enumeration of the first few walks (Martin et al. 1967). In either case the problem can only conveniently be attacked with the aid of a computer.

We have carried out an exact enumeration of self-avoiding walks on the hydrogen peroxide and hyper-triangular lattices. Such a calculation is most easily carried out by means of a chain counting theorem derived by Sykes (1961). In this section we shall briefly outline the derivation of this theorem along the lines originally followed by Sykes.

We focus our attention on a self-avoiding walk of $(n-1)$ steps on a lattice of coordination number q . If we add one more step to the walk in any one of the $(q-1) = \sigma$ allowable directions, one of three things can occur. We can form a self-avoiding walk of n steps, or one of two topologically distinct linear graphs (Fig. 6.1).

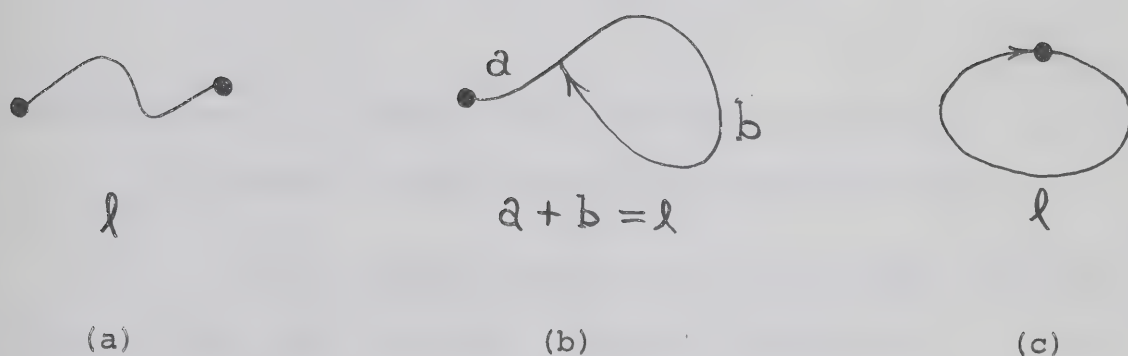


Fig. 6.1. The result of adding a step to a self avoiding walk of $(n-1)$ steps. (a) Self-avoiding walk of l steps. (b) Tadpole, $T_{a,b}$. (c) Polygon, p_l .

In Fig. 6.1, graph (b), which is known as a tadpole, results from a self intersection a steps from the origin. The number of such graphs on a lattice is denoted by $T_{a,b}$. Every tadpole will be walked twice, the head being walked once in each sense. Graph (c) results from a self intersection at the origin. The number of such graphs per site is denoted by p_l , the number through a given point on the lattice is given by lp_l . The l steps

forming the polygon will also be walked twice, once in each sense. We can combine the above statements into an equation of the form

$$c_\ell = \sigma c_{\ell-1} - 2 \sum_{a=1}^{\ell-3} T_{a,\ell-a} - 2\ell p_\ell, \quad (6-3)$$

which gives us a simple recursive relation between c_ℓ and $c_{\ell-1}$ in terms of tadpoles and polygons of order ℓ .

We can extend the idea of the previous paragraph and use the same technique to count the tadpoles. If we add a step to the tail of a tadpole $T_{x-1,y}$, the result will be either a new tadpole $T_{x,y}$ or one of three topologically distinct linear graphs shown in Fig. 6.2.



(a)



(b)



(c)

Fig. 6.2. The three topologically distinct linear graphs that result from the addition of a step to the tail of a tadpole. (a) Dumbbell, $(a,b,c)_{db}$. (b) Figure eight, $(a,b)_8$. (c) Theta graph, $(a,b,c)_\theta$.

For a given lattice the number of dumbbells, figure eights, and theta graphs per site are denoted by $(a,b,c)_{db}$, $(a,b)_8$, and $(a,b,c)_\theta$ respectively. Thus by eliminating the tadpoles the number of self-avoiding walks of order ℓ can be made to depend on four types of topologically distinct linear graphs, namely polygons, dumbbells, figure eights, and theta graphs.

The mathematical steps involved in eliminating the tadpoles from the recursive relation (6-3) are straight forward but rather lengthy and we shall not reproduce them here, but quote only the final result, i.e.

$$c_{\ell+1} - 2\sigma c_\ell + \sigma^2 c_{\ell-1} = 2\ell p - 2(\ell+1)p_{\ell+1} + 8 \sum_{\ell+1} (a,b,c)_{db} \\ + 8 \sum_{\ell+1} (a,b)_8 + 12 \sum_{\ell+1} (a,b,c)_\theta, \quad (6-4)$$

where $\ell > 1$ and the summations are over all dumbbells, figure eights, and theta graphs of order $\ell+1$ on the lattice. Equation (6-4) is known as Sykes' chain counting theorem. The great advantage of this theorem is that the polygons, dumbbells etc. are much less numerous than the walks themselves, resulting in a large saving of computer time, which enables one to calculate walks of higher order

than would otherwise be possible.

Equation (6-4) can be cast into the alternative form

$$\begin{aligned}
 C(x) = & 1 + (1 - \sigma x)^{-2} [qx(1 - \sigma x) - 2(1 - x) \sum_{\ell} \ell \dot{p}_{\ell} x^{\ell} \\
 & + 8 \sum_{\ell} (a, b, c)_{db} x^{\ell} + 8 \sum_{\ell} (a, b)_{\theta} x^{\ell} \\
 & + 12 \sum_{\ell} (a, b, c)_{\theta} x^{\ell}].
 \end{aligned} \tag{6-5}$$

It is perhaps worth mentioning that (6-5) is not simply a restricted form of the susceptibility counting theorem of the Ising model (c.f. eqn. (3-31) Chapter III). If one restricts the susceptibility in the Ising model to a sum over polygons, dumbbells, figure eights, and theta graphs, the counting weights for polygons and theta graphs differ from the counting weights for the same graphs in (6-5). In both cases, (3-31) and (6-5), the counting weights for dumbbells and figure eights remain the same. This simply points out the well known fact that although the expansions for self-avoiding walks and the Ising model susceptibility appear to be similar, there are fundamental differences between the two problems, namely that the counting weights in (6-5) not only depend on the degree of the vertices but also on the topology of the graphs as well.

Using (6-5) we have enumerated walks of up to thirty steps for the hydrogen peroxide lattice and walks of up to fourteen steps for the hypertriangular lattice. The self-avoiding walk generating functions for these two lattices are given by

(Hydrogen Peroxide)

$$\begin{aligned}
 C(x) = & 1 + 3x + 6x^2 + 12x^3 + 24x^4 + 48x^5 + 96x^6 + 192x^7 \\
 & + 384x^8 + 768x^9 + 1506x^{10} + 2982x^{11} + 5904x^{12} \\
 & + 11688x^{13} + 23094x^{14} + 45678x^{15} + 90000x^{16} \\
 & + 177660x^{17} + 349938x^{18} + 690192x^{19} + 1359288x^{20} \\
 & + 2678808x^{21} + 5271558x^{22} + 10381926x^{23} \\
 & + 20419224x^{24} + 40191204x^{25} + 79025742x^{26} \\
 & + 155470668x^{27} + 305587564x^{28} + 600950160x^{29} \\
 & + 1180825386x^{30} + \dots
 \end{aligned} \tag{6-6}$$

and

(Hypertriangular)

$$\begin{aligned}
 C(x) = & 1 + 6x + 30x^2 + 144x^3 + 696x^4 + 3330x^5 + 15774x^6 \\
 & + 74484x^7 + 351192x^8 + 1651806x^9 + 7753182x^{10} \\
 & + 36342882x^{11} + 170163366x^{12} + 795893904x^{13} \\
 & + 3719252820x^{14} + \dots
 \end{aligned} \tag{6-7}$$

The number of polygons, dumbbells, figure eights, and theta graphs of order k embeddable in the hydrogen peroxide and hypertriangular lattices are listed in Appendix J.

CHAPTER VII

ANALYSIS OF SERIES EXPANSIONSA. Methods of Analysis

The thermodynamic functions of the three dimensional Ising model, initial susceptibility, specific heat, spontaneous magnetization, etc., are known to us only through their power series expansions, which for the hydrogen peroxide and hypertriangular lattices have been derived by methods outlined in previous chapters. From these series we hope to locate the position of the critical point and predict the behaviour of the various thermodynamic functions near the critical point.

Power series expansions for the Ising model generally fall into three categories (see C. Domb in Proceedings of the International Conference on Phenomena near Critical Points 1965):

- (1) The coefficients are all of the same sign,
- (2) The coefficients alternate in sign,
- (3) The magnitudes and signs of the coefficients exhibit more complicated behavior than (1) or (2).

In (1) the dominant singularity (the physical singularity or

critical point) lies on the positive real axis, while in (2) the dominant singularity lies on the negative real axis and in (3) the dominant singularity lies elsewhere in the complex plane. We are primarily interested in series of type (1) or (2).

For the Ising model of a ferromagnet in zero field we expect to find a singularity on the positive real axis (the Curie point or critical point) and possibly a singularity on the negative real axis corresponding to the antiferromagnetic Néel point.

The power series for the high temperature initial susceptibility of the spin one-half Ising model ferromagnet is of type (1) for all regular lattices and experience has shown this series to be the most useful for obtaining estimates of the critical point. The power series for the spontaneous magnetization of the hydrogen peroxide lattice is also of type (1), the only three dimensional lattice other than diamond for which this is so.

Assuming that the asymptotic form of the thermodynamic functions of the three dimensional Ising model is the same as that for the two dimensional Ising model (see Chap. I), i. e.

$$W(x) \approx A (1 - x/x_C)^{-P} \quad x \rightarrow x_C, \quad (7-1)$$

there are two methods which have been shown capable of giving accurate results from an analysis of the power series expansions. These two methods are the ratio method (Domb and Sykes 1961) and the Padé approximant method (Baker 1961).

The ratio method follows directly from (7-1), where the ratio of successive terms is given by

$$a_n/a_{n-1} \approx \mu_C [1 + (p-1)/n], \quad (7-2)$$

where $\mu_C = 1/x_C$. Provided the assumption (7-1) is valid and the convergence of the series is fairly rapid, a plot of a_n/a_{n-1} against $1/n$ should yield a straight line. The intercept of this line with the $(1/n) = 0$ axis gives the critical point μ_C , and from the slope one can find the critical index p , i. e. slope = $\mu_C(p-1)$.

Given an estimate of the critical point we can obtain successive estimates of the critical index p from the relation

$$(p)_n = 1 + n [(\mu_n/\mu_C) - 1], \quad (7-3)$$

where $\mu_n = a_n/a_{n-1}$. If we have an accurate estimate of the critical index p , a refined estimate of the critical point can be obtained by calculating the successive estimates

$$(\mu_C)_n = (n\mu_n)/(n + p-1). \quad (7-4)$$

Provided we have accurate estimates of both the critical point μ_C and the critical index p we can obtain successive estimates of the amplitude A by factoring out of the n th term of the power series expansion that part arising from the binomial expansion, i. e.

$$(A)_n = a_n / \binom{n+p-1}{n} \mu_C^n. \quad (7-5)$$

The Padé approximant method, which was first applied to the Ising model by Baker (1961), approximates a function by the ratio of two polynomials. The (L, M) Padé approximant to a power series is defined by

$$W(x) = \frac{Q_L(x)}{P_M(x)} = \frac{b_0 + b_1x + b_2x^2 + \dots + b_Lx^L}{c_0 + c_1x + c_2x^2 + \dots + c_Mx^M}. \quad (7-6)$$

The coefficients $b_0, b_1, \dots, b_L, c_0, c_1, \dots, c_M$ are calculated by requiring the expansion of the right hand side of (7-6) to agree exactly with the given power series, $W(x)$, through order $(L + M) \leq R$, where R is the order of the term at which $W(x)$ terminates.

In order to use the Padé approximant method most effectively for the type of functions we are dealing with one takes the logarithmic derivative of (7-1),

$$(d/dx) \ln W(x) \approx -p/(x-x_C), \quad (7-7)$$

a process which converts the singularity into a simple pole. The (L,M) Padé approximant has M simple poles in its denominator and hence there is the possibility that the Padé approximant may be able to locate the pole we are seeking.

If we have an accurate estimate of the critical index p we can obtain estimates of the critical point by forming Padé approximants to

$$[W(x)]^{1/p} \approx -A^{1/p} x_C / (x - x_C) \quad (7-8)$$

which has a simple pole at $x = x_C$.

Having obtained estimates of the critical point from Padé approximants to (7-7) or (7-8) we can use that estimate to obtain estimates of the critical index p by forming Padé approximants to

$$(x - x_C) (d/dx) \ln W(x) = -p \quad (7-9)$$

and evaluating them at the critical point $x = x_C$. Another technique for obtaining estimates of the critical index was introduced by Baker et al. (1967). This method consists of forming Padé approximants to the function

$$(d/dx) \ln [(d/dx) W(x)] / (d/dx) \ln W(x) = (p + 1)/p \quad (7-10)$$

and evaluating them at the critical point.

One can also use the Padé approximant method to calculate estimates of the amplitude. Taking Padé approximants to the function

$$(x-x_c) [W(x)]^{1/p} = -A^{1/p} x_c, \quad (7-11)$$

and evaluating them at the critical point we can get estimates of A.

B. The Ising Model

The series expansions derived in Chapter III and IV have been analyzed using the methods outlined in the previous section. The results of a Padé approximant analysis are most conveniently displayed in the form of a table consisting of a rectangular array of the (L,M) approximants. As we have several such tables they have been grouped together to form Appendix K. The results of the ratio analysis are displayed in Fig. 7.1 and Table 7.1.

The series expansion for the high temperature initial susceptibility of the hypertriangular lattice was analyzed first. Since it has been rather well established for some time that the susceptibility critical index $\gamma = 5/4$, we have obtained estimates of the critical point, v_C , from Padé approximants to $[\chi(v)]^{4/5}$, as shown in Table K.1. Without assuming a value for γ , estimates of v_C were obtained from $(d/dv) \ln \chi(v)$, and are listed in Table K.2. The two methods yield results consistent to five decimal places. Taking as our best estimate of the critical point of the hypertriangular lattice, $v_C = 0.222087 \pm 0.000005$ from Table K.1, estimates of γ were obtained from Padé approximants to $(v_C - v) (d/dv) \ln \chi(v)$

and are listed in Table K.3. Estimates of γ obtained from Padé approximants to $(d/dv)[\ln(d/dv) \chi(v)]/(d/dv) \ln \chi(v)$ are listed in Table K.4. The results of the two methods are quite consistent and to four decimal places the entries of Table K.3 are consistent with $\gamma = 5/4$.

The amplitude, $C_+(v_C)$, of the susceptibility singularity in $\chi(v) \approx C_+(1-v/v_C)^{-\gamma}$ has been estimated from Padé approximants to $(v_C-v) [\chi(v)]^{4/5}$; the results are shown in Table K.5. Padé approximant estimates of the dimensionless free energy per site and internal energy, evaluated at the critical point, are given in Tables K.6 and K.7 respectively. Finally, estimates of the amplitude, $A_+(K_C)$, of the specific heat singularity in $C(K) \approx A_+(1-K/K_C)^{-\alpha}$ were obtained from Padé approximants to $(K-K_C) \{ (d^2/dK^2) C(K) \}^{1/(2+\alpha)}$ and are listed in Table K.8.

The high temperature series expansions for the hydrogen peroxide lattice have been analyzed in the same way as those for the hypertriangular lattice, with one important difference. Our best estimate of the critical point v_C of the hydrogen peroxide lattice, taken from Table K.9 is $v_C = 0.51815 \pm 0.00006$. However, using our best estimate of the critical point of the hypertriangular lattice, $v_C = 0.222087 \pm 0.000005$, and the star-triangle

relation (5-12), we get $v_c = 0.518140 \pm 0.000006$ for the critical point of the hydrogen peroxide lattice. It is this latter estimate that we have used in calculations requiring an estimate of the critical point of the hydrogen peroxide lattice. As an indication of the precision that has been achieved in estimating the critical points of the hypertriangular and hydrogen peroxide lattices, it may be noted that the best estimates obtained from Tables K.1 and K.9 satisfy the relation (5-12) to five figures with an error of only 4 parts in 10^5 .

We have also used the ratio method to analyze the susceptibility and specific heat series of the hypertriangular lattice and the susceptibility series of the hydrogen peroxide lattice. A plot of b_n/b_{n-1} against $1/n$ for the susceptibility of the hypertriangular lattice is given in Fig. 7.1, where $g = \gamma - 1$ and $\mu_c = 1/v_c$. A comparison of the estimates listed in Table 7.1 with the corresponding estimates obtained from Padé analysis shows that the two methods have yielded consistent results.

For the hydrogen peroxide lattice it was not possible to obtain any meaningful estimates for the specific heat singularity amplitude. In principle it is possible to obtain A_+^{HP} from A_+^{HT} using (5-46). However,

Fig. 7.1. Plot of successive ratios b_n/b_{n-1} against $1/n$ for the initial susceptibility of the hypertriangular lattice. $\mu_c = 1/v_c$, $g = \gamma - 1$.

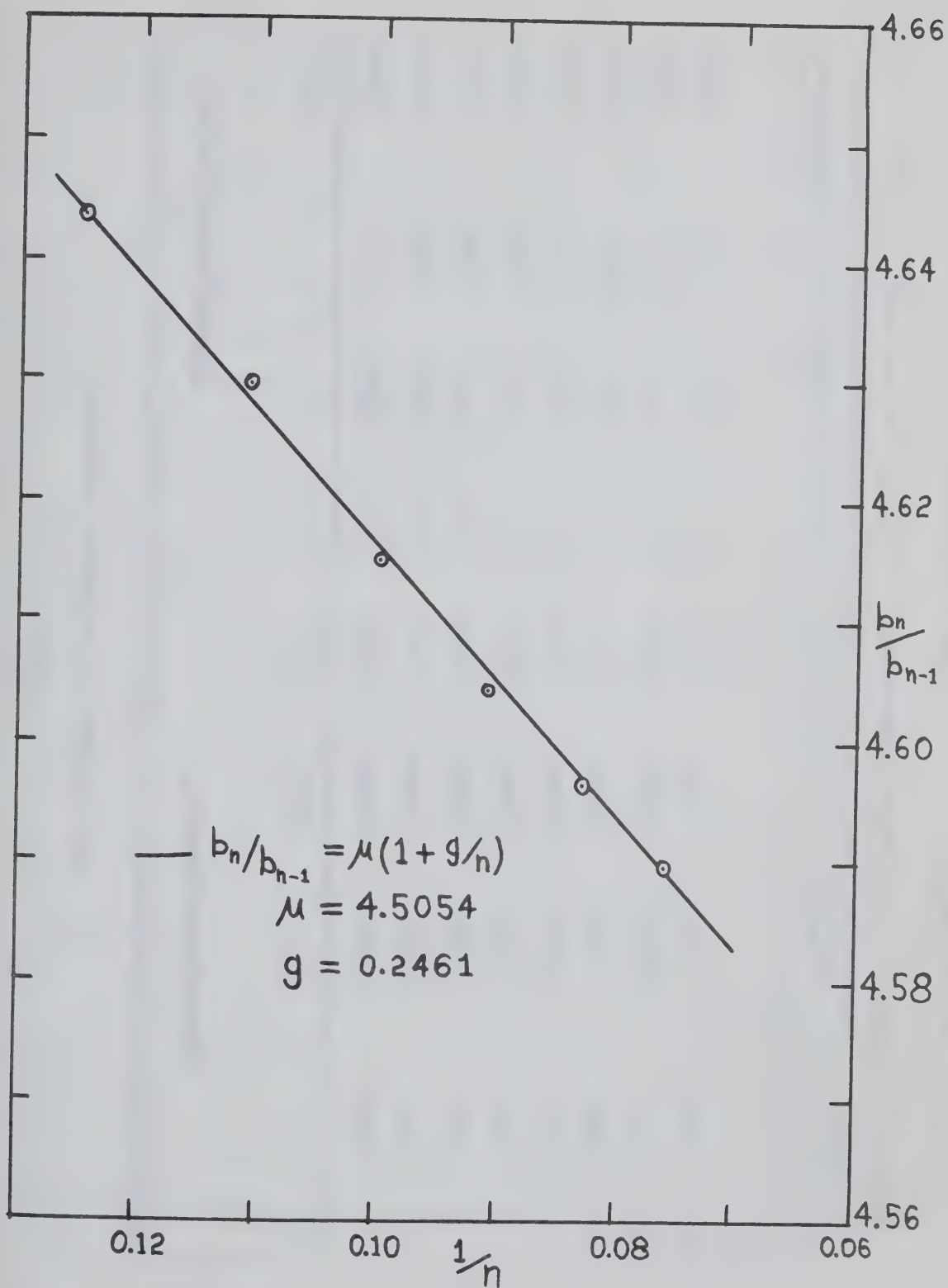


TABLE 7.1
Ratio estimates of the critical parameters

hypertriangular lattice*				hydrogen peroxide lattice				
n	μ_c	γ	$C_+(v_c)$	$A_+(K_c)$	n	μ_c	γ	$C_+(v_c)$
6	4.5011	1.2478	1.04102	2.115	20	1.9305	1.2550	1.0454
7	4.4964	1.2401	1.03956	1.508	21	1.9312	1.2629	1.0461
8	4.5029	1.2504	1.03960	0.496	22	1.9290	1.2380	1.0455
9	4.5046	1.2538	1.04002	0.834	23	1.9297	1.2468	1.0454
10	4.5025	1.2490	1.03997	1.492	24	1.9288	1.2357	1.0448
11	4.5019	1.2486	1.03979	1.320	25	1.9295	1.2440	1.0445
12	4.5027	1.2496	1.03978	0.917	26	1.9296	1.2452	1.0443
13	4.5030	1.2509	1.03984	0.998	27	1.9301	1.2522	1.0444
14				1.238				

* The estimates for γ , C_+ , and A_+ for the hypertriangular lattice were obtained using the best estimate $v_c = 0.222087$. Estimates for γ and C_+ for the hydrogen peroxide lattice were obtained using the best estimate $v_c = 0.518140$. In calculating estimates for μ_c , C_+ , and A_+ we have taken $\gamma = 5/4$ and $\alpha = 1/8$.

$$\mu_c = v_c^{-1} = (nb_n/b_{n-1})(n + \gamma - 1) \qquad \gamma = 1 + n [v_c (b_n/b_{n-1}) - 1]$$

$$C_+(v_c) = b_n v_c^n / (v_c^n + \gamma - 1) \qquad A_+(K_c) = d K_c^n / (v_c^n + \alpha - 1)$$

we have only rough estimates of A_+^{HT} (c.f. Tables K.8 and 7.1) and so we can do no better for A_+^{HP} .

Precise estimates of the amplitude of the susceptibility have been obtained for both lattices and thus a comparison with the ratio predicted by (5-51) is possible. From (5-51), taking $K_C^{HT} = 0.225850$ and $K_C^{HP} = 0.573794$ we find

$$C_+^{HP}(K_C)/C_+^{HT}(K_C) = 1.248055,$$

whereas from separate estimates from Tables K.5 and K.13 we find

$$C_+^{HP}(K_C)/C_+^{HT}(K_C) = 1.2488,$$

where

$$C_+(K_C) = (\sinh 2K_C/2K_C)^Y C_+(v_C).$$

The coefficients in the low temperature series expansions for the hydrogen peroxide lattice are all of the same sign and thus the dominant singularity is the physical singularity or critical point. As pointed out in Section A of this chapter the ratio method is applicable to such series. However, the convergence of the various low temperature series expansions for the hydrogen peroxide lattice has proven to be painfully slow and as a consequence

it has been impossible to draw any conclusion about the behaviour of these functions from a ratio analysis. By necessity then we have been forced to rely solely on the Padé approximant method.

In Table K.16 we have listed for the hydrogen peroxide lattice, estimates of the critical point $z_c = \exp(-2J/kT_c)$ obtained from Padé approximants to $(d/dz) \ln I(z)$. A critical point given by $z_c = 0.316 \pm 0.002$ is consistent with the entries of Table K.16. However, our best estimate of the critical point of the hydrogen peroxide lattice is given by $v_c = 0.518140 \pm 0.000006$, or since $z_c = (1-v_c)/(1+v_c)$ by $z_c = 0.317402 \pm 0.000005$. It is this value that we have used in all calculations requiring an estimate of z_c .

Estimates of the critical indices α' , β and γ' , the critical indices of the specific heat, spontaneous magnetization, and susceptibility respectively, have been obtained by employing the Padé approximant method as given by (7-10). The estimates of β given in Table K.17 are consistent with the value $\beta = 0.305 \pm 0.005$. The estimates of γ' listed in Table K.18 show a fair amount of scatter and no one particular value occurs with any frequency. However, as it is generally thought that the

diagonal and near diagonal Padé approximants are the most reliable, we estimate $\gamma' = 1.27 \pm 0.02$. Estimates of α' given in Table K.19 like those of β are fairly consistent, and we take as our best estimate $\alpha' = 0.23 \pm 0.01$.

In Table K.20 we have listed estimates of $(-f_c/kT_c)$ (the dimensionless free energy per site) obtained from Padé approximants to f/kT evaluated at the critical point. As our best estimate we take $(f_c/kT_c) = 0.931$, which to three figures agrees exactly with the estimate obtained from the high temperature series.

We have also calculated estimates of the critical energy by forming Padé approximants to $U(z)/J$ and evaluating them at the critical point. These results are shown in Table K.21. The entries in Table K.21 seem to indicate a value for U_c/kT_c of ≈ 0.51 . However, it should be noted that the (8,8) Padé approximant, a diagonal approximant making use of all the terms of the series, is in good agreement with the high temperature result $U_c/kT_c = -0.479$. Since the entropy is related to the free energy and the internal energy through (3-28), our best estimate of the critical entropy for the hydrogen peroxide lattice obtained from low temperature series expansions is $S_c/k = 0.458$, as opposed to the high temperature estimate of $S_c/k = 0.451$.

C. The Self-Avoiding Walk Problem

The generating functions for self avoiding walks on the hypertriangular and hydrogen peroxide lattices have also been analyzed by the ratio and Padé approximant methods. In Fig. 7.2 we have plotted the ratios of successive terms of $C(x)$ for the hypertriangular lattice. Nearly all the points lie on a straight line, which indicates that (7-1) is probably a valid assumption for this problem also. From Fig. 7.2 we estimate that $\mu = 4.6179$ and $g = 0.1665$, from which we conjecture that $g = 1/6$ exactly, in agreement with estimates from other three dimensional lattices (Essam and Sykes 1963, Martin et al. 1967, Guttman et al. 1968).

In Table 7.2 we have listed estimates of the attrition parameter μ , and the singularity amplitude A , for the hypertriangular and hydrogen peroxide lattices. The estimates of the attrition parameter are calculated from (7-4) and the estimates of the amplitude from (7-5). In calculating both μ_n and A_n we have assumed $g = 1/6$ exactly. For the hypertriangular lattice the limiting value of μ in Table 7.2 agrees very well with the value of μ taken from Fig. 7.2, which indicates that the conjecture $g = 1/6$ is probably correct.

Because of a very troublesome oscillation in the

Fig. 7.2. Plot of successive ratios c_n/c_{n-1} against $1/n$ for the self-avoiding walk generating function of the hypertriangular lattice.

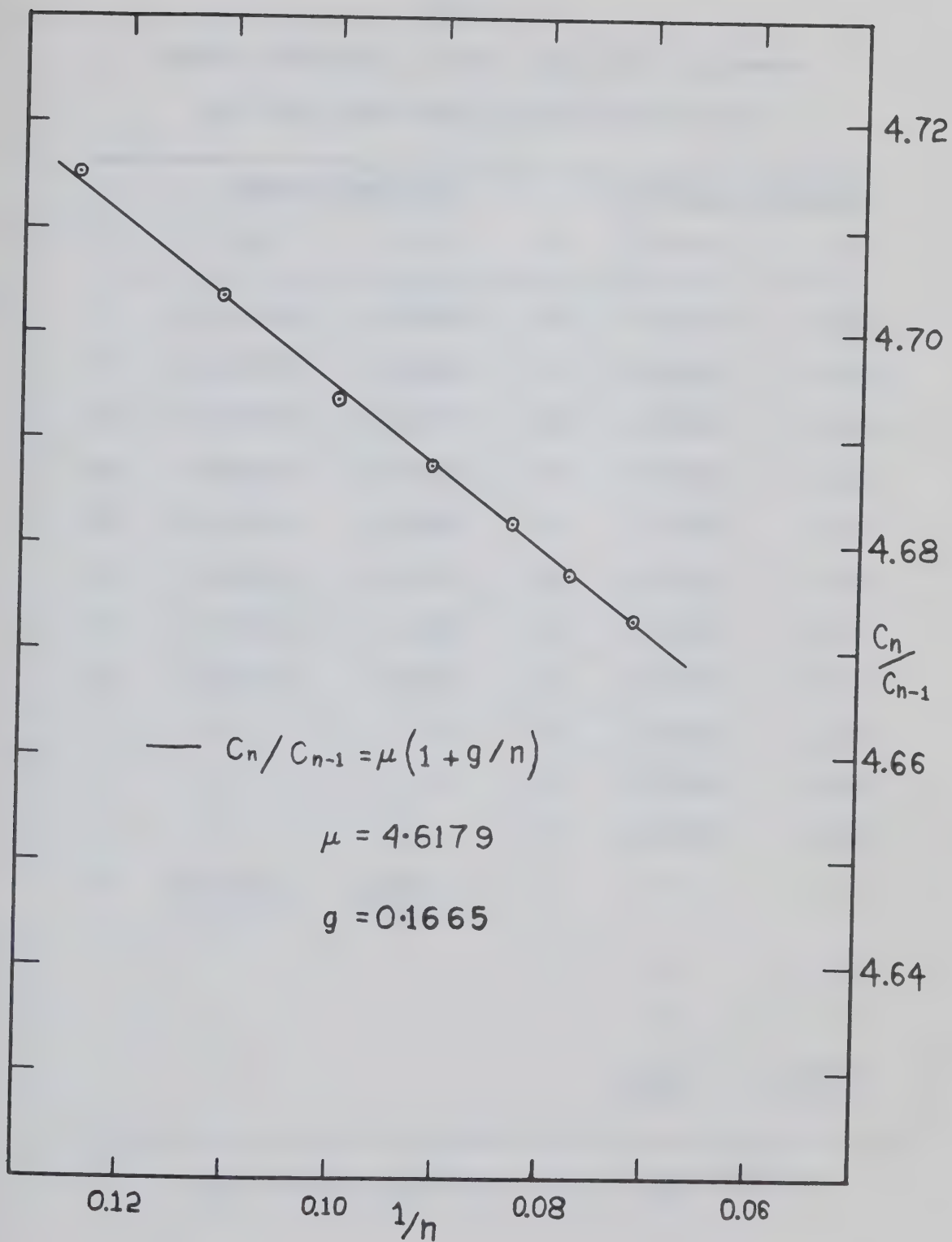


TABLE 7.2

Ratio estimates of the attrition parameter
and the amplitude of the singularity

Hypertriangular			Hydrogen Peroxide		
n	μ_n	A_n	n	$\frac{1}{2}(\mu_n + \mu_{n-1})$	A_n
7	4.612135	1.09898	20	1.95417	1.1226
8	4.618775	1.09894	21	1.95419	1.1216
9	4.617910	1.09870	22	1.95415	1.1194
10	4.616814	1.09819	23	1.95416	1.1184
11	4.617517	1.09786	24	1.95424	1.1163
12	4.618026	1.09764	25	1.95426	1.1153
13	4.618029	1.09742	26	1.95450	1.1135
14	4.618074	1.09722	27	1.95450	1.1125
'	---	---	28	1.95460	1.1108
'	---	---	29	1.95462	1.1099
'	---	---	30	1.95469	1.1083
∞	4.6181 ± 0.0046	1.095 ± 0.011	'	---	---
			'	---	---
			'	---	---
			∞	1.956 ± 0.020	1.10 ± 0.11

$$\mu_n = (nc_n/c_{n-1})/(n+g) \quad A_n = c_n \mu_\infty^n / \binom{n+g}{n}$$

ratios of successive terms of $C(x)$ for the hydrogen peroxide lattice, we have calculated an average of successive pairs of estimates of μ . For the same reason we have not attempted to estimate μ and g for the hydrogen peroxide lattice from a ratio plot such as Fig. 7.2.

We have also obtained estimates of the inverse of the attrition parameter using the Padé approximant method (see Table K.22 and Table K.23 of Appendix K). These estimates are quite consistent with those obtained from the ratio method.

On the basis of successive estimates of the attrition parameter and singularity amplitude shown in Table 7.2 our best estimates for the hydrogen peroxide lattice are $\mu = 1.956 \pm 0.020$, $A = 1.10 \pm 0.11$, and for the hypertriangular lattice they are $\mu = 4.6181 \pm 0.0046$ and $A = 1.095 \pm 0.011$.

CHAPTER VIII

REVIEW AND DISCUSSIONA. The Ising Model

Our primary goal in this work as stated in the Introduction was to obtain improved estimates of the low temperature critical indices of the three dimensional Ising model. It is the opinion of the author that we have obtained improved estimates of the low temperature critical indices, though admittedly we have not obtained the precision we had hoped for. However, we intend to pursue this problem in the future with the hope of extending the low temperature series. This combined with a more sophisticated analysis should shed further light on this problem.

The first stage of this work consisted in deriving high temperature series expansions for the hydrogen peroxide and hypertriangular lattices. The reason for this was to obtain a highly precise value for the critical temperature of the hydrogen peroxide lattice. This precision was achieved by first obtaining a highly precise estimate of the critical temperature of the hypertriangular lattice from the series expansion for the initial susceptibility and then using the star-triangle transformation to obtain the final estimate

for the critical temperature of the hydrogen peroxide lattice.

A further result of this work is that critical parameters for the three dimensional Ising model are now known for the very lowest coordination number, i.e. $q=3$, hence we are in a position to examine the dependence of these parameters on coordination number. In Table 8.1 we have tabulated most of the known results for the two dimensional Ising model. For the three dimensional Ising model we have listed the critical parameters in Table 8.2. For a given dimension the linear chain represents the lower limit of coordination number ($q=2$) while the mean field theory represents the upper limit ($q=\infty$). Although Tables 8.1 and 8.2 represent almost all that is known about high temperature lattice dependent critical parameters, the dependence of these parameters on coordination number is better appreciated when displayed graphically.

In Fig. 8.1 we have displayed the dependence of $v_c = \tanh(J/kT_c)$ on coordination number q for two and three dimensional lattices. The letters labelling the calculated critical temperatures are obvious abbreviations for the lattices listed in Tables 8.1 and 8.2. The curves are not a best fit to all the calculated points but are obtained by a simple procedure. They represent the function

TABLE 8.1

High temperature critical properties of the two dimensional Ising model

Lattice	q	v_c	K_c	$A_+(K_c)$	$C_+(K_c)$	$-U_c/kT_c$	S_c/k	$p_c/\rho_c kT_c$
linear chain	2	1	∞	0	∞	∞	0	0
decorated honeycomb	12/5	0.7598357	0.9958263					
honeycomb	3	0.5773503	0.6584788	0.478106	1.0466	0.760346	0.26471	0.07468
kagome	4	0.4354206	0.4665661	0.480062	1.0176	0.694266	0.28052	0.08330
square	4	0.4142136	0.4406868	0.494538	0.9627	0.623225	0.30647	0.09664
triangular	6	0.2679492	0.2746531	0.499070	0.9244	0.549306	0.33028	0.11126
sq.(1,2) *	8	0.1879	0.1901		0.830	0.456	0.361	0.113
t(1,2)	12	0.1131	0.1136			0.330	0.443	0.183
sq.(1,2,3)	12	0.1130	0.1135		0.641	0.316	0.453	0.176
t(1,2,3)	18	0.0711	0.0712		0.559	0.222	0.511	0.184
mean field	∞	0	0	0	0	0	ln2	2ln2-1
							≈ 0.69315	≈ 0.38630

* sq(1,2) means a square lattice with equal first and second neighbour interactions.

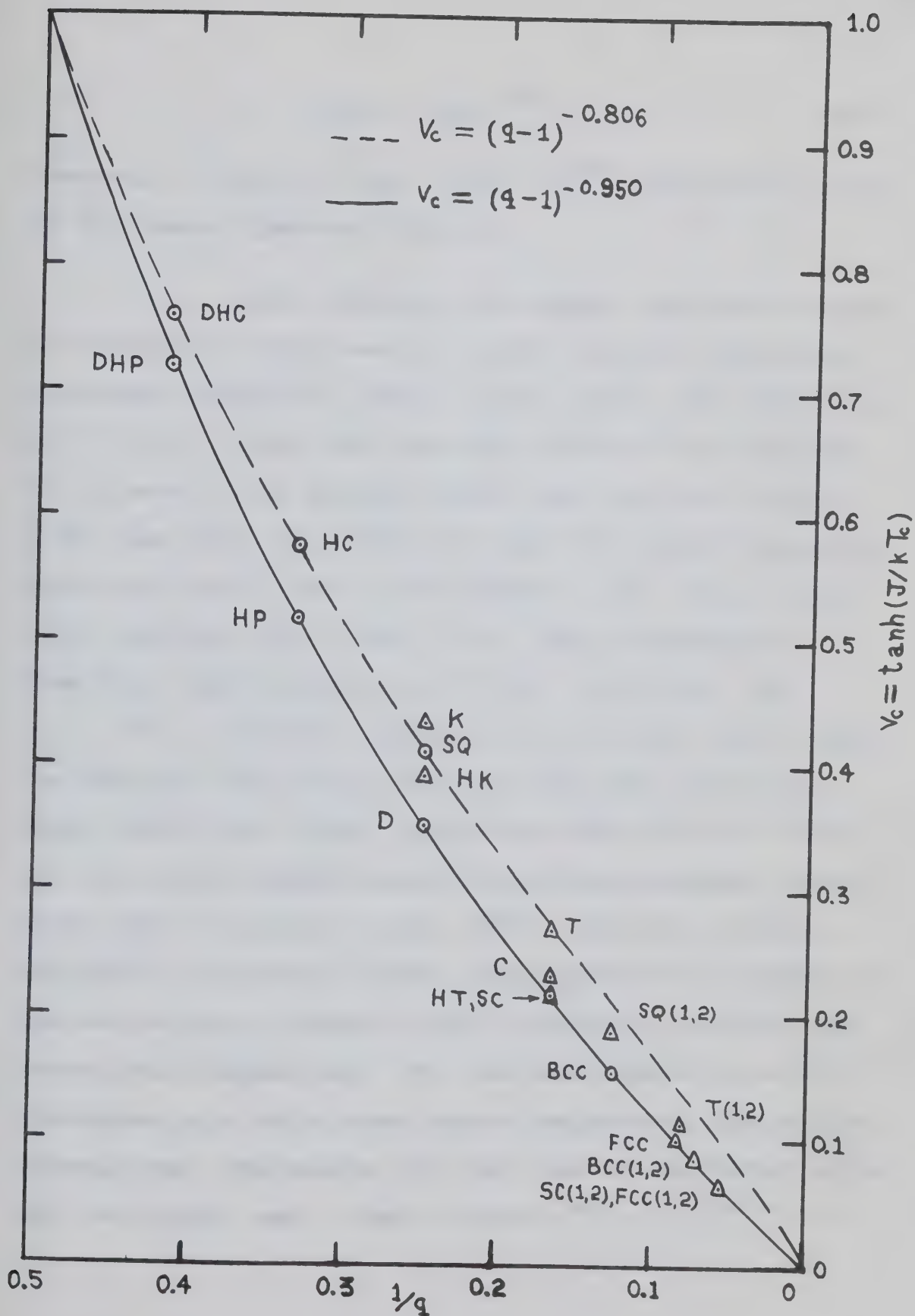
Following symbols have analogous meanings.

TABLE 8.2

High temperature critical properties of the three dimensional Ising model

Lattice	q	v_c	K_c	$A_+(K_c)$	$C_+(K_c)$	$-U_c/kT_c$	S_c/k	$p_c/\rho kT_c$
linear chain	2	1	∞	0	∞	∞	0	0
decorated hydrogen peroxide	12/5	0.719819	0.407269					
hydrogen peroxide	3	0.518140	0.573794	-1.20	1.353583	0.480	0.451	0.141
hyperkagome	4	0.394384	0.416982	-1.17	1.579062			
diamond	4	0.35383	0.36982	-1.2	1.1741	0.320	0.511	0.183
cristobalite	6	0.2330	0.2374		1.100	0.268	0.548	0.208
hypertriangular	6	0.222087	0.225850	-1.18	1.084554	0.228	0.558	0.217
simple cubic	6	0.21815	0.22171	-1.13	1.0604	0.2184	0.560	0.226
body centered cubic	8	0.15617	0.15746	-1.11	0.9929	0.170	0.586	0.252
face centered cubic	12	0.10175	0.10210	1.091	0.975	0.150	0.591	0.258
b.c.c. (1,2)	14	0.0857	0.0859		0.947	0.129	0.607	0.269
s.c. (1,2)	18	0.0644	0.0645		0.878	0.098	0.628	0.291
f.c.c. (1,2)	18	0.0644	0.0645		0.878	0.098	0.628	0.291
s.c. (1,2,3)	26	0.0432	0.0432		0.825	0.069	0.637	0.289
b.c.c. (1,2,3)	26	0.0429	0.0429		0.796	0.066	0.643	0.303
f.c.c. (1,2,3)	42	0.0257	0.0257		0.733	0.041	0.665	0.333
mean field	∞	0	0	0	0	0	$\ln 2$	$2\ln 2 - 1$
							≈ 0.693	≈ 0.386

Fig. 8.1. The dependence of the critical point, $v_c = \tanh(J/kT_c)$, on coordination number q for two and three dimensional Ising models. Circles indicate calculated points for loose-packed lattices; triangles, close-packed lattices. The dashed curve represents the function $v_c = (q-1)^{-0.806}$; the solid curve the function $v_c = (q-1)^{-0.950}$.



$$v_c(q) = (q-1)^{-a_d}, \quad (8-1)$$

where a_d is chosen so that $v_c(2d) = v_c^{\text{shc}}$, the critical point of the simple hypercubic lattice.

In two dimensions the simple hypercubic lattice is the square lattice and $a_2 = 0.806$; in three dimensions the simple hypercubic lattice is the simple cubic lattice and $a_3 = 0.950$. We see that the curve for $d=3$ is an excellent fit to most of the critical points over the whole range of q and thus (8-1) has predictive value for higher dimensions. Fisher and Gaunt (1964) have computed v_c for simple hypercubic lattices only in four, five, and six dimensions. From their data we obtain $a_4 = 0.984$, $a_5 = 0.996$, and $a_6 = 1.000$. Since the completion of this work, Moore (1969) has obtained the critical points of the four dimensional hyper-simple cubic (hsc), hyper-body-centered cubic (hbcc), and hyper-face-centered cubic (hfcc) Ising lattices. Moore found $v_c^{\text{hsc}} = 1/6.725 = 0.149$, $v_c^{\text{hbcc}} = 1/14.510 = 0.0690$, and $v_c^{\text{hfcc}} = 1/21.984 = 0.0455$. The coordination numbers of the hsc and hfcc lattices in four dimensions are eight and twenty-four respectively. For the hbcc lattice Moore has considered only the sixteen nearest neighbours lying on the crystal axes, overlooking the eight nearest neighbours lying off the crystal axes. Hence, taking $q^{\text{hsc}} = 8$, $q^{\text{hbcc}} = 16$,

$q^{hfcc} = 24$, and using (8-1) we find $v_C^{hsc} = 0.149$,
 $v_C^{hbcc} = 0.0700$, and $v_C^{hfcc} = 0.0460$, all in excellent
 agreement with Moore's results and further substantiating
 the usefulness of (8-1) for estimating critical points of
 Ising models.

The amplitude of the specific heat singularity,
 A_+ , is rather insensitive to q and also is not well known
 for most lattices. C_+ , on the other hand, is well deter-
 mined for most lattices and varies appreciably from lattice
 to lattice. However, the variation depends strongly on other
 aspects of lattice structure besides q . Hence we have not
 displayed graphically the q dependence of either A_+ or C_+ .
 The critical energy and entropy both vary rather smoothly
 with q as illustrated in Figs. 8.2 and 8.3, but no such
 simple expression as (8-1) has been found for these quantities.

As is well known, the Ising model serves as a
 model for a lattice gas (Yang and Lee 1952) so we have com-
 puted the critical ratios (Fisher 1964(b)).

$$P_C/\rho_C kT_C = 2[S_C/k - U_C/kT_C - q/2K_C]. \quad (8-2)$$

The dependence of the critical ratio on coordination number
 is displayed in Fig. 8.4.

Fig. 8.2. The dependence of the critical energy, U_c , on coordination number, q , for two and three dimensional Ising models. Circles indicate calculated points for loose packed lattices; triangles, close packed-lattices. The top curve is a best fit for two dimensions; the bottom curve for three dimensions.

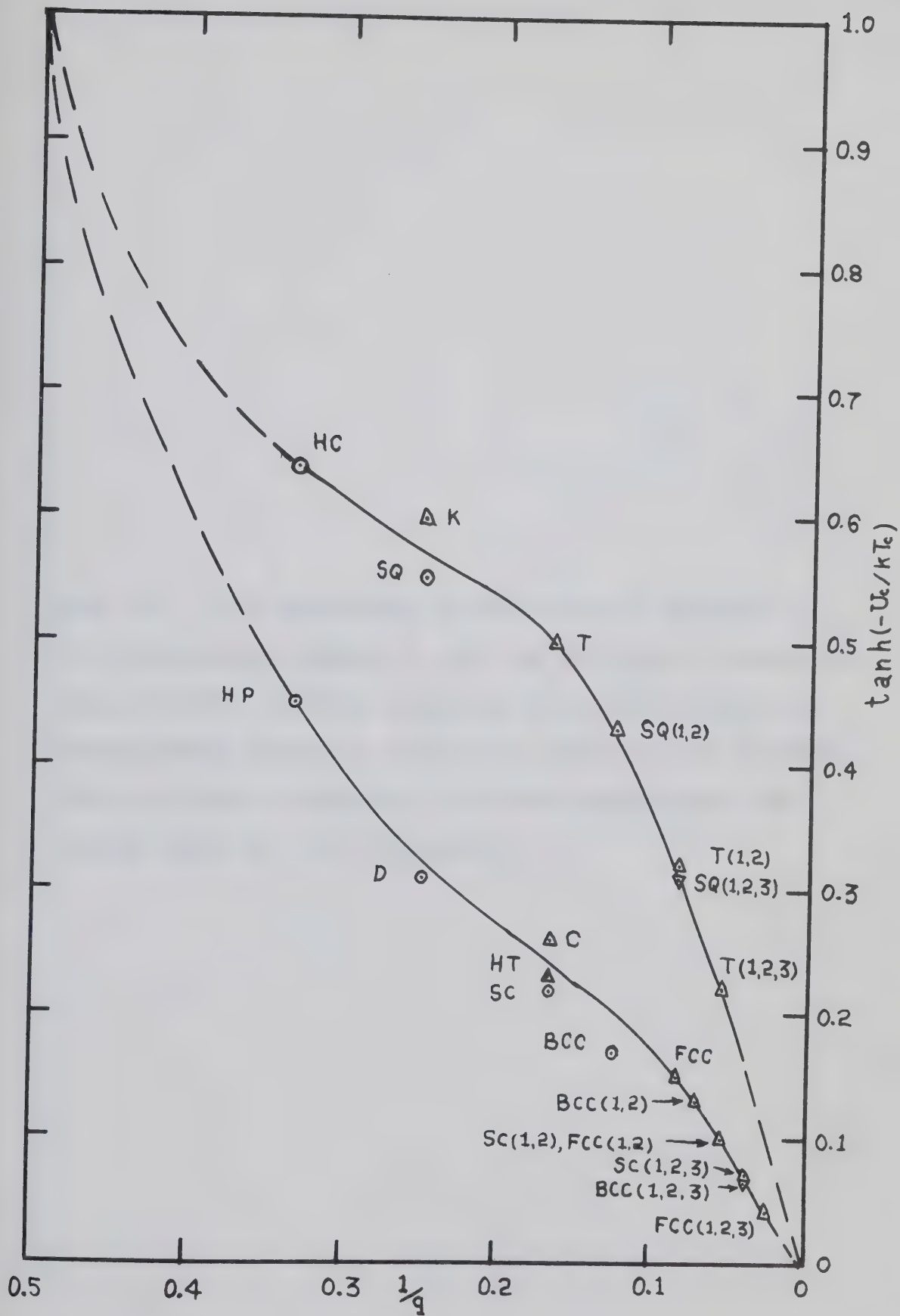


Fig. 8.3. The dependence of the critical entropy, S_c , on coordination number, q , for two and three dimensional Ising models. Circles indicate calculated points for loose-packed lattices; triangles, close-packed lattices. The top curve is best fit for three dimensions; the bottom curve for two dimensions.

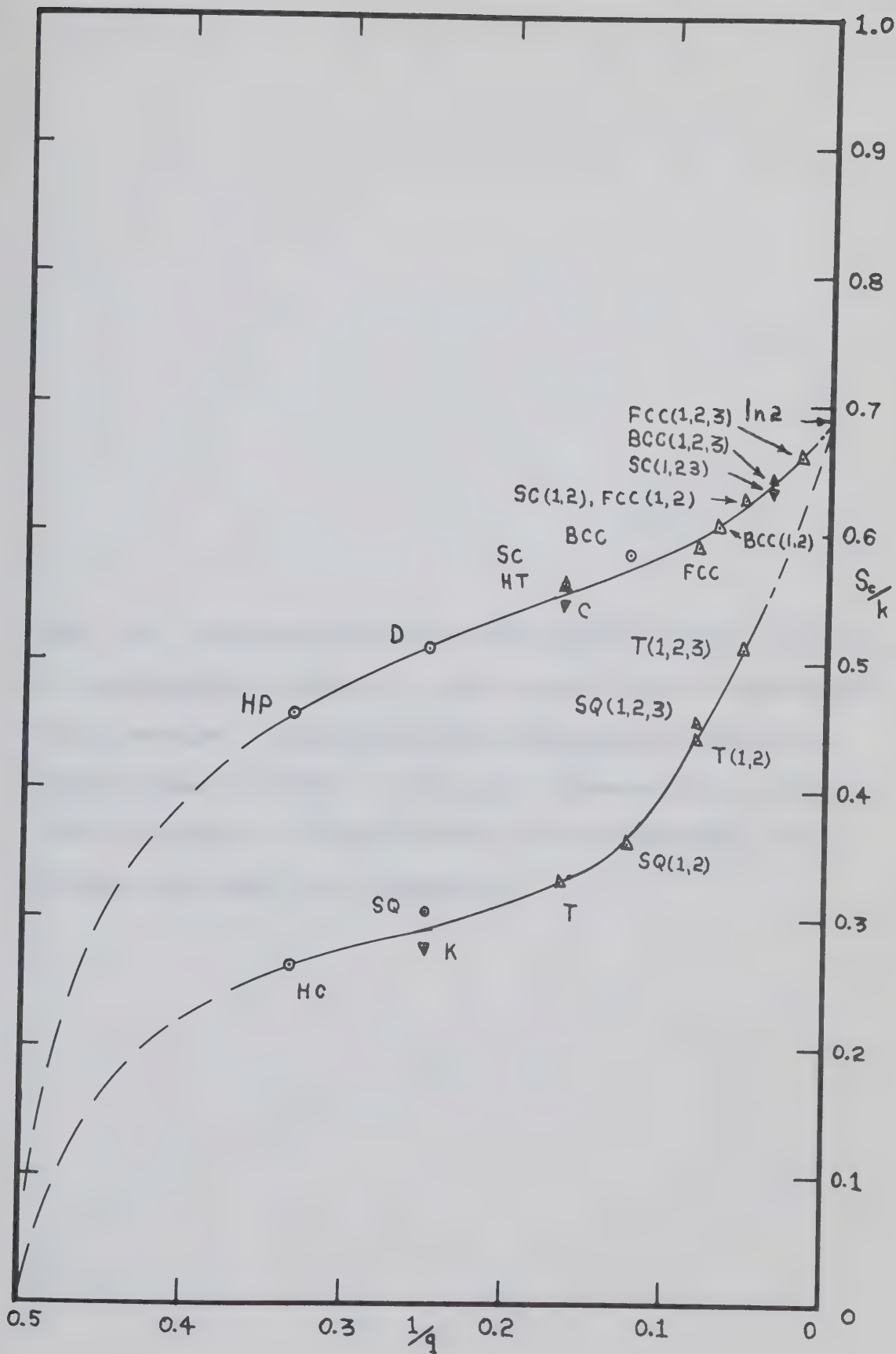
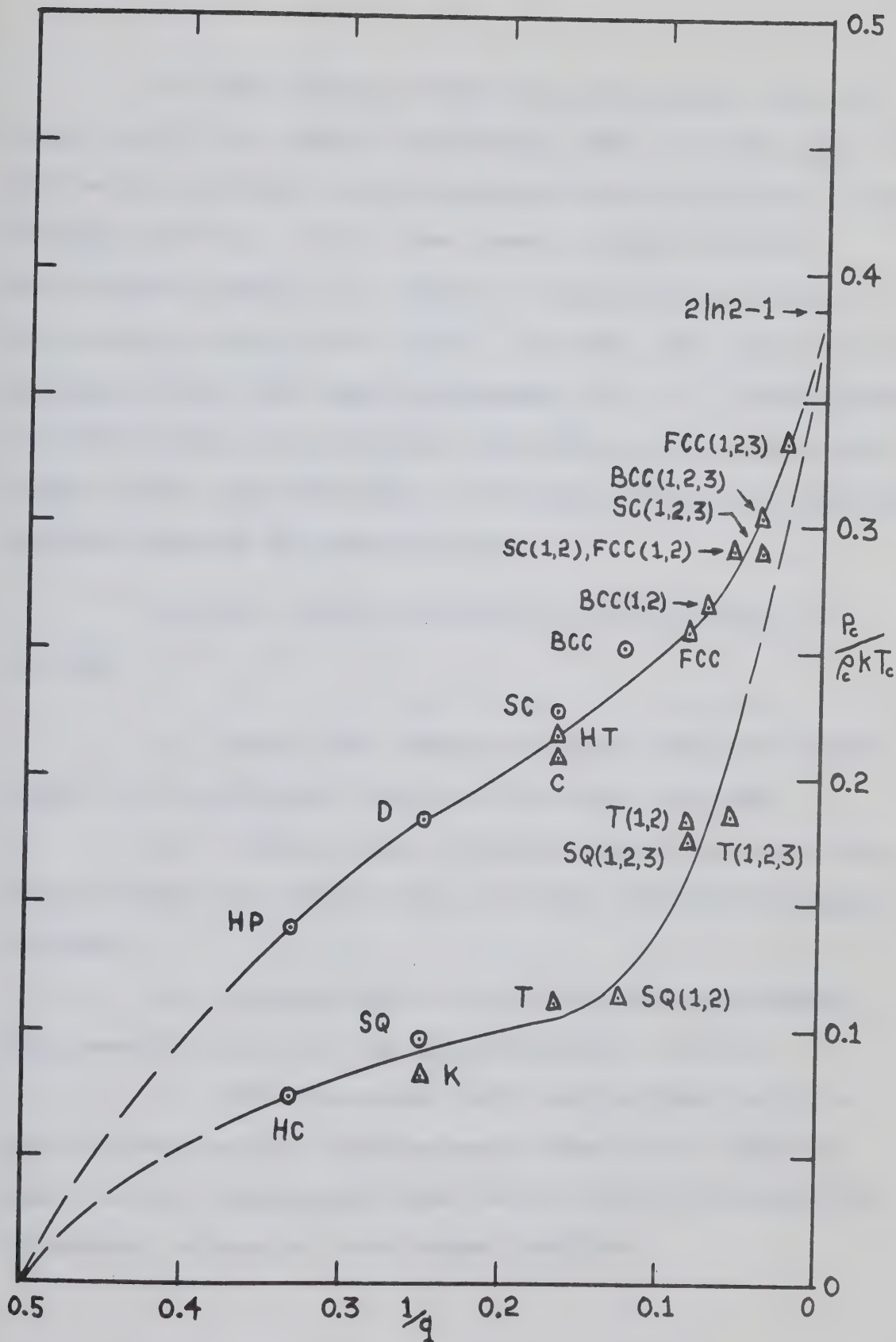


Fig. 8.4. The dependence of the critical ratio, $P_c/\rho_c kT_c$, on coordination number, q , for two and three dimensional Ising models. Circles indicate calculated points for loose packed lattices; triangles, close-packed lattices. The top curve is a best fit for three dimensions; the bottom curve for two dimensions.



At this point it might be worth noting that for argon $S_c/k = 0.43$ (Betts and Ditzian 1968), in very good agreement with the value for the hydrogen peroxide lattice. Also, Mikolaj and Pings (1968) have recently argued that the coordination number of a liquid is meaningful and that $q = 3$ for argon at the critical point. However, the value for the critical energy for argon corresponds to $q = 5$. Nevertheless we believe this is sufficient justification for the further study of the applicability of the Ising model on the hydrogen peroxide lattice to simple liquids.

Briefly the main results of this work are as follows:

1. Three "new" regular lattices have been introduced for the study of lattice statistical problems.
2. A large number of weak lattice constants have been obtained for the hydrogen peroxide and hypertriangular lattices.
3. A large number of strong lattice constants have been obtained for the hypertriangular lattice.
4. Exact relations have been derived, valid in the critical region, relating amplitudes of (a) specific heats and (b) susceptibilities for a triple of generalized honeycomb, triangular, and kagome' lattices.

5. The critical temperatures for the Ising model on all three lattices has been obtained to high precision.

6. The previously accepted value for γ has been confirmed.

7. "Improved" estimates of the low temperature critical indices α' , β , and γ' have been obtained, which indicate the scaling law hypothesis is not valid for the three dimensional Ising model. The estimates found for γ and β are in excellent agreement with the experimental results for beta brass, indicating that the Ising model provides a valid description of the order-disorder transition in binary alloys.

8. The susceptibility amplitude, critical energy, and critical entropy have been determined to reasonable precision on all three lattices.

9. A simple dependence of critical temperature on dimensionality and coordination number has been discovered.

10. The possible relevance of the hydrogen peroxide lattice for simple fluids near the critical point has been indicated.

B. The Self-Avoiding Walk Problem

We have derived exact series expansions of the self-avoiding walk generating functions for the hydrogen peroxide and hypertriangular lattices. From a numerical analysis of the series coefficients we have obtained estimates of the attrition parameter, critical index, and amplitude for both lattices. The value found for the critical index agrees with the value previously found for other three dimensional lattices.

A considerable amount of effort was expended searching for the equivalent of the star-triangle transformation for the self-avoiding walk problem, since such a transformation would provide us with a rigorous check of the numerical analysis and would presumably also show us how to transform the generating function from the hydrogen peroxide lattice to the hypertriangular lattice. However, these efforts have so far been fruitless. It has been pointed out to us by Sykes (Sykes, private communication) that the attrition parameters of the hydrogen peroxide and hypertriangular lattices should obey the following inequality,

$$v \geq \sqrt{\mu^2 / (1 + \mu)} \quad (8-3)$$

where ν and μ denote the attrition parameters of the hydrogen peroxide and hypertriangular lattices respectively. Taking $\mu = 4.6181$ we find $\nu \geq 1.948$ which it just is at 1.956, a difference of only 0.4%. The equality in (8-3) holds for the attrition parameters of Bethe lattices of coordination numbers six and three respectively.

Part of the work reported on in this thesis has also appeared in the physics literature. The high temperature behaviour of the Ising model on the hydrogen peroxide, hypertriangular, and hyperkagomé lattices is discussed in Leu, Betts, and Elliott (1969). A discussion of the self-avoiding walk problem on the hydrogen peroxide and hypertriangular lattices appears in Leu (1969).

APPENDIX A

The first twelve coefficients in the series expansion for the zero field partition function of the hypertriangular lattice.

$$P(1, N) = 0$$

$$P(2, N) = 0$$

$$P(3, N) = N(\triangle) \\ = N$$

$$P(4, N) = 0$$

$$P(5, N) = N(\text{pentagon}) \\ = 3N$$

$$P(6, N) = N(\text{hexagon}) + N(\text{bowtie}) + N(\triangle \triangle) \\ = \frac{1}{2} N^2 + 14 \frac{1}{2} N$$

$$P(7, N) = N(\text{heptagon}) \\ = 33N$$

$$P(8, N) = N(\text{octagon}) + N(\text{pentagon-bowtie}) + N(\text{pentagon} \triangle) \\ = 3N^2 + 57N$$

$$\begin{aligned}
 P(9, N) &= N \left(\text{Octagon} \right) + N \left(\text{Hexagon with one triangle attached} \right) + N \left(\text{Three triangles meeting at a point} \right) \\
 &\quad + N \left(\text{Three triangles in a row} \right) + N \left(\text{Hexagon and triangle} \right) + N \left(\text{Three triangles in a V-shape} \right) \\
 &\quad + N \left(\text{Three triangles in a triangle} \right) \\
 &= 1/6 N^3 + 14 \frac{1}{2} N^2 + 218 \frac{1}{3} N
 \end{aligned}$$

$$\begin{aligned}
 P(10, N) &= N \left(\text{Nonagon} \right) + N \left(\text{Hexagon with two triangles attached} \right) + N \left(\text{Two hexagons} \right) \\
 &\quad + N \left(\text{Pentagon and pentagon} \right) + N \left(\text{Heptagon and triangle} \right) \\
 &= 37 \frac{1}{2} N^2 + 961 \frac{1}{2} N
 \end{aligned}$$










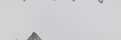


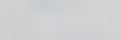









$$\begin{aligned}
 P(11, N) &= N \left(\text{Decagon} \right) + N \left(\text{Hexagon with three triangles attached} \right) + N \left(\text{Heptagon with triangle attached} \right) \\
 &\quad + N \left(\text{Pentagon with three triangles attached} \right) + N \left(\text{Two hexagons with triangle attached} \right) + N \left(\text{Three triangles in a complex shape} \right) \\
 &\quad + N \left(\text{Two hexagons} \right) + N \left(\text{Pentagon with triangle and hexagon} \right) + N \left(\text{Pentagon with two triangles} \right) \\
 &\quad + N \left(\text{Pentagon and hexagon} \right) + N \left(\text{Octagon and triangle} \right) + N \left(\text{Pentagon and two triangles} \right) \\
 &= 1 \frac{1}{2} N^3 - 121 \frac{1}{2} N^2 + 3045 N
 \end{aligned}$$

$$\begin{aligned}
 P(12, N) &= N \left(\text{Undecagon} \right) + N \left(\text{Heptagon with four triangles attached} \right) + N \left(\text{Octagon with two triangles attached} \right) \\
 &\quad + N \left(\text{Hexagon with four triangles attached} \right) + N \left(\text{Hexagon with triangle and pentagon} \right) + N \left(\text{Two hexagons with triangle attached} \right) \\
 &\quad + N \left(\text{Two hexagons with triangle attached} \right) + N \left(\text{Hexagon with four triangles attached} \right) + N \left(\text{Two hexagons with triangle attached} \right) \\
 &\quad + N \left(\text{Two hexagons with triangle attached} \right) + N \left(\text{Hexagon with triangle and pentagon} \right) + N \left(\text{Octagon and triangle} \right) \\
 &\quad + N \left(\text{Hexagon with triangle and pentagon} \right) + N \left(\text{Two triangles and pentagon} \right) + N \left(\text{Three triangles and triangle} \right) \\
 &\quad + N \left(\text{Hexagon and two triangles} \right) + N \left(\text{Hexagon and hexagon} \right) + N \left(\text{Octagon and pentagon} \right) \\
 &\quad + N \left(\text{Hexagon and two triangles} \right) + N \left(\text{Three triangles and triangle} \right) + N \left(\text{Four triangles and triangle} \right) \\
 &= 1/24 N^4 + 7 \frac{1}{4} N^3 + 369 \frac{13}{24} N^2 + 8931 \frac{1}{4} N
 \end{aligned}$$









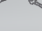























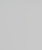
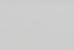
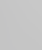



APPENDIX B















































Weak lattice constants of non-magnetic graphs required to calculate the partition function and initial susceptibility of the hypertriangular lattice.


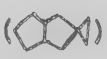

























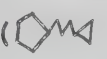





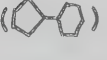





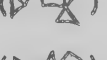




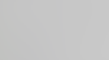

<u>Graph</u>	<u>Lattice Constant</u>	<u>Graph</u>	<u>Lattice Constant</u>
(Δ)	1	(∞)	51
(\diamond)	3	($\infty \Delta$)	33 N-462
(\hexagon)	15	($\diamond \diamond$)	4 1/2 N-76 1/2
(\bowtie)	3	(\bigcirc)	3846
($\Delta \Delta$)	1/2 N-3 1/2	(∞)	459
(\hexagon)	33	(\bowtie)	651
(\bigcirc)	72	($\diamond \Delta \Delta$)	60
($\diamond \bowtie$)	15	($\Delta \bowtie$)	15
($\diamond \Delta$)	3 N-30	($\bowtie \bowtie$)	15
(\bigcirc)	293	($\diamond \diamond$)	18
(\bowtie)	105	($\bigcirc \Delta$)	72 N-1134
($\Delta \bowtie$)	1	($\bigcirc \diamond$)	45 N-840
($\Delta \Delta \Delta$)	12	($\diamond \bowtie$)	9 N-135
($\bigcirc \Delta$)	15 N-180	($\bowtie \Delta$)	15 N-210
($\Delta \Delta \Delta$)	3 N-33	($\bigcirc \Delta \Delta$)	1 1/2 N ² - 19 1/2 N + 300
($\Delta \Delta \Delta$)	1/6 N ² - 3 1/2 N + 20 1/3	(\bigcirc)	13229
(\bigcirc)	1158	($\bigcirc \bowtie$)	2664
(\bowtie)	291	($\infty \bowtie$)	972















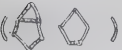

<u>Graph</u>	<u>Lattice Constant</u>	<u>Graph</u>	<u>Lattice Constant</u>
()	1179	()	99 N-2037
()	408	()	112 $1/2$ N-2353 $1/2$
()	120	()	45 N-804
()	120	()	4 $1/2$ N-76 $1/2$
()	54	()	7 $1/2$ N ² -232 $1/2$ N
()	15		+ 1974
()	48	()	1 $1/2$ N ² -43 $1/2$ N + 351
()	8	()	$1/24$ N ³ -1 $3/4$ N ²
()	12		+ 26 $11/24$ N-147 $3/4$
()	132		
()	6		
()	293 N-5079		
()	105 N-1668		
()	N-15		
()	12 N-180		

Weak lattice constants of magnetic graphs which are required to calculate the initial susceptibility of the hypertriangular lattice from Sykes' theorem.

<u>Graph</u>	<u>Lattice Constant</u>	<u>Graph</u>	<u>Lattice Constant</u>
()	15	()	12
()	12	()	30
()	60	()	30
()	6	()	30
()	60	()	15
()	111	()	96
()	18	()	12
()	36	()	1302
()	12	()	522
()	15	()	648
()	120	()	15 N-180
()	273	()	12 N-156
()	354	()	1866
()	258	()	690
()	78	()	699
()	102	()	276
()	66	()	570
()	45	()	114
()	12	()	117

<u>Graph</u>	<u>Lattice Constant</u>	<u>Graph</u>	<u>Lattice Constant</u>
()	66	()	60
()	60	()	180
()	24	()	60 N-840
()	48	()	6 N-78
()	36	()	60 N-885
()	60	()	7392
()	63	()	1566
()	3	()	3288
()	15	()	1536
()	120	()	780
()	6	()	666
()	150	()	576
()	150	()	1326
()	120	()	49
()	24	()	288
()	6	()	246
()	1542	()	36
()	2928	()	216
()	2484	()	432
()	6174	()	36
()	222	()	144
()	72	()	132
()	450	()	72

<u>Graph</u>	<u>Lattice Constant</u>	<u>Graph</u>	<u>Lattice Constant</u>
	84		36
	48		216
	9		84
	456		48
	18		72
	18		84
	6		36
	6		15
	30		60
	12		30
	12		30
	78		3852
	222		7134
	6		13644
	36		11616
	12		28971
	204		1194
	102		2628
	312		2094
	282		642
	135		258
	75		234
	72		240

<u>Graph</u>	<u>Lattice Constant</u>
	228
	462
	60
	60
	816
	648
	72
	111 N-1680
	18 N-270
	36 N-558
	12 N-180
	15 N-210
	120 N-1896
	273 N-4581
	45 N-828
	36 N-648

APPENDIX C

Symbolic equations for calculating the lattice constants of separated non-magnetic graphs for the hypertriangular lattice.

$$N(\triangle) N(\triangle) = N(\triangle) + 2N(\triangle\triangle) + 2N(\triangle\triangle\triangle)$$

$$N(\text{pentagon}) N(\triangle) = N(\text{pentagon with triangle}) + N(\text{pentagon with triangle}) + N(\text{pentagon with triangle})$$

$$N(\text{bowtie}) N(\triangle) = 2N(\triangle\triangle) + 3N(\text{bowtie with triangle}) + 2N(\triangle\triangle\triangle) + N(\triangle\triangle\triangle)$$

$$N(\triangle\triangle) N(\triangle) = 2N(\triangle\triangle) + 2N(\triangle\triangle\triangle) + N(\triangle\triangle\triangle) + 3N(\triangle\triangle\triangle)$$

$$N(\text{hexagon}) N(\triangle) = N(\text{hexagon with triangle}) + N(\text{hexagon with triangle}) + N(\text{hexagon with triangle}) + N(\text{hexagon with triangle})$$

$$N(\text{pentagon}) N(\text{pentagon}) = N(\text{pentagon}) + 2N(\text{pentagon with pentagon}) + 2N(\text{pentagon with pentagon}) + 2N(\text{pentagon with pentagon}) + 2N(\text{pentagon with pentagon})$$

$$N(\text{heptagon}) N(\triangle) = N(\text{heptagon with triangle}) + N(\text{heptagon with triangle}) + N(\text{heptagon with triangle}) + N(\text{heptagon with triangle})$$

$$N(\text{bowtie}) N(\triangle) = N(\text{bowtie}) + N(\text{bowtie with triangle}) + N(\text{bowtie with triangle}) + N(\text{bowtie with triangle}) + N(\text{bowtie with triangle}) + N(\text{bowtie with triangle}) + 2N(\text{bowtie with triangle}) + 2N(\text{bowtie with triangle}) + N(\text{bowtie with triangle})$$

$$N(\text{pentagon}) N(\text{bowtie}) = N(\text{pentagon with bowtie}) + N(\text{pentagon with bowtie}) + N(\text{pentagon with bowtie}) + N(\text{pentagon with bowtie}) + N(\text{pentagon with bowtie}) + N(\text{pentagon with bowtie})$$

$$N(\text{pentagon}) N(\text{hexagon}) = N(\text{pentagon-hexagon}) + N(\text{pentagon-triangle}) + 2N(\text{pentagon-square}) \\ + 2N(\text{pentagon-pentagon}) + N(\text{hexagon-hexagon}) + N(\text{hexagon-octagon}) \\ + 2N(\text{pentagon-hexagon}) + N(\text{pentagon-hexagon})$$

$$N(\text{octagon}) N(\triangle) = N(\text{octagon-triangle}) + N(\text{octagon-triangle}) + N(\text{octagon-pentagon}) \\ + N(\text{octagon-hexagon}) + N(\text{octagon-triangle})$$

$$N(\text{pentagon}) N(\triangle\triangle) = N(\triangle\triangle) + N(\triangle\triangle) + N(\triangle\triangle) + N(\triangle\triangle) \\ + N(\triangle\triangle) + N(\triangle\triangle) + N(\triangle\triangle) \\ + N(\triangle\triangle\triangle)$$

$$N(\text{octagon}) N(\triangle) = N(\text{octagon-triangle}) + N(\text{octagon-triangle}) + N(\text{octagon-triangle}) \\ + N(\text{octagon-hexagon}) + N(\text{octagon-hexagon}) + N(\text{octagon-triangle})$$

$$N(\text{pentagon-hexagon}) N(\triangle) = N(\text{pentagon-hexagon}) + N(\text{pentagon-hexagon}) + 2N(\text{pentagon-hexagon}) \\ + 2N(\text{pentagon-hexagon}) + 2N(\text{pentagon-hexagon}) + 2N(\text{pentagon-hexagon}) \\ + N(\text{pentagon-hexagon}) + N(\text{pentagon-hexagon}) + N(\text{pentagon-hexagon}) \\ + N(\text{pentagon-hexagon}) + N(\text{pentagon-hexagon}) + N(\text{pentagon-hexagon}) \\ + N(\text{pentagon-hexagon}) + 2N(\text{pentagon-hexagon}) + N(\text{pentagon-hexagon})$$

$$N(\triangle\triangle) N(\triangle) = 3N(\triangle\triangle) + N(\triangle\triangle\triangle) + N(\triangle\triangle\triangle)$$

$$N(\triangle\triangle\triangle) N(\triangle) = 3N(\triangle\triangle\triangle) + 2N(\triangle\triangle\triangle) + 3N(\triangle\triangle\triangle) \\ + 2N(\triangle\triangle\triangle) + N(\triangle\triangle\triangle\triangle)$$

$$N(\triangle\triangle) N(\triangle\triangle) = N(\triangle\triangle) + 6N(\triangle\triangle) + 2N(\triangle\triangle\triangle) \\ + 2N(\triangle\triangle\triangle\triangle) + 2N(\triangle\triangle\triangle\triangle) + 2N(\triangle\triangle\triangle\triangle)$$

$$\begin{aligned}
 N(\text{heptagon}) N(\text{bowtie}) &= N(\text{heptagon-bowtie}) + N(\text{heptagon-triangle}) + N(\text{heptagon-trapezoid}) \\
 &+ N(\text{heptagon-pentagon}) + N(\text{heptagon-diamond}) + N(\text{heptagon-hexagon}) \\
 &+ N(\text{heptagon-octagon}) + N(\text{heptagon-nonagon}) + 2N(\text{heptagon-decagon}) \\
 &+ N(\text{heptagon-undecagon})
 \end{aligned}$$

$$\begin{aligned}
 N(\text{heptagon}) N(\text{heptagon}) &= N(\text{heptagon}) + 2N(\text{heptagon-heptagon}) + 6N(\text{heptagon-heptagon}) \\
 &+ 2N(\text{heptagon-heptagon}) + 2N(\text{heptagon-heptagon}) \\
 &+ 2N(\text{heptagon-heptagon}) + 2N(\text{heptagon-heptagon}) + 2N(\text{heptagon-heptagon}) \\
 &+ 2N(\text{heptagon-heptagon}) + 2N(\text{heptagon-heptagon}) + 2N(\text{heptagon-heptagon}) \\
 &+ 6N(\text{heptagon-heptagon}) + 2N(\text{heptagon-heptagon}) + 2N(\text{heptagon-heptagon}) \\
 &+ 4N(\text{heptagon-heptagon}) + 2N(\text{heptagon-heptagon}) + 2N(\text{heptagon-heptagon}) \\
 &+ 2N(\text{heptagon-heptagon})
 \end{aligned}$$

$$\begin{aligned}
 N(\text{heptagon}) N(\text{pentagon}) &= N(\text{heptagon-pentagon}) + N(\text{heptagon-pentagon}) + N(\text{heptagon-pentagon}) \\
 &+ N(\text{heptagon-pentagon}) + N(\text{heptagon-pentagon}) + N(\text{heptagon-pentagon}) \\
 &+ N(\text{heptagon-pentagon}) + N(\text{heptagon-pentagon}) + N(\text{heptagon-pentagon}) \\
 &+ N(\text{heptagon-pentagon}) + N(\text{heptagon-pentagon}) + 2N(\text{heptagon-pentagon}) \\
 &+ N(\text{heptagon-pentagon})
 \end{aligned}$$

$$\begin{aligned}
 N(\text{heptagon-triangle}) N(\text{triangle}) &= N(\text{heptagon-triangle}) + N(\text{heptagon-triangle}) + N(\text{heptagon-triangle}) \\
 &+ N(\text{heptagon-triangle}) + N(\text{heptagon-triangle}) + N(\text{heptagon-triangle}) \\
 &+ 2N(\text{heptagon-triangle}) + 2N(\text{heptagon-triangle})
 \end{aligned}$$

$$\begin{aligned}
 N(\text{triangle-triangle}) N(\text{triangle}) &= + 2N(\text{triangle-triangle}) + N(\text{triangle-triangle}) + 3N(\text{triangle-triangle}) \\
 &+ 4N(\text{triangle-triangle}) + 2N(\text{triangle-triangle}) \\
 &+ 3N(\text{triangle-triangle}) + 2N(\text{triangle-triangle})
 \end{aligned}$$

$$\begin{aligned}
 N(\triangle\triangle\triangle) N(\triangle) &= N(\triangle\triangle\triangle) + N(\triangle\triangle\triangle\triangle) + 3N(\triangle\triangle\triangle) \\
 &\quad + 2N(\triangle\triangle\triangle\triangle) + 4N(\triangle\triangle\triangle\triangle)
 \end{aligned}$$

Symbolic equations for calculating the lattice constants of separated magnetic graphs for the hypertriangular lattice.

$$N(\text{triangle with two internal lines}) N(\Delta) = 2N(\text{triangle with one internal line}) + N(\text{triangle with two internal lines and a vertex}) + 2N(\text{triangle with three internal lines}) + N(\text{triangle with one internal line and a vertex}) + N(\text{triangle with two internal lines and a vertex})$$

$$N(\text{triangle with one internal line}) N(\Delta) = N(\text{triangle with one internal line}) + 2N(\text{triangle with one internal line and a vertex}) + 2N(\text{triangle with one internal line and a vertex}) + N(\text{triangle with one internal line and a vertex}) + N(\text{triangle with one internal line and a vertex}) + N(\text{triangle with one internal line and a vertex}) + N(\text{triangle with one internal line and a vertex})$$

$$N(\text{triangle with two internal lines}) N(\Delta) = 2N(\text{triangle with two internal lines}) + N(\text{triangle with two internal lines and a vertex}) + 2N(\text{triangle with two internal lines and a vertex}) + N(\text{triangle with two internal lines and a vertex}) + N(\text{triangle with two internal lines and a vertex}) + N(\text{triangle with two internal lines and a vertex}) + N(\text{triangle with two internal lines and a vertex})$$

$$N(\text{triangle with one internal line}) + N(\Delta) = N(\text{triangle with one internal line}) + N(\text{triangle with one internal line and a vertex}) + N(\text{triangle with one internal line and a vertex}) + N(\text{triangle with one internal line and a vertex}) + N(\text{triangle with one internal line and a vertex}) + 2N(\text{triangle with one internal line and a vertex}) + 2N(\text{triangle with one internal line and a vertex}) + 2N(\text{triangle with one internal line and a vertex}) + 2N(\text{triangle with one internal line and a vertex}) + N(\text{triangle with one internal line and a vertex})$$

$$N(\text{triangle with two internal lines}) N(\Delta) = N(\text{triangle with two internal lines}) + N(\text{triangle with two internal lines and a vertex}) + N(\text{triangle with two internal lines and a vertex}) + N(\text{triangle with two internal lines and a vertex}) + N(\text{triangle with two internal lines and a vertex}) + N(\text{triangle with two internal lines and a vertex}) + N(\text{triangle with two internal lines and a vertex}) + 3N(\text{triangle with two internal lines and a vertex}) + N(\text{triangle with two internal lines and a vertex})$$

$$\begin{aligned}
 N(\text{cyclopentadiene}) \cdot N(\text{cyclopentadiene}) &= N(\text{bicyclopentadiene}) + N(\text{tricyclopentadiene}) + N(\text{tetracyclopentadiene}) \\
 &+ N(\text{pentacyclopentadiene}) + N(\text{hexacyclopentadiene}) + 2N(\text{heptacyclopentadiene}) \\
 &+ N(\text{octacyclopentadiene}) + N(\text{nonacyclopentadiene}) + 2N(\text{decacyclopentadiene}) \\
 &+ 2N(\text{undecacyclopentadiene}) + 2N(\text{dodecacyclopentadiene}) + N(\text{tridecacyclopentadiene}) \\
 &+ 6N(\text{tetradecacyclopentadiene}) + N(\text{pentadecacyclopentadiene}) + N(\text{hexadecacyclopentadiene})
 \end{aligned}$$

$$\begin{aligned}
 N(\text{bicyclopentadiene}) \cdot N(\text{cyclopentadiene}) &= N(\text{tricyclopentadiene}) + N(\text{tetracyclopentadiene}) + N(\text{pentacyclopentadiene}) \\
 &+ N(\text{hexacyclopentadiene}) + N(\text{heptacyclopentadiene}) + N(\text{octacyclopentadiene}) \\
 &+ N(\text{nonacyclopentadiene}) + N(\text{decacyclopentadiene}) + N(\text{undecacyclopentadiene})
 \end{aligned}$$

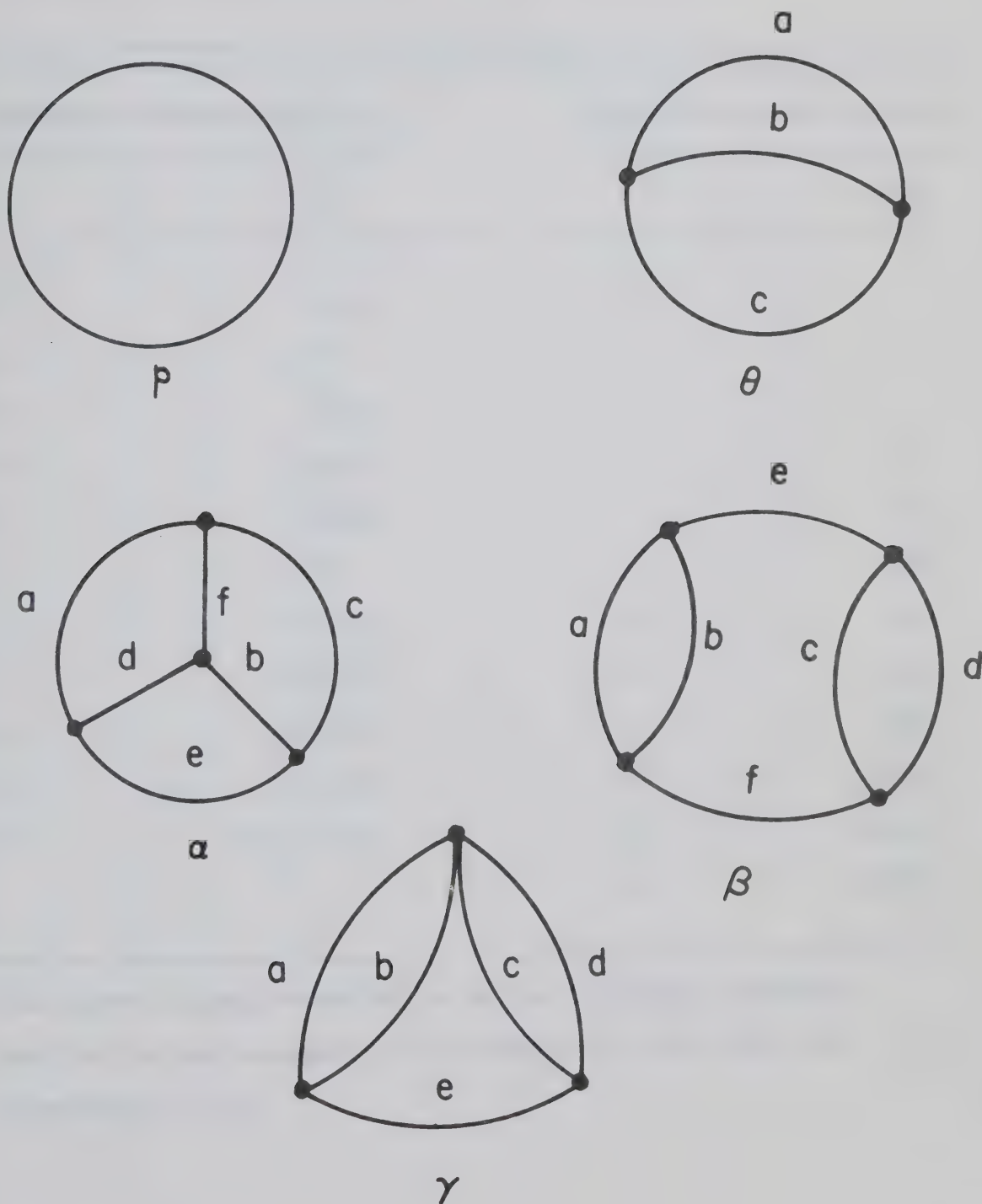
$$\begin{aligned}
 N(\text{cyclopentadiene}) \cdot N(\Delta) &= N(\text{bicyclopentadiene}) + N(\text{tricyclopentadiene}) + 2N(\text{tetracyclopentadiene}) \\
 &+ N(\text{pentacyclopentadiene}) + N(\text{hexacyclopentadiene}) + 2N(\text{heptacyclopentadiene}) \\
 &+ N(\text{octacyclopentadiene}) + N(\text{nonacyclopentadiene}) + N(\text{decacyclopentadiene}) \\
 &+ N(\text{undecacyclopentadiene}) + N(\text{dodecacyclopentadiene}) \\
 &+ N(\text{tridecacyclopentadiene}) + N(\text{tetradecacyclopentadiene}) + N(\text{pentadecacyclopentadiene})
 \end{aligned}$$

$$\begin{aligned}
 N(\text{bicyclopentadiene}) \cdot N(\Delta) &= 2N(\text{tricyclopentadiene}) + N(\text{tetracyclopentadiene}) + N(\text{pentacyclopentadiene}) \\
 &+ N(\text{hexacyclopentadiene}) + 2N(\text{heptacyclopentadiene}) + N(\text{octacyclopentadiene}) \\
 &+ N(\text{nonacyclopentadiene}) + N(\text{decacyclopentadiene}) + N(\text{undecacyclopentadiene}) \\
 &+ N(\text{dodecacyclopentadiene})
 \end{aligned}$$

$$\begin{aligned}
 N(\text{tricyclopentadiene}) \cdot N(\Delta) &= 2N(\text{tetracyclopentadiene}) + 2N(\text{pentacyclopentadiene}) + N(\text{hexacyclopentadiene}) \\
 &+ N(\text{heptacyclopentadiene}) + N(\text{octacyclopentadiene}) + N(\text{nonacyclopentadiene}) \\
 &+ N(\text{decacyclopentadiene}) + N(\text{undecacyclopentadiene})
 \end{aligned}$$

APPENDIX D

Weak lattice constants of polygon, theta, alpha, beta, and gamma star graphs for the hydrogen peroxide and hyper-triangular lattices.



Weak lattice constants of p graphs or polygons

hydrogen peroxide lattice		hypertriangular lattice	
l	$(l)_p$	l	$(l)_p$
10^*	$1\frac{1}{2}$	3	1
12	0	4	0
14	$1\frac{1}{2}$	5	3
16	$10\frac{1}{2}$	6	15
18	$23\frac{1}{2}$	7	33
20	45	8	72
22	$178\frac{1}{2}$	9	293
24	$587\frac{1}{2}$	10	1158
26	$1579\frac{1}{2}$	11	3846
28	$5026\frac{1}{2}$	12	13229
30	$16,603\frac{1}{2}$	13	50145
		14	192054

*The first p graph embeddable on the hydrogen peroxide lattice is the decagon and no graphs of odd order are embeddable on it.

Weak lattice constants of θ graphs
for the hydrogen peroxide lattice*

a	b	c	l	$(a,b,c)_\theta$		a	b	c	l	$(a,b,c)_\theta$	
5	5	5	15	1		1	9	15	25	381	
3	7	7	17	3		3	7	15	25	189	
2	8	8	18	12		3	11	11	25	12	
1	9	9	19	19	1/2	5	5	15	25	61	
5	5	9	19	0		5	9	11	25	24	
4	6	10	20	6		7	7	11	25	12	
3	7	11	21	12		7	9	9	25	42	
5	5	11	21	15		2	8	16	26	483	
7	7	7	21	0		2	12	12	26	12	
2	8	12	22	24		4	6	15	26	249	
4	6	12	22	36		4	10	12	26	42	
6	8	8	22	3		6	8	12	26	15	
1	9	13	23	54		6	10	10	26	30	
3	7	13	23	78		8	8	10	26	18	
5	5	13	23	30		1	9	17	27	882	
5	9	9	23	0		1	13	13	27	34	1/2
7	7	9	23	0		3	7	17	27	552	
2	8	14	24	216		3	11	13	27	120	
4	6	14	24	72		5	5	17	27	240	
4	10	10	24	0		5	9	13	27	48	
6	8	10	24	24		5	11	11	27	120	
8	8	8	24	4		7	7	13	27	21	
						7	9	11	27	84	
						9	9	9	27	7	

a	b	c	ℓ	$(a,b,c)_\theta$	a	b	c	ℓ	$(a,b,c)_\theta$
2	8	18	28	1047	2	8	20	30	4458
2	12	14	28	252	2	12	16	30	522
4	6	18	28	990	2	14	14	30	948
4	10	14	28	150	4	6	20	30	3300
4	12	12	28	237	4	10	16	30	234
6	8	14	28	96	4	12	14	30	870
6	10	12	28	222	6	8	16	30	390
8	8	12	28	78	6	10	14	30	564
8	10	10	28	78	6	12	12	30	342
					8	8	14	30	249
1	9	19	29	2028	8	10	12	30	366
1	13	15	29	489	10	10	10	30	42
3	7	19	29	1890					
3	11	15	29	231					
3	13	13	29	786					
5	5	19	29	984					
5	9	15	29	144					
5	11	13	29	531					
7	7	15	29	48					
7	9	13	29	216					
7	11	11	29	135					
9	9	11	29	72					

* Many θ graphs which are by inspection obviously not embeddable in the hydrogen peroxide lattice are not listed.

Weak lattice constants of θ graphs for the
hypertriangular lattice

a	b	c	ℓ	$(a,b,c)_\theta$	a	b	c	ℓ	$(a,b,c)_\theta$
1	2	4	7	15	1	2	9	12	7392
1	2	5	8	60	1	4	7	12	1566
2	3	3	8	6	1	5	6	12	3288
1	2	6	9	111	2	3	7	12	1326
1	4	4	9	18	2	4	6	12	1536
2	3	4	9	36	2	5	5	12	780
3	3	3	9	12	3	3	6	12	666
1	2	7	10	354	3	4	5	12	576
1	4	5	10	258	4	4	4	12	49
2	3	5	10	78	1	2	10	13	2514
2	4	4	10	102	1	4	8	13	6609
3	3	4	10	66	1	5	7	13	8022
1	2	8	11	1866	1	6	6	13	3579
1	4	6	11	690	2	3	8	13	5403
1	5	5	11	699	2	4	7	13	6678
2	3	6	11	276	2	5	6	13	3756
2	4	5	11	570	3	3	7	13	3234
3	3	5	11	114	3	4	6	13	3165
3	4	4	11	117	3	5	5	13	831
					4	4	5	13	855
					1	2	11	14	101610
					1	4	9	14	29070
					1	5	8	14	35832
					1	6	7	14	18324
					2	3	9	14	20106
					2	4	8	14	28971
					2	5	7	14	16254
					2	6	6	14	4689
					3	3	8	14	11544
					3	4	7	14	13686
					3	5	6	14	7422
					4	4	6	14	4197
					4	5	5	14	4113

* Many θ graphs which are by inspection obviously not embeddable in the hypertriangular lattice are not listed.

Weak lattice constants of α graphs for the hydrogen
peroxide and hypertriangular lattices

a	b	c	d	e	f	l	$(a,b; c,d; e,f)_\alpha$
(i) hydrogen peroxide lattice							
2	2	3	3	5	5	20	1 1/2
1	3	2	4	5	7	22	6
1	4	1	4	5	8	23	12
2	5	2	5	3	6	23	6
1	1	2	6	7	7	24	3
1	5	2	6	3	7	24	6
2	6	2	6	2	6	24	2
1	2	1	6	7	8	25	24
1	6	1	6	3	8	25	12
1	6	2	7	2	7	25	24
2	3	3	8	4	5	25	6
1	1	1	7	8	8	26	36
1	7	1	7	2	8	26	24
2	2	2	8	6	6	26	3
1	8	1	8	1	8	27	13
(ii) hypertriangular lattice							
1	2	1	2	2	1	9	2
1	2	1	2	3	1	10	12
1	1	1	3	1	3	10	6

Weak lattice constants of β graphs for the hydrogen
peroxide and hypertriangular lattices

a	b	c	d	e	f	l	$(a,b; c,d; e,f)_\beta$
(i) hydrogen peroxide lattice							
3	7	5	5	1	1	22	0
2	8	5	5	1	2	23	12
1	9	5	5	1	3	24	18
1	9	5	5	2	2	24	6
3	7	3	7	1	3	24	3
3	7	3	7	2	2	24	3
2	8	3	7	1	4	25	24
2	8	3	7	2	3	25	12
4	6	5	5	1	4	25	0
4	6	5	5	2	3	25	0
1	9	3	7	1	5	26	30
1	9	3	7	2	4	26	30
1	9	3	7	3	3	26	18
1	9	7	7	1	1	26	9
2	8	2	8	1	5	26	36
2	8	2	8	2	4	26	36
2	8	2	8	3	3	26	21
1	9	2	8	1	6	27	120
1	9	2	8	2	5	27	126
1	9	2	8	3	4	27	120
2	12	5	5	1	2	27	12
3	7	4	10	1	2	27	0
4	6	7	7	1	2	27	0
1	9	1	9	1	7	28	102
1	9	1	9	2	6	28	102
1	9	1	9	3	5	28	99
1	9	1	9	4	4	28	52 1/2
2	8	6	10	1	1	28	12
3	7	5	11	1	1	28	6
3	13	5	5	1	1	28	18

(ii) hypertriangular lattice

a	b	c	d	e	f	l	$(a,b; c,d; e,f)_\beta$
3	2	1	2	1	2	9	15
1	2	1	2	1	3	10	30
1	2	1	2	2	2	10	30
1	2	2	3	1	1	10	12
1	2	1	2	1	4	11	36
1	2	1	2	2	3	11	51
1	2	1	4	1	2	11	72
1	2	2	3	1	2	11	36
1	2	2	4	1	1	11	36
1	2	3	3	1	1	11	24

Weak lattice constants of γ graphs for the
hypertriangular lattice

a	b	c	d	e	l	$(a,b; c,d; e)_\gamma$
1	2	1	2	3	9	15
1	2	1	2	4	10	45
1	2	2	3	2	10	12
1	2	3	3	1	10	12
1	2	1	2	5	11	66
1	2	1	4	3	11	60
1	2	2	3	3	11	24
1	2	3	3	2	11	36
1	2	2	4	2	11	48
1	2	3	4	1	11	60
1	4	1	4	1	11	63
2	3	2	3	1	11	3
1	2	1	2	6	12	288
1	2	1	4	4	12	246
1	2	2	3	4	12	36
1	2	2	4	3	12	216
1	2	1	5	3	12	432
1	2	3	3	3	12	36
1	2	2	5	2	12	144
1	2	3	5	1	12	72
1	2	3	4	2	12	132
1	2	4	4	1	12	84
1	4	2	3	2	12	48
1	4	1	5	1	12	9
1	4	3	3	1	12	18
2	3	2	4	1	12	18
2	3	3	3	1	12	6

APPENDIX E

The first nine coefficients, calculated by the direct method, in the power series expansion of the high temperature ferromagnetic initial susceptibility of the hypertriangular lattice.

$$b_1 = (/)$$

$$b_2 = (1)$$

$$b_3 = (\sim)$$

$$b_4 = (\mathcal{M}) + (\mathcal{D}) + (\Delta /)$$

$$b_5 = (\mathcal{W}) + (\mathcal{X}) + (\mathcal{D} /) + (\Delta \wedge)$$


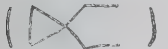




















$$b_6 = (\mathcal{M}) + (\mathcal{D}) + (\mathcal{X}) + (\mathcal{O}) + (\mathcal{O} /) + (\Delta \sim)$$


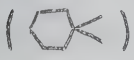











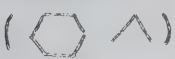








$$b_7 = (\mathcal{W}) + (\mathcal{D}) + (\mathcal{X}) + (\mathcal{O}) + (\mathcal{O} /) + (\mathcal{O} \sim) + (\mathcal{O} \mathcal{O}) + (\mathcal{O} \mathcal{D}) + (\mathcal{O} \mathcal{X}) + (\mathcal{O} \mathcal{O} /) + (\mathcal{O} \mathcal{O} \sim) + (\mathcal{O} \mathcal{O} \mathcal{O}) + (\mathcal{O} \mathcal{O} \mathcal{D}) + (\mathcal{O} \mathcal{O} \mathcal{X}) + (\mathcal{O} \mathcal{O} \mathcal{O} /) + (\mathcal{O} \mathcal{O} \mathcal{O} \sim)$$






















$$b_8 = (\mathcal{W}) + (\mathcal{D}) + (\mathcal{X}) + (\mathcal{O}) + (\mathcal{O} /) + (\mathcal{O} \sim) + (\mathcal{O} \mathcal{O}) + (\mathcal{O} \mathcal{D}) + (\mathcal{O} \mathcal{X}) + (\mathcal{O} \mathcal{O} /) + (\mathcal{O} \mathcal{O} \sim) + (\mathcal{O} \mathcal{O} \mathcal{O}) + (\mathcal{O} \mathcal{O} \mathcal{D}) + (\mathcal{O} \mathcal{O} \mathcal{X}) + (\mathcal{O} \mathcal{O} \mathcal{O} /) + (\mathcal{O} \mathcal{O} \mathcal{O} \sim) + (\mathcal{O} \mathcal{O} \mathcal{O} \mathcal{O}) + (\mathcal{O} \mathcal{O} \mathcal{O} \mathcal{D}) + (\mathcal{O} \mathcal{O} \mathcal{O} \mathcal{X}) + (\mathcal{O} \mathcal{O} \mathcal{O} \mathcal{O} /) + (\mathcal{O} \mathcal{O} \mathcal{O} \mathcal{O} \sim)$$

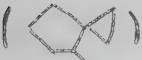


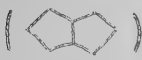









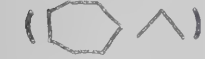
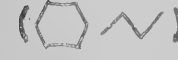


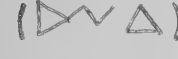



Lattice constants per site of weak graphs required in the calculation, by the direct method, of the high temperature ferromagnetic initial susceptibility of the hypertriangular lattice.




<u>Graph</u>	<u>Number of Edges</u>	<u>Lattice Constant</u>
(/)	1	3
(^)	2	15
(^v)	3	72
(^vv)	4	348
(\triangle)	4	12
(\triangle /)	4	$3N-15$
(^vvv)	5	1665
(\triangle)	5	18
(\triangle ^v)	5	60
(\triangle ^)	5	$15N-105$
(^vvvv)	6	7887
(\triangle ^)	6	168
(\triangle ^v)	6	288
(\square)	6	60
(\square /)	6	$9N-75$
(\triangle ^v)	6	$72N-648$
(^vvvvv)	7	37242

<u>Graph</u>	<u>Number of Edges</u>	<u>Lattice Constant</u>
()	7	1362
()	7	396
()	7	816
()	7	270
()	7	90
()	7	330
()	7	12
()	7	48
()	7	6
()	7	15
()	7	45N-435
()	7	45N-510
()	7	348N-3813
()	7	9N-72
()	7	12N-108
()	7	$1 \frac{1}{2} N^2 - 25 \frac{1}{2} N + 117$
()	8	175596
()	8	6420
()	8	3816
()	8	3810
()	8	1296
()	8	780

<u>Graph</u>	<u>Number of Edges</u>	<u>Lattice Constant</u>
()	8	1518
()	8	450
()	8	804
()	8	60
()	8	72
()	8	240
()	8	72
()	8	30
()	8	3
()	8	60
()	8	6
()	8	90
()	8	99N-1095
()	8	225N-2934
()	8	72N-3108
()	8	7887N-21465
()	8	18N-198
()	8	60N-660
()	8	45N-495
()	8 7 1/2 N ² -157 1/2 N+915	
()	9	825903
()	9	30336

<u>Graph</u>	<u>Number of Edges</u>	<u>Lattice Constant</u>
	9	17808
	9	17628
	9	9072
	9	6096
	9	3768
	9	1680
	9	7236
	9	3924
	9	3726
	9	1041
	9	273
	9	336
	9	96
	9	336
	9	120
	9	1122
	9	672
	9	144
	9	24
	9	120
	9	30

<u>Graph</u>	<u>Number of Edges</u>	<u>Lattice Constant</u>
()	9	120
()	9	120
()	9	111
()	9	18
()	9	36
()	9	12
()	9	420
()	9	330
()	9	36
()	9	135
()	9	15
()	9	216N-2751
()	9	45N-510
()	9	495N-7338
()	9	1080N-17748
()	9	216N-3009
()	9	60N-720
()	9	288N-3714
()	9	168N-2184
()	9	7887N-116979
()	9	36N-480

<u>Graph</u>	<u>Number of Edges</u>	<u>Lattice Constant</u>
()	9	$348N-18108$
()	9	$9N^2-156N+1320$
()	9	$36N^2-900N+6249$

Symbolic equations used to calculate the weak lattice constants of separated configurations required in the calculation by the direct method of the high temperature ferromagnetic initial susceptibility of the hypertriangular lattice.

$$N(\Delta)N(/) = 3N(\Delta) + N(\text{D-}) + N(\Delta /)$$

$$N(\Delta)N(\wedge) = 3N(\Delta) + 2N(\text{D-}) + N(\text{M}) + N(\text{X}) + N(\Delta \wedge)$$

$$N(\Delta)N(\vee) = 2N(\text{D-}) + 2N(\text{M}) + N(\text{C}) + N(\text{DV}) + N(\text{DX}) \\ + N(\Delta \vee)$$

$$N(\text{O})N(/) = 5N(\text{O}) + N(\text{O-}) + N(\text{O}/)$$

$$N(\text{O})N(\wedge) = 6N(\text{O}) + N(\text{O-}) + N(\text{O}) + N(\text{O}/)$$

$$N(\text{X})N(/) = 6N(\text{X}) + N(\text{X}) + N(\text{X}) + N(\text{X}/)$$

$$N(\text{O})N(\wedge) = 5N(\text{O}) + 2N(\text{O-}) + N(\text{O}) + N(\text{O}) + N(\text{O}) \\ + N(\text{O})$$

$$N(\text{D-})N(\Delta) = N(\text{D-}) + 4N(\text{X}) + 2N(\text{X}) + N(\text{X}) \\ + 2N(\text{D-}) + N(\text{D-})$$

$$N(\text{M})N(\Delta) = 2N(\text{M}) + N(\text{C}) + 2N(\text{DV}) + N(\text{A}) \\ + N(\text{DM}) + N(\text{DX}) + N(\text{X}) + N(\text{O}) \\ + N(\Delta \text{M})$$

$$N(\Delta\Delta)N(/) = 6N(\Delta\Delta) + N(\text{bowtie}) + N(\text{bowtie with slash}) + N(\Delta\Delta /)$$

$$N(\text{hexagon})N(/) = 7N(\text{hexagon}) + N(\text{hexagon with line}) + N(\text{hexagon with triangle}) + N(\text{hexagon with slash})$$

$$N(\text{hexagon})N(\wedge) = 6N(\text{hexagon}) + 2N(\text{hexagon with line}) + 4N(\text{hexagon with triangle}) + N(\text{hexagon with wavy line}) \\ + N(\text{hexagon with cross}) + N(\text{hexagon with circle}) + N(\text{hexagon with square}) + N(\text{hexagon with diamond}) \\ + N(\text{hexagon with caret})$$

$$N(\text{bowtie})N(\wedge) = 10N(\text{bowtie with triangle}) + 2N(\text{bowtie with line}) + 4N(\text{bowtie}) \\ + N(\text{bowtie with wavy line}) + N(\text{bowtie with cross}) + N(\text{bowtie with star}) + N(\text{bowtie with circle}) \\ + N(\text{bowtie with caret})$$

$$N(\text{pentagon})N(\wedge) = 5N(\text{pentagon}) + 2N(\text{pentagon with line}) + 2N(\text{pentagon with wavy line}) + 2N(\text{pentagon with triangle}) \\ + N(\text{pentagon with circle}) + N(\text{pentagon with wavy line}) + N(\text{pentagon with cross}) + 2N(\text{pentagon with square}) \\ + N(\text{pentagon with diamond}) + N(\text{pentagon with caret})$$

$$N(\text{bowtie})N(\Delta) = N(\text{bowtie}) + 4N(\text{bowtie with triangle}) + N(\text{bowtie with line}) + 4N(\text{bowtie with wavy line}) \\ + N(\text{bowtie with cross}) + 2N(\text{bowtie with star}) + N(\text{bowtie with circle}) + 2N(\text{bowtie with square}) \\ + N(\text{bowtie with diamond})$$

$$N(\text{bowtie})N(\Delta) = N(\text{bowtie}) + 2N(\text{bowtie with triangle}) + 4N(\text{bowtie with line}) + N(\text{bowtie with wavy line}) \\ + 2N(\text{bowtie with cross}) + N(\text{bowtie with star}) + N(\text{bowtie with circle})$$

$$N(\text{bowtie})N(\Delta) = N(\text{bowtie}) + 2N(\text{bowtie with triangle}) + 4N(\text{bowtie with line}) + N(\text{bowtie with wavy line}) \\ + 2N(\text{bowtie with cross}) + N(\text{bowtie with star}) + N(\text{bowtie with circle})$$

$$N(\text{wavy line})N(\Delta) = 2N(\text{wavy line with triangle}) + N(\text{wavy line with line}) + 2N(\text{wavy line with wavy line}) + 2N(\text{wavy line with triangle}) \\ + N(\text{wavy line with circle}) + N(\text{wavy line with star}) + N(\text{wavy line with wavy line}) + N(\text{wavy line with cross}) \\ + N(\text{wavy line with diamond}) + N(\text{wavy line with caret})$$

$$N(\triangle \triangle)N(\wedge) = 6N(\triangle \triangle) + 4N(\text{butterfly}) + 2N(\triangle \triangle) + N(\text{zigzag}) \\ + N(\text{butterfly}) + N(\text{zigzag}) + N(\triangle \times) \\ + N(\triangle \triangle \wedge)$$

$$N(\text{cycloheptagon})N(/) = 8N(\text{cycloheptagon}) + N(\text{cycloheptagon}) + N(\text{cycloheptagon}) + N(\text{cycloheptagon}) \\ + N(\text{cycloheptagon} /)$$

$$N(\text{cyclopentadiene})N(/) = 8N(\text{cyclopentadiene}) + N(\text{cyclopentadiene}) + N(\text{cyclopentadiene}) \\ + N(\text{cyclopentadiene}) + N(\text{cyclopentadiene}) + N(\text{cyclopentadiene} /)$$

$$N(\text{cyclohexagon})N(\wedge) = 7N(\text{cyclohexagon}) + 2N(\text{cyclohexagon}) + N(\text{cyclohexagon}) + N(\text{cyclohexagon}) \\ + 4N(\text{cyclohexagon}) + N(\text{cyclohexagon}) + N(\text{cyclohexagon}) + N(\text{cyclohexagon}) \\ + N(\text{cyclohexagon}) + N(\text{cyclohexagon} \wedge)$$

$$N(\text{cycloheptagon})N(\vee) = 6N(\text{cycloheptagon}) + 5N(\text{cycloheptagon}) + 2N(\text{cycloheptagon}) + 2N(\text{cycloheptagon}) \\ + N(\text{cycloheptagon}) + 2N(\text{cycloheptagon}) + N(\text{cycloheptagon}) + 2N(\text{cycloheptagon}) \\ + 2N(\text{cycloheptagon}) + 4N(\text{cycloheptagon}) + N(\text{cycloheptagon}) + N(\text{cycloheptagon}) \\ + N(\text{cycloheptagon}) + N(\text{cycloheptagon}) + N(\text{cycloheptagon}) + N(\text{cycloheptagon}) \\ + N(\text{cycloheptagon}) + 3N(\text{cycloheptagon}) + 2N(\text{cycloheptagon}) + N(\text{cycloheptagon} \vee)$$

$$N(\text{cyclopentadiene})N(N) = 8N(\text{cyclopentadiene}) + 4N(\text{cyclopentadiene}) + 4N(\text{cyclopentadiene}) + N(\text{cyclopentadiene}) \\ + N(\text{cyclopentadiene}) + 2N(\text{cyclopentadiene}) + 4N(\text{cyclopentadiene}) + N(\text{cyclopentadiene}) \\ + N(\text{cyclopentadiene}) + N(\text{cyclopentadiene}) + N(\text{cyclopentadiene}) + N(\text{cyclopentadiene}) \\ + N(\text{cyclopentadiene} \vee)$$

$$N(\text{cyclohexagon})N(\triangle) = 2N(\text{cyclohexagon}) + N(\text{cyclohexagon}) + N(\text{cyclohexagon}) + N(\text{cyclohexagon}) \\ + 2N(\text{cyclohexagon}) + N(\text{cyclohexagon}) + N(\text{cyclohexagon}) + N(\text{cyclohexagon}) \\ + N(\text{cyclohexagon}) + N(\text{cyclohexagon} \triangle)$$

$$\begin{aligned}
 N(\text{W})N(\Delta) = & N(\text{W}) + N(\text{W}) + 4N(\text{W}) + N(\text{W}) \\
 & + N(\text{W}) + 4N(\text{W}) + N(\text{W}) \\
 & + 2N(\text{W}) + N(\text{W}) + N(\text{W}) \\
 & + 2N(\text{W}) + 2N(\text{W}) + N(\text{W})
 \end{aligned}$$

$$\begin{aligned}
 N(\text{W})N(\Delta) = & N(\text{W}) + 4N(\text{W}) + N(\text{W}) + 4N(\text{W}) \\
 & + N(\text{W}) + 2N(\text{W}) + 2N(\text{W}) \\
 & + N(\text{W}) + N(\text{W}) + 2N(\text{W}) + N(\text{W}) \\
 & + N(\text{W})
 \end{aligned}$$

$$\begin{aligned}
 N(\text{W})N(\Delta) = & N(\text{W}) + N(\text{W}) + 2N(\text{W}) + N(\text{W}) \\
 & + N(\text{W}) + 2N(\text{W}) + N(\text{W}) \\
 & + N(\text{W}) + N(\text{W}) + N(\text{W}) \\
 & + N(\text{W}) + 2N(\text{W}) + 2N(\text{W}) + N(\text{W}) \\
 & + N(\text{W}) + N(\text{W}) + N(\text{W}) + N(\text{W})
 \end{aligned}$$

















$$\begin{aligned}
 N(\text{W})N(\Delta) = & 2N(\text{W}) + N(\text{W}) + N(\text{W}) + 2N(\text{W}) \\
 & + N(\text{W}) + N(\text{W}) + N(\text{W}) \\
 & + N(\text{W})
 \end{aligned}$$

$$\begin{aligned}
 N(\text{W})N(\Delta) = & 5N(\text{W}) + 2N(\text{W}) + 2N(\text{W}) + N(\text{W}) \\
 & + 3N(\text{W}) + 2N(\text{W}) + N(\text{W}) + N(\text{W}) \\
 & + N(\text{W}) + N(\text{W}) + N(\text{W}) + N(\text{W}) \\
 & + 2N(\text{W}) + N(\text{W}) + N(\text{W}) + 2N(\text{W}) \\
 & + N(\text{W}) + N(\text{W}) + N(\text{W})
 \end{aligned}$$

$$\begin{aligned}
 N(\text{W})N(\Delta) = & 8N(\text{W}) + N(\text{W}) + N(\text{W}) + N(\text{W}) \\
 & + N(\text{W})
 \end{aligned}$$

$$\begin{aligned}
N(\triangle \triangle) N(V) = & 8N(\text{diagram 1}) + 2N(\text{diagram 2}) + 2N(\text{diagram 3}) \\
& + N(\text{diagram 4}) + 4N(\text{diagram 5}) + N(\text{diagram 6}) \\
& + 2N(\text{diagram 7}) + N(\text{diagram 8}) + N(\text{diagram 9}) \\
& + N(\text{diagram 10}) + N(\text{diagram 11}) + N(\text{diagram 12}) \\
& + N(\text{diagram 13}) + N(\text{diagram 14})
\end{aligned}$$

Lattice constants of weak graphs, with more than two odd vertices, required in the calculation of the lattice constants of the separated graphs

<u>Graph</u>	<u>Number of Edges</u>	<u>Lattice Constant</u>
	5	48
	6	480
	7	1185
	7	2274
	7	240
	7	225
	8	11130
	8	10656
	8	2040
	8	1140
	8	96
	8	96
	8	192
	8	60
	8	120
	8	60

APPENDIX F

The first seven low temperature ferromagnetic polynomials for the hypertriangular lattice

$$L_1 = u^3$$

$$L_2 = 3u^5 - 3 \frac{1}{2} u^6$$

$$L_3 = u^6 - 12u^7 - 33u^8 + 20 \frac{1}{3} u^9$$

$$L_4 = 12u^8 + 41u^9 - 256 \frac{1}{2} u^{10} + 351u^{11} - 147 \frac{3}{4} u^{12}$$

$$L_5 = 3u^9 + 111u^{10} - 24u^{11} - 1673u^{12} + 4164u^{13} - 3798u^{14} + 1217 \frac{1}{5} u^{15}$$

$$L_6 = 81u^{11} + 765 \frac{1}{2} u^{12} - 2481u^{13} - 7644u^{14} + 39481u^{15} - 61267 \frac{1}{2} u^{16} + 41928u^{17} - 10863 \frac{1}{6} u^{18}$$

$$L_7 = 45u^{12} + 1059u^{13} + 3186u^{14} - 31423u^{15} + 12628u^{16} + 296067u^{17} - 762932u^{18} + 859836u^{19} - 470943u^{20} + 102477 \frac{1}{7} u^{21}$$

Low temperature ferromagnetic series expansions for the Ising model on the hypertriangular lattice.

free energy

$$\begin{aligned}
 (-f/kT) &= (q/2) K + u^3 + 3 u^5 - 2 \frac{1}{2} u^6 - 12 u^7 \\
 &\quad - 21 u^8 + 64 \frac{1}{3} u^9 - 145 \frac{1}{2} u^{10} \\
 &\quad + 408 u^{11} - 1010 \frac{1}{4} u^{12} + \dots
 \end{aligned}$$

configurational energy

$$\begin{aligned}
 (U/J) &= - (q/2) + 12 u^3 + 60 u^5 - 60 u^6 - 336 u^7 \\
 &\quad - 672 u^8 + 2316 u^9 - 5820 u^{10} + 17952 u^{11} \\
 &\quad - 48492 u^{12} + \dots
 \end{aligned}$$

specific heat

$$\begin{aligned}
 C/k(\ln u)^2 &= 9 u^3 + 75 u^5 - 90 u^6 - 588 u^7 - 1344 u^8 \\
 &\quad + 5211 u^9 - 14550 u^{10} + 49368 u^{11} \\
 &\quad - 145476 u^{12} + \dots
 \end{aligned}$$

spontaneous magnetization

$$\begin{aligned}
 I &= 1 - 2 u^3 - 12 u^5 - 8 u^6 - 72 u^7 - 102 u^8 \\
 &\quad + 480 u^9 - 942 u^{10} + 3540 u^{11} \\
 &\quad - 8096 u^{12} + \dots
 \end{aligned}$$

initial susceptibility

$$\begin{aligned}\bar{\chi} = & 4 u^3 + 48 u^5 - 20 u^6 - 432 u^7 - 420 u^8 \\ & + 3656 u^9 - 5316 u^{10} + 31728 u^{11} \\ & - 57704 u^{12} + \dots\end{aligned}$$

APPENDIX G

Partial Generating Functions for the Hydrogen Peroxide Lattice.

$$F_0 = \ln(1+X)$$

$$F_1 = (3,3)$$

$$F_2 = 3(5,4,1) - 3 \frac{1}{2} (6,6)$$

$$F_3 = 12(7,5,2) + (7,6,0,1) - 33(8,7,1) + 20 \frac{1}{3} (9,9)$$

$$F_4 = 56(9,6,3) + 12(9,7,1,1) - 256 \frac{1}{2} (10,8,2) \\ - 15(10,9,0,1) + 351(11,10,1) - 147 \frac{3}{4} (12,12)$$

$$F_5 = 3(10,5,5) + 273(11,7,4) + 108(11,8,2,1) + 3(11,9,0,2) \\ - 1862(12,9,3) - 297(12,10,1,1) + 4164(13,11,2) \\ + 189(13,12,0,1) - 3798(14,13,1) + 1217 \frac{1}{5} (15,15)$$

$$F_6 = 30(12,6,6) + 15(12,7,4,1) + 1329(13,8,5) \\ + 820(13,9,3,1) + 66(13,10,1,2) - 12918(14,10,4) \\ - 3810(14,11,2,1) - 84 \frac{1}{2} (14,12,0,2) + 41753(15,12,3) \\ + 5274(15,13,1,1) - 61267 \frac{1}{2} (16,14,2) - 2272(16,15,0,1) \\ + 41928(17,16,1) - 10863 \frac{1}{6} (18,18)$$

$$F_7 = 2(13,6,6,1) + 237(14,7,7) + 213(14,8,5,1) + 30(14,9,3,2) \\ + 6321(15,9,6) + 4524(15,10,5,1) + 846(15,11,2,2) \\ + 13(15,12,0,3) - 86502(16,11,5) - 39370(16,12,3,1) \\ - 2475(16,13,1,2) + 378465(17,13,4) + 89130(17,14,2,1) \\ + 1626(17,15,0,2) - 789853(18,15,3) - 82398(18,16,1,1) \\ + 859836(19,17,2) + 26921(19,18,0,1) - 470943(20,19,1) \\ + 102477 \frac{1}{7} (21,21)$$

$$F_9 = 12(15,6,9) + 30(15,7,7,1) + 12(15,8,5,2) + 1653(16,8,8) \\ + 2119(16,9,6,1) + 585(16,10,4,2) + 30(16,11,2,3) \\ + \dots$$






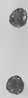




$$F_9 = 3(16,7,7,2) + 6(16,7,9) + 144(17,7,10) + 429(17,8,8,1) \\ + 237(17,9,6,2) + 30(17,10,4,3) + \dots$$

$$F_{10} = 54(18,8,8,2) + 21(18,9,6,3) + \dots$$

$$F_{10} = 12(19,8,8,3) + \dots$$

APPENDIX H

Shadow configurations for the hydrogen peroxide lattice. The lattice constants are the number of strong embeddings of a given graph in the hypertriangular lattice. The codes refer to the partial generating functions of the hydrogen peroxide lattice.

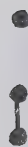
Shadow	Graph	Lattice Constant	Code
		1	(3,3)
		3	3(5,4,1)
		$\frac{1}{2} \quad N \quad -3 \quad \frac{1}{2}$	$-3 \quad \frac{1}{2} \quad (6,6)$
		12	12 (7,5,2)
		1	(7,6,0,1)

Shadow

Graph

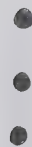
Lattice Constant

Code



-33 (8,7,1)

3N -33



20 1/3 (9,9)

1/6 N² -3 1/2 N + 20 1/3



8 (9,6,3)

8



48 (9,6,3)

48



12 (9,7,1,1)

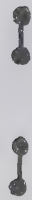
12

Shadow

Graph

Lattice Constant

Code



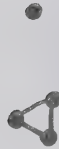
$$4 \frac{1}{2} N - 76 \frac{1}{2}$$

$$-76 \frac{1}{2} (10, 8, 2)$$



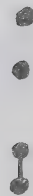
$$12 N - 180$$

$$-180 (10, 8, 2)$$



$$N - 15$$

$$-15 (10, 9, 0, 1)$$



$$1 \frac{1}{2} N^2 - 43 \frac{1}{2} N + 351$$

$$351 (11, 10, 1)$$



$$\frac{1}{24} N^3 - 1 \frac{3}{4} N^2$$

$$-147 \frac{3}{4} (12, 12)$$

$$+ 26 \frac{11}{24} N - 147 \frac{3}{4}$$

Shadow	Graph	Lattice Constant	Code
		3	3 (10,5,5)
		177	177 (11,7,4)
		96	96 (11,7,4)
		12	11 (8,2,1)
		48	11 (8,2,1)

Shadow

Graph

Lattice Constant

Code



48

11 (8,2,1)



3

3 (11,9,0,2)



8 N -152

-152 (12,9,3)



48 N -897

-897 (12,9,3)



36 N -813

-813 (12,9,3)

Shadow

Graph

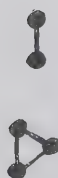
Lattice Constant

Code



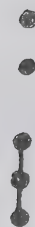
12 N -228

-228 (12,10,1,1)



3 N -69

-69 (12,10,1,1)



6 N² -222 N + 2253

2253 (13,11,2)







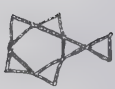
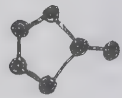




4 1/2 N² -175 1/2 N + 1911

1911 (13,11,2)



1/2 N² -18 1/2 N + 189

189 (13,12,0,1)

Shadow	Graph	Lattice Constant	Code
		$\frac{1}{2} N^3 - 27 N^2$ $+ 527 \frac{1}{2} N - 3798$	-3798 (14,13,1)
		$\frac{1}{120} N^4 - \frac{7}{12} N^3 + 16 \frac{7}{24} N^2$ $-218 \frac{11}{12} N + 1217 \frac{1}{5}$	1217 $\frac{1}{5}$ (15,15)
		30	30 (12,6,6)
		15	15 (12,7,4,1)
		3 N -60	-60 (13,8,5)

Shadow

Graph

Lattice Constant

Code



663

663 (13,8,5)



324

324 (13,8,5)



354

354 (13,8,5)



48

48 (13,8,5)



162

162 (13,9,3,1)

Shadow

Graph

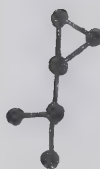
Lattice Constant

Code



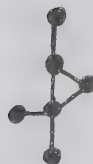
354

354 (13,9,3,1)



48

48 (13,9,3,1)



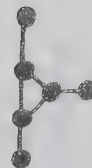
96

96 (13,9,3,1)



96

96 (13,9,3,1)



64

64 (13,9,3,1)

Shadow	Graph	Lattice Constant	Code
		6	6 (13,10,1,2)
		48	48 (13,10,1,2)
		12	12 (13,10,1,2)
		177 N -3981	-3981 (14,10,4)
		96 N -2148	-2148 (14,10,4)

Shadow	Graph	Lattice Constant	Code
		24 N -666	-666 (14,10,4)
		144 N -3996	-3996 (14,10,4)
		72 N -2127	-2127 (14,10,4)
		12 N -276	-276 (14,11,2,1)
		48 N -1089	-1089 (14,11,2,1)

Shadow

Graph

Lattice Constant

Code



48 N -1074 -1074 (14,11,2,1)



12 N -357 -357 (14,11,2,1)



36 N -1014 -1014 (14,11,2,1)













3 N -69 -69 (14,12,0,2)



1/2 N -15 1/2

-15 1/2
(14,12,0,2)

Shadow	Graph	Lattice Constant	Code
		$4 N^2 - 180 N + 2186$	2186 (15,12,3)
		$24 N^2 - 1065 N + 12831$	12831 (15,12,3)
		$36 N^2 - 1749 N + 23400$	23400 (15,12,3)
		$4 \frac{1}{2} N^2 - 229 \frac{1}{2} N + 3336$	3336 (15,12,3)
		$6 N^2 - 270 N + 3294$	3294 (15,13,1,1)

Shadow

Graph

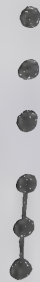
Lattice Constant

Code



$$3 N^2 - 147 N + 1980$$

1980 (15, 13, 1, 1)



$$2 N^3 - 132 N^2 + 3127 N - 26949$$

-26949 (16, 14, 2)



$$2 \frac{1}{4} N^3 - 153 N^2 + 3776 \frac{1}{4} N$$

-34318 $\frac{1}{2}$

(16, 14, 2)



$$\frac{1}{6} N^3 - 11 N^2 + 261 \frac{5}{6} N$$







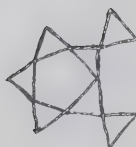
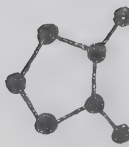

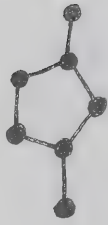
-2272 (16, 15, 0, 1)



$$\frac{1}{8} N^3 - 10 \frac{3}{4} N^2 + 370 \frac{3}{8} N$$

41928 (17, 16, 1)

211

Shadow	Graph	Lattice Constant	Code
		$1/720 N^5 - 7/48 N^4$ $+ 6 \ 65/144 N^3 - 152 \ 3/16 N^2$ $+ 1941 \ 17/360 N - 10863 \ 1/6$	-10863 1/6 (18,18)
			2 (13,6,6,1)
			114 (14,7,7)
			60 (14,7,7)
			60 (14,7,7)

Shadow

Graph

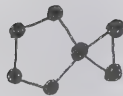
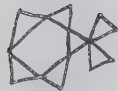
Lattice Constant

Códe



3 (14,7,7)

3



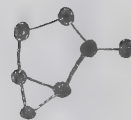
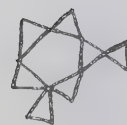
15 (14,8,5,1)

15



60 (14,8,5,1)

60













60 (14,8,5,1)

60



24 (14,8,5,1)

24

Shadow	Graph	Lattice Constant	Code
		54	54 (14,8,5,1)
		15	15 (14,9,3,2)
		15	15 (14,9,3,2)
		2463	2463 (15,9,6)
		1236	1236 (15,9,6)

Shadow

Graph

Lattice Constant

Code



2424 2424 (15,9,6)



648 648 (15,9,6)



132 132 (15,9,6)



396 396 (15,9,6)



-714 -714 (15,9,6)

Shadow

Graph

Lattice Constant

Code



-264 -264 (15,9,6)



618 618 (15,10,4,1)













1218 1218 (15,10,4,1)



663 663 (15,10,4,1)



294 294 (15,10,4,1)

Shadow	Graph	Lattice Constant	Code
		324	324 (15,10,4,1)
		324	324 (15,10,4,1)
		138	138 (15,10,4,1)
		324	324 (15,10,4,1)
		708	708 (15,10,4,1)

Shadow

Graph

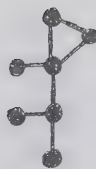
Lattice Constant

Code



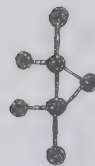
177

177 (15,10,4,1)



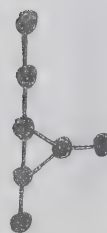
96

96 (15,10,4,1)



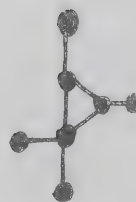
48

48 (15,10,4,1)













654

654 (15,10,4,1)



192

192 (15,10,4,1)

Shadow	Graph	Lattice Constant	code
		-354	-354 (15,10,4,1)
		162	162 (15,11,2,2)
		162	162 (15,11,2,2)
		33	33 (15,11,2,2)
		177	177 (15,11,2,2)

Shadow

Graph

Lattice Constant

Code



48

48 (15,11,2,2)



48

48 (15,11,2,2)



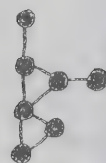
96

96 (15,11,2,2)



24

24 (15,11,2,2)



96

96 (15,11,2,2)

Shadow

Graph

Lattice Constant

Code



1

1 (15,12,0,3)



12

12 (15,12,0,3)



-17409

-17409 (16,11,5)















-8520

-8520 (16,11,5)



-9150

-9150 (16,11,5)

Shadow	Graph	Lattice Constant	Code
 		-17565	-17565 (16,11,5)
		-9366	-9366 (16,11,5)
		-3444	-3444 (16,11,5)
		-1236	-1236 (16,11,5)
 		-20706	-20706 (16,11,5)

Shadow

Graph

Lattice Constant

Code



894 894 (16, 11, 5)



-4266 -4266 (16, 12, 3, 1)



-9270 -9270 (16, 12, 3, 1)



-1236 -1236 (16, 12, 3, 1)



-2532 -2532 (16, 12, 3, 1)

Shadow

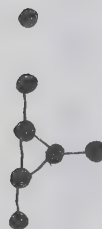
Graph

Lattice Constant

Code



-2502 -2502 (16,12,3,1)



-1670 -1670 (16,12,3,1)













-284 -284 (16,12,3,1)



-1185 -1185 (16,12,3,1)



-1737 -1737 (16,12,3,1)

Shadow	Graph	Lattice Constant	Code
		-4740	-4740 (16, 12, 3, 1)
		-4746	-4746 (16, 12, 3, 1)
		-5202	-5202 (16, 12, 3, 1)
		-162	-162 (16, 13, 1, 2)
		-1266	-1266 (16, 13, 1, 2)

Shadow

Graph

Lattice Constant

Code



-309 -309 (16,13,1,2)



-438 -438 (16,13,1,2)



-300 -300 (16,13,1,2)



64359 64359 (17,3,4)



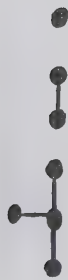
34488 34488 (17,13,4)

Shadow

Graph

Lattice Constant

Code



21726

21726 (17,13,4)



129348

129348 (17,13,4)



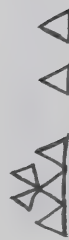
69360

69360 (17,13,4)



59184

59184 (17,13,4)



4497

4497 (17,14,2,1)

Shadow

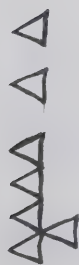
Graph

Lattice Constant

Code



17649 17649 (17,14,2,1)



17304 17304 (17,14,2,1)








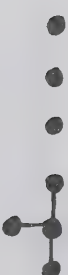




11628 11628 (17,14,2,1)













33012 33012 (17,14,2,1)



5040 5040 (17,14,2,1)

Shadow	Graph	Lattice Constant	Code
		1128	1128 (17,15,0,2)
		498	498 (17,15,0,2)
		-28638	-28638 (18,15,3)
		-167895	-167895 (18,15,3)
		-461823	-461823 (18,15,3)

Shadow	Graph	Lattice Constant	Code
		-131497	-131497 (18,15,3)
		-43332	-43332 (18,16,1,1)
		-39066	-39066 (18,16,1,1)
		318363	318363 (19,17,2)
		541473	541473 (19,17,2)

Shadow	Graph	Lattice Constant	Code
		26921	26921 (19,18,0,1)
		-470943	-470943 (20,19,1)
		102477 1/7	102477 1/7 (21,21)

APPENDIX I

Low Temperature Ferromagnetic Polynomials $L_s(z)$ for the Hydrogen Peroxide Lattice.

$$\begin{aligned}
 L_1 &= z^3 \\
 L_2 &= 1 \frac{1}{2} z^4 - 2z^6 \\
 L_3 &= 3z^5 - 9z^7 + 6 \frac{1}{3} z^9 \\
 L_4 &= 7z^6 - 33 \frac{3}{4} z^8 + 51z^{10} - 24 \frac{1}{2} z^{12} \\
 L_5 &= 18z^7 - 121z^9 + 288z^{11} - 291z^{13} + 106 \frac{1}{5} z^{15} \\
 L_6 &= 49 \frac{1}{2} z^8 - 429z^{10} + 1410 \frac{1}{2} z^{12} - 2220z^{14} \\
 &\quad + 1684 \frac{1}{2} z^{16} - 495(2/3)z^{18} \\
 L_7 &= 143z^9 - 1521z^{11} + 6420z^{13} - 13872z^{15} + 16271z^{17} \\
 &\quad - 9888z^{19} + 2437 \frac{1}{7} z^{21} \\
 L_8 &= 429z^{10} - 5414 \frac{1}{2} z^{12} + 27999z^{14} - 77398 \frac{7}{8} z^{16} \\
 &\quad + 124165z^{18} - 116077 \frac{1}{2} z^{20} + 58755z^{22} - 12457 \frac{1}{4} z^{24} \\
 L_9 &= 1326z^{11} - 19380z^{13} + 118864z^{15} - 401793z^{17} \\
 &\quad + 822360z^{19} - 1047420z^{21} + 813216z^{23} - 352791z^{25} \\
 &\quad + 65618 \frac{1}{9} z^{27} \\
 L_{10} &= 1 \frac{1}{2} z^{10} + 4184z^{12} - 69700 \frac{1}{2} z^{14} \\
 &\quad + 495463 \frac{1}{2} z^{16} - 1984976z^{18} + 4959838 \frac{4}{5} z^{20} \\
 &\quad - 8042325z^{22} + 8485862 \frac{1}{2} z^{24} - 5631619 \frac{1}{2} z^{26} \\
 &\quad + 2137315 \frac{1}{2} z^{28} - 354044 \frac{9}{10} z^{30}
 \end{aligned}$$

$$L_{11} = 15z^{11} + 13371z^{13} - 251461z^{15} + 2037402z^{17} \\ - 9458250z^{19} + 27985130z^{21} - 55320660z^{23} \\ + 74182779z^{25} - 66776053z^{27} + 38687790z^{29} \\ - 13048224z^{31} + 1948161 \frac{1}{11} z^{33}$$

$$L_{12} = 97 \frac{1}{2} z^{12} + 43029z^{14} - 908463 \frac{3}{4} z^{16} + 8286908 \frac{1}{3} z^{18} \\ - 43833172 \frac{1}{2} z^{20} + 150201585z^{22} - 351274376 \frac{1}{4} z^{24} \\ + 573569217z^{26} - 655220490z^{28} + 514088399z^{30} \\ - 264244883 \frac{1}{4} z^{32} + 80188977z^{34} - 10896827 \frac{1}{6} z^{36}$$

$$L_{13} = 525z^{13} + 138830z^{15} - 3281880z^{17} + 33392535z^{19} \\ - 198665785z^{21} + 775265400z^{23} - 2098448703z^{25} \\ + 4050218774z^{27} - 5627965959z^{29} + 5597194944z^{31} \\ - 3891121690z^{33} + 1797133827z^{35} - 495661896z^{37} \\ + 61800078 \frac{1}{13} z^{39}$$

$$L_{14} = z^{12} + 2536 \frac{1}{2} z^{14} + 447481 \frac{1}{2} z^{16} - 11841776z^{18} \\ + 133444096 \frac{1}{2} z^{20} - 883929669z^{22} + 3877211902z^{24} \\ - 11944978402 \frac{1}{2} z^{26} + 26666016898 \frac{5}{7} z^{28} \\ - 43765361029 \frac{1}{2} z^{30} + 52896457630 \frac{1}{2} z^{32} \\ - 46565246611z^{34} + 29055837352z^{36} - 12182650104z^{38} \\ + 3079314606z^{40} - 354674912 \frac{11}{14} z^{42}$$

$$L_{15} = 12z^{13} + 11425z^{15} + 1436253z^{17} - 42636642z^{19} \\ + 529247008z^{21} - 3871587153z^{23} + 18889738137 \frac{3}{5} z^{25} \\ - 65375406444 \frac{1}{3} z^{27} + 166021444314z^{29} \\ - 314961411369z^{31} + 449306269607z^{33} - 480296343859 \frac{4}{5} z^{35} \\ + 379171416132z^{37} - 214589972615z^{39} + 82377179820z^{41} \\ - 19215911169z^{43} + 2056526543 \frac{3}{5} z^{45}$$

$$L_{16} = 93z^{14} + 49072 \frac{1}{2} z^{16} + \dots$$

$$L_{17} = 598z^{15} + \dots$$

$$L_{18} = 1 \frac{1}{2} z^{14} + 3433 \frac{1}{2} z^{16} + \dots$$

$$L_{19} = 21z^{15} + \dots$$

$$L_{20} = 184 \frac{1}{2} z^{16}$$

$$L_{21} = (\quad) z^{17} + \dots$$

$$L_{22} = 6z^{16} + \dots$$

APPENDIX J

The number of polygons (p graphs), theta graphs, dumbbell graphs, and figure eight graphs on the hypertriangular lattice.

l	$l(l)_p$	$\sum_l (a,b,c)_\theta$	$\sum_l (a,b,c)_{db}$	$\sum_l (a,b)_8$
3	3	0	0	0
4	0	0	0	0
5	15	0	0	0
6	90	0	0	3
7	231	15	12	0
8	576	66	60	15
9	2637	177	393	105
10	11580	858	2472	342
11	42306	4332	13350	1110
12	158748	17179	69039	4815
13	651885	68046	355116	20136
14	2688756	295818	1787898	77334
15	10897530			

The number of polygons (p graphs), theta graphs, and dumbbell graphs on the hydrogen peroxide lattice

l	$l(l)_p$	$\sum_l (a,b,c)_\theta$	$\sum_l (a,b,c)_{db}$
10	15	0	0
11	0	0	0
12	0	0	0
13	0	0	0
14	21	0	0
15	0	1	0
16	168	0	0
17	0	3	0
18	423	12	0
19	0	19 1/2	0
20	900	6	0
21	0	27	37 1/2
22	3927	63	72
23	0	162	141
24	14100	316	270
25	0	721	645
26	41067	849	1221
27	0	2108 1/2	3135
28	140742	3150	6318
29	0	7554	14305 1/2
30	498105	12285	27474

Weak lattice constants of dumbbell graphs for the hydrogen peroxide lattice.

a	b	c	ℓ	$(a,b,c)_{db}$
10	1	10	21	37 1/2
10	2	10	22	72
10	3	10	23	141
10	4	10	24	270
10	1	14	25	93
10	5	10	25	552
10	2	14	26	174
10	6	10	26	1047
10	1	16	27	708
10	3	14	27	372
10	7	10	27	2055
10	2	16	28	1470
10	4	14	28	714
10	8	10	28	4134

a	b	c	ℓ	$(a, b, c)_{db}$
10	1	18	29	1830
10	3	16	29	2802
10	5	14	29	1398
10	9	10	29	8217
14	1	14	29	$58 \frac{1}{2}$
10	2	18	30	3366
10	4	16	30	5382
10	6	14	30	2688
10	10	10	30	15933
14	2	14	30	105

Weak lattice constants of dumbbell graphs for the hypertriangular lattice.

a	b	c	ℓ	$(a,b,c)_{db}$
3	1	3	7	12
3	2	3	8	60
3	3	3	9	273
3	1	5	9	120
3	4	3	10	1302
3	2	5	10	522
3	1	6	10	648
3	1	7	11	1542
3	2	6	11	2928
3	3	5	11	2484
3	5	3	11	6174
5	1	5	11	222

a	b	c	ℓ	$(a, b, c)_{db}$
3	1	8	12	3852
3	2	7	12	7134
3	3	6	12	13644
3	4	5	12	11616
3	6	3	12	28971
5	1	6	12	2628
5	2	5	12	1194
3	1	9	13	17634
3	2	8	13	17412
3	3	7	13	32880
3	4	6	13	64182
3	5	5	13	54606
3	7	3	13	135807
5	1	7	13	6594
5	2	6	13	13098
5	3	5	13	5439
6	1	6	13	7464

a	b	c	ℓ	$(a,b,c)_{db}$
3	1	10	14	74730
3	2	9	14	77754
3	3	8	14	80724
3	4	7	14	155202
3	5	6	14	301944
3	6	5	14	255570
3	8	3	14	636798
5	1	8	14	15438
5	2	7	14	31506
5	3	6	14	60228
5	4	5	14	25389
6	1	7	14	36570
6	2	6	14	36045

Weak lattice constants of figure eight graphs for the hypertriangular lattice.

a	b	ℓ	$(a,b)_8$	a	b	ℓ	$(a,b)_8$
3	3	6	3	3	10	13	12036
3	5	8	15	5	8	13	2619
				6	7	13	5481
3	6	9	105	3	11	14	44814
3	7	10	291	5	9	14	12243
5	5	10	51	6	8	14	13554
				7	7	14	6723
3	8	11	651				
5	6	11	459				
3	9	12	2664				
5	7	12	972				
6	6	12	1179				

APPENDIX K

Table of Padé approximant estimates of critical parameters for the hypertriangular and hydrogen peroxide lattices.

TABLE K.1

Estimates of the critical point, v_G , of the hypertriangular lattice

obtained from Padé approximants to $[\chi(v)]^{1/5}$.

M^L	3	4	5	6	7	8
3				0.2220855	0.2220898	
4			0.2220807	0.2220915	0.2220896	0.2220898
5		0.2220860	0.2220855	0.2220892	0.2220144	0.2220872
6	0.2220807	0.2220855	0.2220859	0.2220877	0.222086	
7	0.2220906	0.2220892	0.2220877	0.2220873		
8		0.2220922	0.2220868			

TABLE K.2

Estimates of the critical point, v_c , of the hypertriangular lattice
obtained from Padé approximants to $\frac{d}{dv} \ln \chi(v)$.

$M \backslash L$	2	3	4	5	6	7	8
2					0.2201692		
3				0.2221757	0.2220570	0.2220913	
4			0.2221729	0.2221626	0.2220833	0.2220836	0.2220412
5		0.2221737	0.2221648	0.2222835	0.2220836	0.2220833	
6	0.2221779	0.2221551	0.2218872	0.2220894	0.2220770		
7		0.2220814	0.2220842	0.2220784			
8			0.2220823				

TABLE K.3
Estimates of the critical index, γ , of the hypertriangular lattice
obtained from Padé approximants to $(v_c - v) \frac{d}{dv} \ln \chi(v)$
evaluated at $v = v_c = 0.222087$

$M \backslash L$	2	3	4	5	6	7	8
2					1.24979		
3				1.25282	1.24991	1.24994	
4			1.25391	1.24924	1.24993	1.25018	1.24992
5		1.25144	1.24965	1.24996	1.24995	1.24992	
6	1.24974	1.24991	1.24994	1.24995	1.24996		
7		1.24994	1.24997	1.24993			
8			1.24994				

TABLE K.4

Estimates of the critical index, γ , of the hypertriangular lattice obtained from Padé approximants to $\frac{d}{dv} \{ \ln[\frac{d}{dv} \chi(v)] \} / \frac{d}{dv} [\ln \chi(v)]$ evaluated at $\frac{1}{4}$

$$v = v_C = 0.222087$$

$M \backslash L$	2	3	4	5	6	7	8
2					1.24559		
3				1.26378	1.24820	1.25056	
4			1.29244	1.25360	1.24936	1.24963	1.25056
5		1.25965	1.25282	1.25036	1.24958	1.24936	
6	1.24820	1.24886	1.24931	1.24952	1.25036		
7		1.25047	1.24973	1.24931			
8			1.25047				

TABLE K.5

Estimates of the amplitude of the susceptibility $C_+(v_c)$, of the hypertriangular lattice obtained from Padé approximants to $(v_c - v) [\chi(v)]^{1/5}$ evaluated at $v = v_c = 0.222087$

$M \backslash L$	2	3	4	5	6	7	8	9
2						1.039740		
3					1.039741	1.039734	1.039550	
4				1.039714	1.039726	1.039700	1.039717	1.039716
5			1.039714	1.039696	1.039721	1.039715	1.039716	
6		1.039740	1.039726	1.039721	1.039718	1.039716		
7	1.039739	1.039735	1.039692	1.039715	1.039716			
8		1.039573	1.039719	1.039716				
9			1.039716					

TABLE K.6
Estimates of $(-f_C/kT_C)$ for the hypertriangular lattice obtained from Padé approximants to $(-f/kT)$ evaluated at $v = v_C = 0.222087$

$M \backslash L$	4	5	6	7	8	9
4					0.7859	
5				0.7862	0.7869	0.7862
6			0.7861	0.7874	0.7863	
7		0.7858	0.7864	0.7862		
8	0.7861	0.7859	0.7862			
9		0.7859				

TABLE K.7

Estimates of the critical energy, $-U_C/kT_C$, of the hypertriangular lattice
obtained from Padé approximants to U/J evaluated at $v = v_C = 0.222087$

M^L	3	4	5	6	7	8	9
3						0.224	
4					0.214	0.235	0.228
5				0.218	0.245	0.225	
6			0.207	0.230	0.227		
7		0.227	0.231	0.226			
8	0.223	0.227	0.228				
9		0.228					

TABLE K.8

Estimates of the amplitude of the specific heat, $A_+(K_C)$, of the hypertriangular lattice obtained from Padé approximants to $(K_C - K) \{d/dK C(K)\}^{1/2+\alpha}$ evaluated at $K=K_C=0.573794$

$M \backslash L$	3	4	5	6	7	8
3						
4						
5		1.085	0.958	1.260	1.314	
6	1.085	1.091	1.043	1.326		
7	0.983	1.047	1.073			
8		1.356				

TABLE K.9

Estimates of the critical point, v_c , of the hydrogen peroxide lattice
obtained from Padé approximants to $[X(v)]^{4/5}$

$M \backslash L$	9	10	11	12	13	14	15	16
8						0.518193	0.518182	
9					0.518180	0.518225	0.518170	0.518279
10				0.518148	0.518092	0.518113	0.518154	0.518156
11			0.509147	0.518033	0.518110	0.518083	0.518156	0.518155
12		0.518170	0.518047	0.518219	0.518276	0.518143	0.518153	
13	0.518174	0.518202	0.518126	0.518278	0.518224	0.518151		
14	0.518147	0.518143	0.518157	0.518152	0.518154			
15	0.518143	0.518146	0.518153	0.518153				
16	0.518156	0.518154	0.518153					
17		0.518152						

TABLE K.10

Estimates of the critical point, v_c , of the hydrogen peroxide lattice
obtained from Padé approximants to $\frac{d}{dv} \ln \chi(v)$

$M \backslash L$	8	9	10	11	12	13	14	15
7							0.510108	
8						0.518063	0.518035	0.518079
9					0.517982	0.518043	0.518052	0.518064
10				0.518092	0.518088	0.518068	0.518078	0.518082
11			0.518132	0.518087	0.518093	0.518073	0.518083	0.518078
12		0.518080	0.518092	0.518021	0.518069	0.518076	0.518070	
13	0.518009	0.518095	0.518084	0.518072	0.518081	0.518177		
14	0.518055	0.518068	0.518075	0.518077	0.518015			
15	0.518061	0.518085	0.518080	0.518073				
16		0.518079	0.518084					

TABLE K.11

Estimates of the critical index, γ of the hydrogen peroxide lattice obtained from
 Padé Approximants to $(v_c - v) \frac{d}{dv} \ln \chi(v)$ evaluated at $v = v_c = 0.518140$

$M \backslash L$	8	9	10	11	12	13	14	15
7							1.2479	
8						1.2480	1.2472	1.2485
9					1.2485	1.2486	1.2493	1.2498
10				1.2484	1.2471	1.2482	1.2503	1.2520
11			1.2484	1.2484	1.2482	1.2478	1.2512	
12		1.2485	1.2489	1.2482	1.2486	1.2494	1.2494	
13	1.2480	1.2487	1.2484	1.2474	1.2496	1.2494		
14	1.2477	1.2496	1.2502	1.2521	1.2493			
15	1.2484	1.2500	1.2487	1.2506				
16		1.2511	1.2504					

TABLE K.12

Estimates of the critical index, γ , of the hydrogen peroxide lattice obtained from

Padé approximants to $\frac{d}{dv} \left\{ \ln \frac{d}{dv} x(v) \right\} / \frac{d}{dv} \ln x(v)$ evaluated at

$$v = v_C = 0.518140.$$

M ^L	8	9	10	11	12	13	14	15
7							1.2452	
8						1.3203	1.2511	1.2461
9					1.2378	1.2489	1.1876	1.2466
10				1.2340	1.2419	1.2405	1.2447	1.2467
11			1.2415	1.2446	1.2404	1.2417	1.2489	1.2442
12		1.2413	1.2405	1.2424	1.2433	1.2453	1.2405	
13	1.2402	1.2456	1.2421	1.2364	1.2349	1.2432		
14	1.2368	1.2413	1.2432	1.2349	1.2204			
15	1.2463	1.2508	1.2472	1.2428				
16		1.2483	1.2506					

TABLE K.13

Estimates of the amplitude of the susceptibility, $C_+(v_G)$, of the hydrogen peroxide lattice obtained from Padé approximants to $(v_G - v) [X(v)]^{1/5}$ evaluated at $v = v_G = 0.518140$

$M \backslash L$	9	10	11	12	13	14	15	16
8						1.0408	1.0412	
9					1.0410	1.0410	1.0411	1.0410
10				1.0410	1.0410	1.0412	1.0411	1.0414
11			1.0410	1.0412	1.0411	1.0410	1.0410	1.0409
12		1.0409	1.0411	1.0411	1.0416	1.0410	1.0410	
13	1.0411	1.0411	1.0411	1.0411	1.0410	1.0410		
14	1.0411	1.0411	1.0411	1.0409	1.0413			
15	1.0411	1.0411	1.0411	1.0421				
16	1.0410	1.0407	1.0406					
17		1.0405						

TABLE K.14

Estimates of $(-f_c/kT_c)$ for the hydrogen peroxide lattice obtained from Padé approximants to $(-f/kT)$ evaluated at $v = v_c = 0.518140$

$M \backslash L$	10	11	12	13	14	15	16	17
10						0.9304	0.9306	
11					0.9304	*	0.9306	*
12				0.9308	0.9306	0.9306	0.9306	
13			0.9308	*	0.9306	*		
14		0.9306	0.9306	0.9306	0.9306			
15	0.9306	*	0.9306	*				
16	0.9306	0.9306	0.9308					
17		*						

*padé approximants have no solution.

TABLE K.15

Estimates of the critical energy, $-U_C/kT_C$, of the hydrogen peroxide lattice obtained from Padé approximants to U/J evaluated at $v=v_C=0.518140$

$M \backslash L$	10	11	12	13	14	15	16
9						0.4777	*
10				0.5079		0.4792	0.4792
11				0.5079	*	0.4792	*
12			0.5144	0.4757	0.4757	0.4798	
13		0.5144	*	0.4757	*		
14	0.4780	0.4793	0.4793	0.4799			
15	*	0.4793	*				
16		0.4803					

*Padé approximants have no solution.

TABLE K.16

Estimates of z_c for the hydrogen peroxide lattice
obtained from Padé approximants to $\frac{d}{dz} \ln I(z)$.

$M \backslash L$	5	6	7	8	9
5			0.3174	0.3166	
6		0.3112	0.3162	0.3163	0.3169
7	0.3085	0.3180	0.3164	0.3162	
8	0.3153	0.3163	0.3142		
9		No solution			

TABLE K.17
Estimates of β for the hydrogen peroxide lattice obtained from
Padé approximants to $(z_C - z) \frac{d}{dz} \ln I(z)$ evaluated at $z = z_C = 0.317402$

$M \backslash L$	4	5	6	7	8	9	10	11
4			0.306	0.304	0.304	0.303	0.329	0.287
5		no solution	0.301	0.304	0.304	0.301	0.302	
6	0.304	0.300	0.306	0.305	0.310	0.302		
7	0.301	0.302	0.305	0.305	0.304			
8	0.305	0.311	0.307	0.304				
9	0.307	0.308	0.310					
10	0.308	0.307						
11	0.310							

TABLE K.18

Estimates of γ' for the hydrogen peroxide lattice
obtained from Padé approximants to $(z_c - z) \frac{d}{dz} \ln [\bar{X}(z)/z^3]$
evaluated at $z = z_c = 0.317402$

$M \backslash L$	4	5	6	7	8
4			1.222	1.288	1.313
5		1.287	1.261	1.377	
6			1.265	1.275	
7				1.221	
8					1.289

TABLE K.19

Estimates of α' for the hydrogen peroxide lattice
 obtained from Padé approximants to $(z_c - z) \frac{d}{dz} [C(z)/kz^3(\ln z)^2]$
 evaluated at $z = z_c = 0.317402$

$\frac{L}{M}$	4	5	6	7	8
4			0.217	0.226	0.228
5		0.243	0.224	0.187	
6	0.230	0.226	0.229		
7	0.225	0.228			
8	0.232				

TABLE K.20

Estimates of $(-f_c/kT_c)$ for the hydrogen peroxide lattice obtained from Padé approximants to $(-f/kT)$ evaluated at $z = z_c = 0.317402$

$M \backslash L$	5	6	7	8	9	10
5				0.9292	0.9341	
6			0.9290	0.9301	0.9304	0.9307
7		0.9292	0.9362	0.9304	0.9327	
8	0.9298	0.9304	0.9305	0.9307		
9	0.9301	0.9305	0.9302			
10		0.0317				

TABLE K.21

Estimates of U_C/kT_C for the hydrogen peroxide lattice obtained from Padé approximants to $U(z)/J$ evaluated at $z = z_C = 0.317402$

$M \backslash L$	5	6	7	8	9	10
5				0.5200	0.5209	
6			0.5286	0.5068	0.5070	0.4780
7		0.5285	0.5214	0.5079	0.5070	
8	0.5168	0.5018	0.5074	0.4732		
9	0.5110	0.5066	0.5038	0.5196		
10		0.5197				

TABLE K.22
Estimates of the inverse of the attrition parameter, μ^{-1} , for the
hypertriangular lattice obtained from Padé approximants
to $\frac{d}{dx} [\ln C(x)]$

$M \backslash L$	4	5	6	7	8
4			0.21634	0.21642	
5		0.21634	0.21633	0.21643	0.21642
6	0.21636	0.21640	0.21641	0.21646	
7	0.21634	0.21641	0.21640		
8		0.21647			

TABLE K.23

Estimates of the inverse of the attrition parameter μ^{-1} for the
hydrogen peroxide lattice obtained from Padé approximants
to $\frac{d}{dx}[\ln C(x)]$

$M \backslash L$	10	11	12	13	14	15
10	0.51094	0.51106				
11	0.51114	0.51109	0.51106			
12		0.51109	0.51054	0.51118		
13			0.51123	0.51124	0.51128	
14				0.51123	0.51125	0.51122
15					0.51124	

REFERENCES

- Als-Nielsen, J. and Dietrich, O. W. 1967. Phys. Rev. 153, 706, 711.
- Abrahams, S. C., Collin, R. C., and Lipscomb, W. W. 1951. Acta. Cryst. 4, 15.
- Andrews, Th. 1869. Phil. Trans. 159, 575.
- Baker, G. A., Jr., 1961. Phys. Rev. 122, 1477.
- Baker, G. A., Jr., and Gaunt, D. S. 1967. Phys. Rev. 155, 545.
- Baker, G. A., Jr., Gilbert, H. E., Eve, J., and Rushbrooke, G. S. 1967. Phys. Rev. 164, 800.
- Betts, D. D. and Ditzian, R. V. 1968. Can. J. Phys. 46, 971.
- Brush, S. G. 1967. Rev. Mod. Phys. 39, 883.
- Domb, C. 1960. Adv. Phys. 9, 149, 245.
- Domb, C. 1966. Critical Phenomena, Misc. Publ. No. 273, Eds. M. S. Green and J. V. Sengers (Washington: National Bureau of Standards).
- Domb, C. 1969. Advances in Chemical Physics XV, Ed. K. E. Schuler (New York: Interscience).
- Domb, C., and Dalton, N. W. 1966. Proc. Phys. Soc. (London) 89, 859.
- Domb, C. and Sykes, M. F. 1961. J. Math. Phys. 2, 63.
- Essam, J. W. and Sykes, M. F. 1963. Physica 29, 378.
- Fisher, M. E. 1959(a). Physica 25, 521.
- Fisher, M. E. 1959(b). Phys. Rev. 113, 969.
- Fisher, M. E. 1964(a). J. Math. Phys. 5, 944.
- Fisher, M. E. 1964(b). Phys. Rev. 136, A1599.

- Fisher, M. E. 1967. Rep. Progr. Phys. 30, 615
- Fisher, M. E. and Gaunt, D. S. 1964. Phys. Rev. 113, A224.
- Fisher, M. E. and Sykes, M. F. 1959. Phys. Rev. 114, 45.
- Gans, P. J. 1965. J. Chem. Phys. 42, 4159.
- Gaunt, D. S., Fisher, M. E., Sykes M. F., and Essam, J. W. 1964. Phys. Rev. Letters 13, 713.
- Griffiths, R. B. 1964. Phys. Rev. 136, A437.
- Griffiths, R. B. 1965. Phys. Rev. Letters 14, 623.
- Griffiths, R. B. 1967. J. Math. Phys. 8, 478, 484.
- Guggenheim, E. A. 1945. J. Chem. Phys. 13, 253.
- Guttmann, A. J., Ninham, B. W., and Thompson, C. J. 1968. Phys. Rev. 172, 559.
- Hammersley, J. M. 1957. Proc. Camb. Phil Soc. 53, 642.
- Heesch, H. and Laves, F. 1933. Z. Krist. 85, 443.
- Heisenberg, W. 1928. Z. Physik. 49, 619.
- Heller, P. 1967. Rep. Progr. Phys. 30, 731.
- Heller, P. and Benedeck, G. B. 1962. Phys. Rev. Letters 8, 428.
- Heller, P. and Benedeck, G. B. 1965. Phys. Rev. Letters 14, 71.
- Henry, N. F. M. and Lonsdale, K., Eds. 1952. International Tables for X-Ray Crystallography I, (Birmingham, England: Kynoch Press).
- Ising, E. 1925. Z. Phys. 31, 253.
- Kac, M., Uhlenbeck, G. E., and Hemmer, P. 1963. J. Math. Phys. 4, 216, 229.
- Kadanoff, L. P. 1966. Physics 2, 263.

- Kadanoff, L. P., Götze, W., Hamblen, D., Hecht, R.,
Lewis, E. A. S., Palciauskas, V. V., Rayl, M.,
Swift, J., Aspnes, D., and Kane, J. Rev. Mod.
Phys. 39, 395.
- Kouvel, J. S. and Fisher, M. E. 1964. Phys. Rev. 136, A1626.
- Krammers, H. A. and Wannier, G. H. 1941. Phys. Rev. 60,
252, 263.
- Leu, J. A. 1969. Phys. Letters 29A, 641.
- Leu, J. A., Betts, D. D., and Elliott, C. J. 1969.
Can. J. Phys. 47, 1671.
- Lieb, E. H. 1967(a). Phys. Rev. Letters 18, 692.
- Lieb, E. H. 1967(b). Phys. Rev. Letters 18, 1046.
- Lieb, E. H. 1967(c). Phys. Rev. Letters 19, 108.
- Martin, J. L., Sykes, M. F., and Hioe, F. T. 1967. J. Chem.
Phys. 46, 3478.
- Mikolaj, P. G. and Pings, C. J. 1968. Phys. Chem. Liquids 1, 93.
- Moldover, M. R. 1966. Thesis, Stanford University.
- Moore, M. A. 1969. Preprint.
- Nagle, J. F. and Temperley, H. N. V. 1968. J. Math Phys.
9, 1020.
- Naya, S. 1954. Prog. theor. Phys. 11, 53.
- Noakes, J. E. Tornberg, N., and Arrot, A. 1966. J. Appl.
Phys. 37, 1264.
- Onsager, L. 1944. Phys. Rev. 65, 117.
- Onsager, L. 1949. Nuovo Cim (Suppl.) 6, 261.
- Ore, O. 1963. Graphs and Their Uses (New York: Random
House).
- Peierls, R. 1936. Proc. Camb. Phil. Soc. 32, 477.
- Rushbrooke, G. S. 1963. J. Chem. Phys. 39, 842.

- Schumb, W. C., Satterfield, C. N., and Wentworth, R. L.
1955. Hydrogen Peroxide (New York: Reinhold).
- Sykes, M. F. 1961. J. Math. Phys. 2, 52.
- Sykes, M. F., Essam, J. W., and Gaunt, D. S. 1965. J. Math. Phys. 6, 283.
- Sykes, M. F., Essam, J. W., Heap, B. R., and Hiley, B. J.
1966. J. Math. Phys. 7, 1577.
- Sykes, M. F., Martin, J. L., and Hunter, D. L. 1967. Proc. Phys. Soc. (London) 91, 671.
- Syozi, I. 1951. Prog. theor. Phys. 6, 306.
- Teaney, D. T. 1965. Phys. Rev. Letters 14, 898.
- Teaney, D. T. 1966. Critical Phenomena, Misc. Publ. No. 273, Eds. M. S. Green and J. V. Sengers (Washington: National Bureau of Standards).
- Temperley, H. N. V. 1956. Phys. Rev. 103, 1.
- Thompson, D. R. and Rice, O. K. 1964. J. Amer. Chem. Soc. 86, 3547.
- Van der Waerden, B. L. 1941. Z. Phys. 118, 473.
- Voronel', A. V., Snigrev, V. G., and Chashkin, Yu. R.
1965. Soviet Physics-JETP 21, 653.
- Wannier, G. H. 1945. Rev. Mod. Phys. 17, 50.
- Weingerger, M. A. and Schneider, W. G. 1952. Canad. J. Chem. 30, 422.
- Wells, A. F. 1954. Acta. Cryst. 7, 535.
- Widom, B. 1965. J. Chem. Phys. 43, 3892. 3898.
- Widom, B. and Rice, O. K. 1955. J. Chem. Phys. 23, 1250.
- Yang, C. N. 1952. Phys. Rev. 85, 808.
- Yang, C. N. and Lee, T. K. 1952. Phys. Rev. 87, 404, 410.

B29946